Characterization of a DNAPL Release into a Structured Heterogeneous Porous Medium and Remediation by Soil Vapor Extraction: Physical and Numerical Modeling

Jane Elizabeth Allan
B.A.Sc., Civil Engineering, University of Waterloo, 1990

A dissertation submitted to the faculty of the
Oregon Graduate Institute of Science & Technology
in partial fulfillment of the
requirement for the degree
Doctor of Philosophy
in
Environmental Science and Engineering

October 1995

This dissertation "Characterization of a DNAPL Release into a Structured Heterogeneous Porous Medium and Remediation by Soil Vapor Extraction: Physical and Numerical Modeling" by Jane Elizabeth Allan has been examined and approved by the following examination committee:

Dr. Richard L. Johnson, Dissertation Advisor

Dr. William Fish

Dr. Carl D. Palmer

Dr. Neil R. Thomson (University of Waterloo)

ACKNOWLEDGEMENTS

One month and several thousand miles away from Portland, I am looking back at five years packed with adventures and new experiences, but especially, with great people. This is my chance to thank the people that played an important part in helping me achieve this goal as well as making my time in Portland memorable.

First and foremost, I would like to thank my advisor Dr. Rick Johnson for everything! His encouragement and contagious enthusiasm kept me moving along in the right direction. He has been EXTREMELY generous with funding, particularly regarding professional and personal development. Although I never quite got used to his last-minute style, I learned that I could always count on him coming through in the end.

A special thanks to Dr. Neil Thomson for his modeling expertise and support during the last few months. He has been very generous with his time and always approachable - I rarely needed to knock on his door because it was always open. I would also like to thank the other members of my committee, Dr. Bill Fish and Dr. Carl Palmer, for reviewing my dissertation.

Financial support for this project was provided by the University of Waterloo's Solvents in Groundwater Consortium and its corporate sponsors Boeing, Ciba-Geigy and Kodak (check with Rick - I'm missing some), as well as a separate grant from IBM.

I am grateful to many individuals for their time and expertise over the course of this project: construction and instrumentation of the physical model (Bill, Jay and Matt), anything from the machine shop (Doug and Matt), anything electrical (Gerry, Gordon and Matt), anything computer related (Don, Claude, Rick S. and Matt), and anything that required alot of muscle (Matt). Did I mention Matt?

I would also like to acknowledge the people (like Donna, Margaret, Lorne, and many others) that make OGI feel more like a community than an institute; and a special

thanks also to Judi - my Portland mom. Thanks to Tim, Matt, Allison, Eric, Diane, Dirk, Patty, Michelle and Cheryl for the good times and laughs. I think that I will always look back on my five years in Portland as "the good old days!" (well... except maybe the last few months).

Many people helped make those last few months more bearable. Thanks to Greg and Jimmy for commiserating with me while we were in the same deadline situation - misery loves company! Diane was a great outlet for venting and also provided further incentive for me to finish for fear that she would 'lap' me by two years. After long days in front of the computer it was always great to come home to my housemates Paul, Trig and Andrew.

I owe a great deal to my family for providing a constant source of love and encouragement. As my long distance phone bills will show, I still look homeward for comfort during stressful periods.

And finally, I will always be grateful to Mike Elovitz. His confidence in my abilities (academic and otherwise) has really changed the way I perceive myself. I have often relied on his emotional support to get me through difficult times. Even when we were separated by 3000 miles of telephone lines I have always felt his support as though he were still just around the corner.

TABLE OF CONTENTS

LIST OF FIGURES

LIST OF TABLES

ABSTRACT

Characterization of a DNAPL Release into a Structured Heterogeneous Porous Medium and Remediation by Soil Vapor Extraction: Physical and Numerical Modeling

Jane E. Allan, Ph.D.

Oregon Graduate Institute of Science & Technology, 1995

Supervising Professor: Richard L. Johnson

The research presented here examines the movement of the dense non-aqueous phase liquid (DNAPL), tetrachloroethylene (PCE), in a well-characterized heterogeneous medium and identifies and quantifies the factors which control mass removal by soil vapor extraction (SVE).

PCE was released into a large-scale structured physical model made up of layers of sand, gravel, silica flour and clay with the water table at the clay bottom. Movement of the PCE was tracked using two non-destructive techniques: a neutron moisture probe and a down-hole video camera. PCE was observed to pool then drain to residual from a low permeability silica flour lens, then pool and spread laterally above the clay bottom. After redistribution approximately 80-90% of the PCE was located above the sand-clay interface. The final PCE distribution was confirmed by soil cores.

Air flow during SVE was examined using tracer tests and numerical modeling. Air flow was controlled by the permeability structure of the medium and influenced by leakage from the surface (despite the presence of a surface cover). Less than 10% if the total mass released into the physical model was recovered by conventional SVE. The primary limitation was mass transfer from the zone near the water table, where airflow

was negligible. Diffusion from the pool of PCE near the clay bottom was simulated using a one-dimensional diffusion model. Calculated mass flux agreed well with removal rates observed during sustained SVE.

Two- and three-dimensional simulations of the PCE release into the physical model reproduced general trends in the redistribution of PCE observed in the physical model. Numerical model results were sensitive to small change in the sand permeability and the slope of the silica flour layer. Mass removal by SVE was simulated in two-dimensions. Trends in mass removal were similar to those observed in the physical model (*i.e.*, a short period of high mass removal followed by a long period of slow mass removal). The distribution of remaining PCE matched distributions measured in the physical model (*i.e.*, all mass above the gravel removed, and little change in the high water content zone).

CHAPTER 1

INTRODUCTION

PROBLEM STATEMENT

In the past several decades, a great deal of effort has been spent studying the behavior of dense non-aqueous phase liquids (DNAPLs, *e.g.*, chlorinated solvents) in the subsurface. Both theoretical and experimental work by engineers and scientists have investigated the important processes for two- and three-phase flow and the implications for groundwater contamination and subsequent remediation. The processes have proven to be complex and difficult to characterize. Work at contaminated sites has also shown the complex nature of DNAPL movement and the difficulties associated with remediating DNAPL-contaminated sites. Much of this difficulty stems from the chemical and physical characteristics of DNAPLs and their interactions with heterogeneous subsurface soils and water. Some of these characteristics are outlined below.

DNAPLs released in the subsurface move as a separate liquid phase. Most soils are preferentially wetted by water, followed by the DNAPL phase, and the air phase as the least wetting (Schwille, 1988). Because they are less wetting than water and because DNAPL viscosities are often low, distributions are erratic even in homogeneous porous media (Kueper and Frind, 1992). In water-saturated systems the result of this will often be that when a DNAPL is spilled, only a small fraction of soil within the spill zone is actually contaminated with DNAPL (Poulsen and Kueper, 1992). Furthermore, in the portions of the soil where DNAPLs are present, saturations are often high. As a result, the relative permeability of the water in those regions may be low. Figure 1.1 presents a typical relative permeability - saturation relationship for a DNAPL/water system (van

Dam, 1967). Low aqueous solubilities combined with generally poor contact between immobile DNAPL and flowing groundwater, mean that the removal of DNAPL by dissolution will occur very slowly. Drinking water limits for many DNAPL compounds (e.g., the chlorinated solvents) are very low. As a result, unless the DNAPL source is completely removed, groundwater concentrations will remain above drinking water limits for many decades.

When a DNAPL is present above the water table, generally three fluid phases are present (i.e., air, water and DNAPL). A three-phase relative permeability-phase saturation relationship diagram is shown in Figure 1.2. As with the two-phase system, when the saturation of a phase is low (relative in this case to the sum of the other two phases) the relative permeability of that phase is low. In the vadose zone, regions with high DNAPL content are often perched above lower permeability lenses which act as capillary barriers. Those same regions often have elevated water contents. Because the DNAPLs are more dense than water, they can become encapsulated in water perched above the lower-permeability lens.

Many DNAPLs (e.g., most chlorinated solvents) are volatile, therefore, above the water table, soil vapor extraction (SVE) is a widely-used approach both for reducing vapor concentrations and for source removal. Volatilization of DNAPL adjacent to a moving air stream occurs fairly quickly. However, many field investigations show that initially high extraction concentrations are followed by low concentrations giving rise to very long cleanup times. The primary reason for these long times is low mass removal rates due to mass-transfer limitations resulting from 1) non-uniform DNAPL distributions, 2) non-uniform air flow (due to porous media heterogeneity and variable water contents), and 3) the coexistence of high DNAPL and water contents.

Mass transfer limitations for the removal of DNAPL encapsulated in a high water content zone are both due to the lack of air flow in the region and because transport within the high-water-content zone is controlled by molecular diffusion. Because aqueous diffusion coefficients are up to four orders of magnitude smaller than gas phase diffusion coefficients, the mass transfer rate is determined primarily by the saturated thickness through which the dissolved contaminants must diffuse.

The mechanisms of multiphase fluid flow and soil vapor extraction have been

examined mathematically, and sophisticated computer models have been developed based on our understanding of the important processes. However, assessment of the accuracy of these mathematical models generally relies on comparisons with experimental results. For many of the chemical and physical processes described in the numerical models, laboratory experiments provide the best means of comparison. However, laboratory-scale experiments can not capture some of the large-scale processes that play an important role in controlling DNAPL movement, air flow and mass removal by SVE. Actual field studies, on the other hand, usually do not provide sufficient information to adequately describe the porous media properties and DNAPL distribution. This is mainly due to the limitations of standard field monitoring equipment and the high cost of data collection. Quantitative data from large-scale investigations conducted under controlled "field-like" conditions (non-homogenous and three-dimensional), but which have detailed characterization of the DNAPL distribution remain scarce. The following conceptional spill and remediation scenario illustrates how the lack of understanding of air flow and mass removal can seriously limit our ability to predict SVE performance in field settings.

Conceptual Spill and Remediation by Soil Vapor Extraction

If a DNAPL such as tetrachloroethylene (PCE) is released from a point source at or near the surface (e.g. from a drum, pipe-line or underground storage tank), it will generally migrate downward through the vadose zone. Heterogeneities in the structure of the porous medium and spatially-variable water content will cause movement to be erratic. After the release has stopped, the DNAPL may become distributed in the medium as residual or become trapped above a low permeability lenses as connected-phase pools with high DNAPL saturations. Water saturations in the DNAPL pool areas may also be high, since infiltrating water may also become trapped by the capillary barrier (Figure 1.3). Our current understanding of the processes suggests that frequently a large percentage of the released DNAPL mass will end up as pools in high-water-content areas.

Installation of monitoring devices for soil, vapor and groundwater sampling in the vicinity of the release are generally some of the first activities conducted at a site. The drilling logs from a site such as the one shown in Figure 1.3 might indicate zones of

sands and gravels with continuous and discontinuous layers of silt/clay. Soil gas samples might indicate high vapor concentrations throughout the region. However, soil samples from such a site will frequently indicate very low contaminant concentrations due to the highly-irregular distribution of the DNAPLs. Groundwater concentrations are also likely to be low. If the DNAPL is volatile and a vadoze zone is present, then soil vapor concentrations are likely to be high.

If the unsaturated zone contains a significant volume of DNAPL, or if the vapors pose a risk to groundwater or human health, soil vapor extraction (SVE) is frequently used to reduce that risk. Most vapor extraction systems consist of one or more extraction wells connected to an extraction blower and an off-gas treatment system. Frequently, when the SVE operation is started-up, the initial concentrations are quite high, but drop rapidly to a small fraction of the initial concentrations within a matter of days to weeks. The high concentration period is followed by a prolonged period where concentrations remain quite low but steady. This latter stage is generally thought to be a result of mass transfer limited transport of the DNAPLs to the gas phase.

To assess SVE performance, subsurface vacuum measurements are frequently used to characterize the "radius of influence" of the SVE system. A frequently-used rule of thumb is that the radius of influence is the region in which subsurface vacuums are greater than one inch of water. However, this measure tells little about the volume of air that is flowing through the affected region.

Frequently, some effort is made to maximize either the off-gas concentrations or the mass removal rate. To increase the average off-gas cncentration, the SVE system can be pulsed. With each pulse cycle, elevated concentrations may be observed for a short period, however, they usually drop off quickly to previous low levels. As a result, total mass removed during pulsing is generally lower than for continuous SVE. Mass removal rate can sometimes be increased by increasing the flow rate/vacuum of the extraction system. The increase in mass removal may be due either to increased air flow within the region of influence and/or an expanded radius of influence. Generally, no additional measures are taken to assess the details of air flow within the system.

EXPERIMENTAL OBJECTIVES AND TASKS

The primary objectives of the research presented here were to examine the movement of a DNAPL in an a well-characterized heterogeneous porous medium and to identify and quantify the factors which control mass removal by SVE of the DNAPL from the medium. Tetrachloroethylene (PCE) was chosen as a representative DNAPL because it is a common subsurface contaminant and its physical and chemical properties are well known. Experiments were conducted in an 8.3 x 8.3 x 2.9 m deep physical model made up of layers of sand, gravel, silica flour and bentonite. The water table was positioned near the bottom such that the model included a tension saturated capillary fringe and transition zone. To meet the objectives of this research three major tasks were completed.

DNAPL release experiments

Approximately 200 liters of PCE were released at a constant rate from near the surface of the physical model. Movement of the PCE was tracked using a down-hole video camera and a neutron moisture probe (NP). The down-hole video camera enabled direct observation of the lateral and vertical extend of the pools as well as qualitative assessment of pore-scale distributions. The NP was calibrated for chlorine content and measurements from the physical model are presented as %PCE content. Since both sampling techniques are non-destructive the migration of the spill was tracked as a function of time. The final DNAPL distribution in the physical model was determined by the non-destructive techniques as well as soil cores. These experiments are discussed in Chapter 2.

SVE experiments

Mass removal by conventional SVE (i.e. low soil vacuum, high air flow) was examined initially and continued until mass recovery was very low. Subsequently, mass recovery using enhanced SVE (high-vacuum extraction from drive points and air injection into the drive points) was examined. Air flow rates during conventional SVE were

examined using tracer tests and numerical modeling. Mass transfer limitations due to diffusion were evaluated using a one-dimensional diffusion model. These experiments are described in Chapter 3.

Numerical modeling

The numerical modeling was conducted in four phases:

1) The movement and final distribution of the PCE was simulated using a three-dimensional, three-phase numerical model. All input parameters were determined independently (i.e., with no fitting of simulated to observed results). Model sensitivity to the measured input parameters was performed. These experiments are discussed in Chapter 4.

2) Air flow during SVE was simulated using a two-dimensional, two-phase (air and water) model. A leakage term was included (and fitted) to describe the air leakage from the surface observed in the physical model. These experiments are discussed in Chapter 3.

3) Mass transfer of DNAPL from the high-water-content pool areas to the region of flowing air was modeled with a one-dimensional, variable water content diffusion model. This is discussed in Chapter 3.

4) Air flow and PCE movement simulations described above were used to define the air flow and initial NAPL distribution for the simulation of mass removal by SVE. The results of these simulations are discussed in Chapter 4.

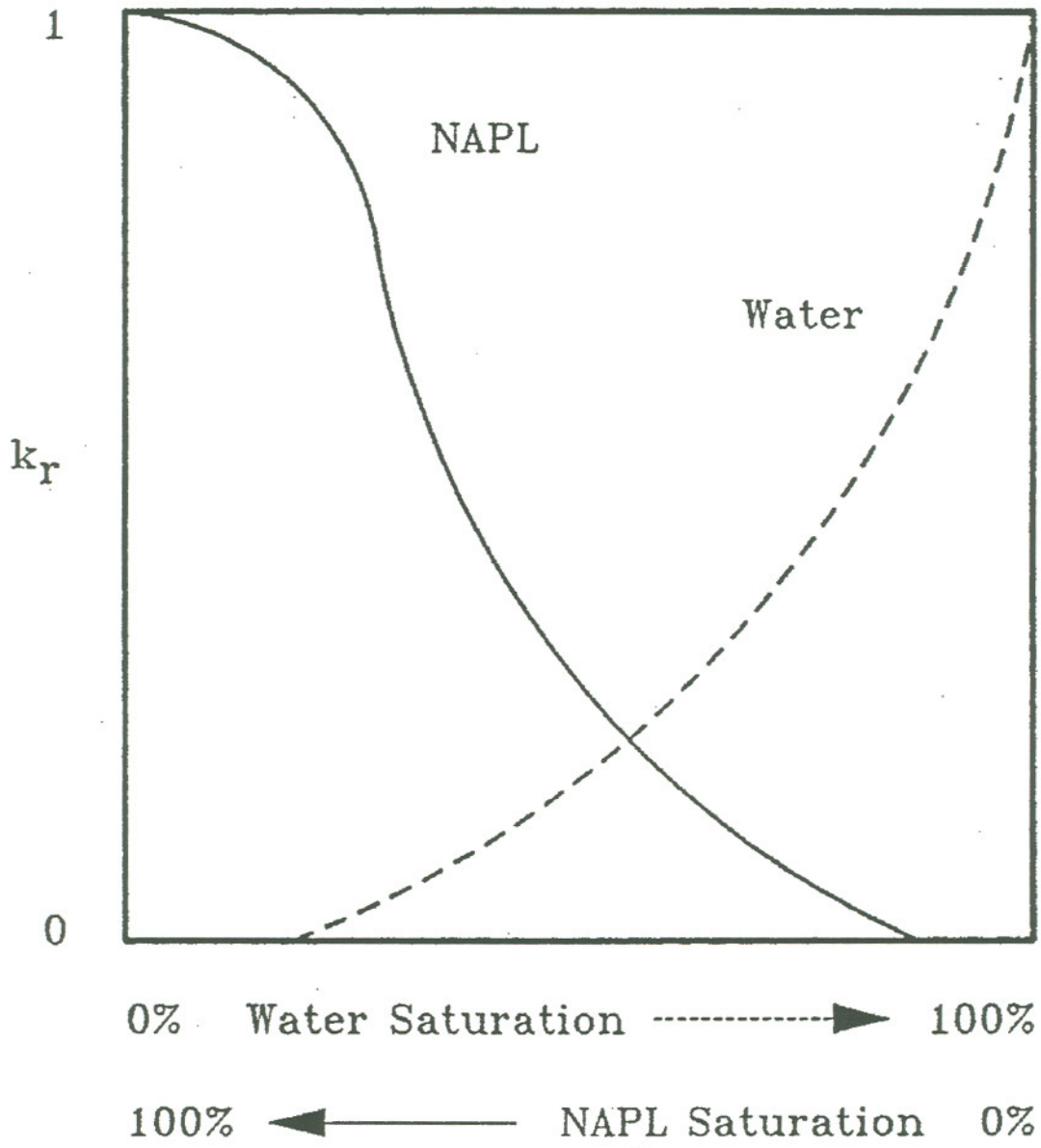

Figure 1.1 Relative permeability curves for two-phase flow (van Dam, 1967).

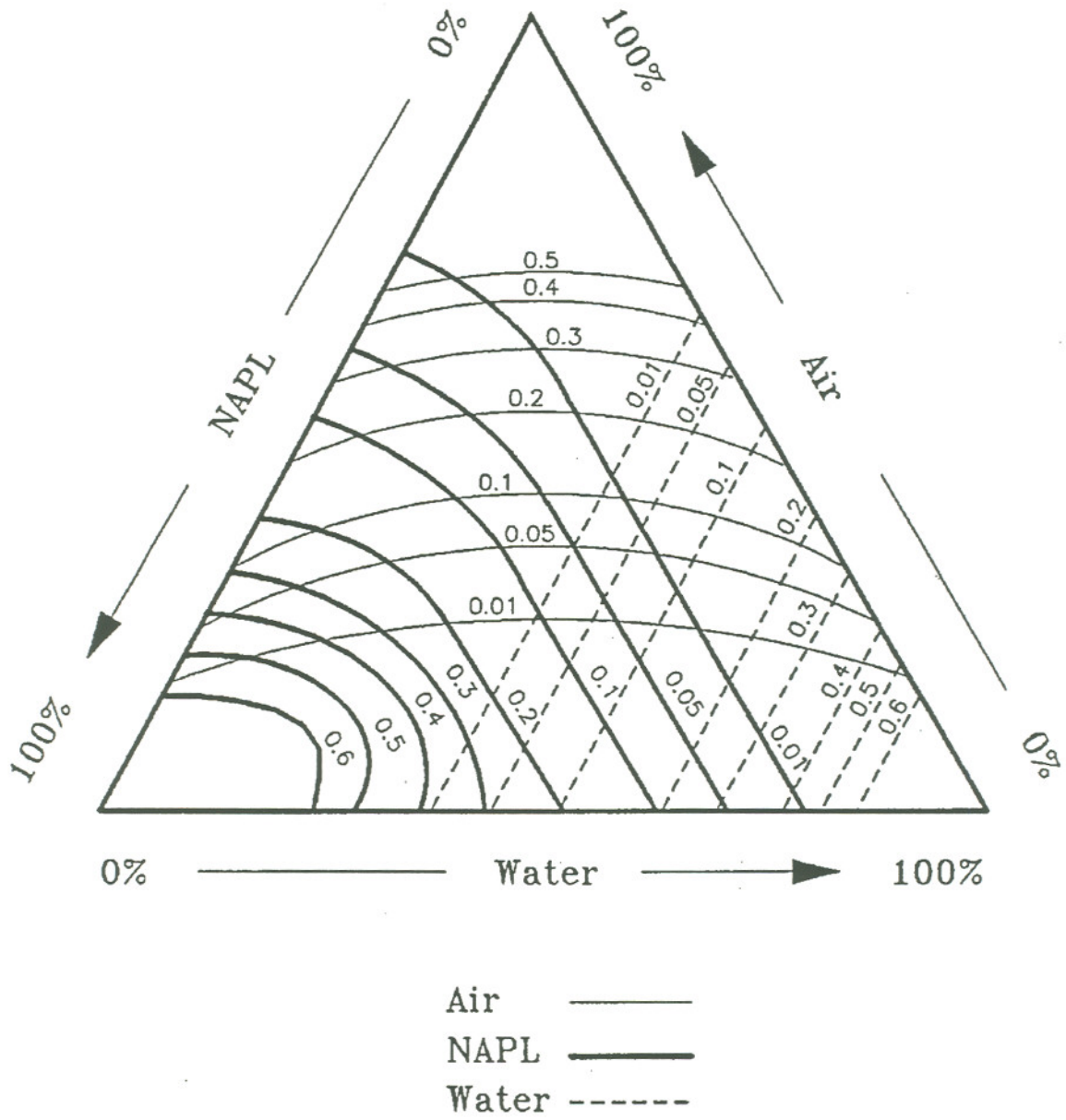

Figure 1.2 Relative permeability curves for three-phase flow (van Dam, 1967).

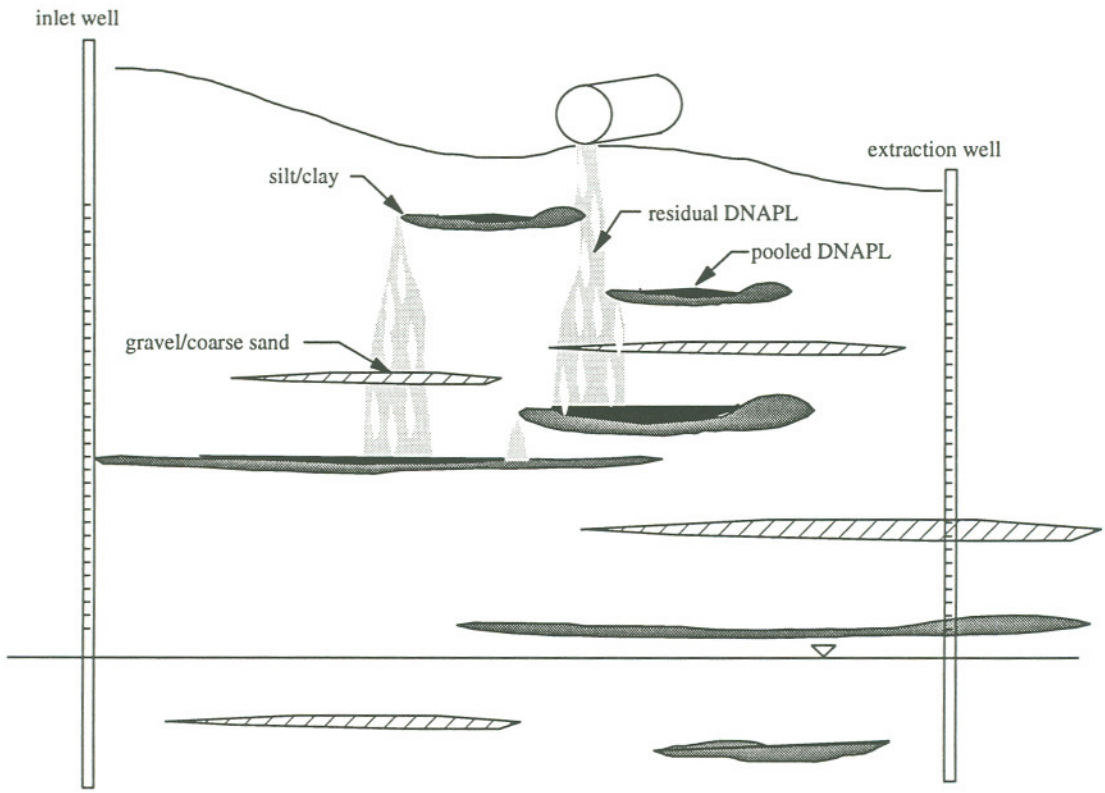

Figure 1.3 Schematic drawing of a DNAPL spill into a heterogeneous porous medium.

REFERENCES

Kueper, B.H. and E.O Frind, Two-phase flow in heterogeneous porous media 2. model application, *Water Resour. Res., 27(2)*, 1059-1070, 1992.

Poulsen, M.M. and B.H. Kueper, A field experiment to study the behavior of tetrachloroethylene in unsaturated porous media, *Environ. Sci. Technol., 25(5)*, 889-895, 1992.

Schwille, F., *Dense Chlorinated Solvents in Porous and Fractured Media*, Chelsea, MI, Lewis, 1988.

van Dam, J., The migration of hydrocarbons in a water-bearing stratum, *The Joint Problems of Oil and Water Industries*, London, The Institute of Petroleum, 55-96, 1967.

CHAPTER 2

CHARACTERIZATION OF A DNAPL RELEASE INTO A HETEROGENEOUS POROUS MEDIUM

INTRODUCTION

In recent years, contamination of groundwater by dense, non-aqueous phase liquids (DNAPLs) has become a common and widely recognized problem. The most frequently cited group of DNAPL contaminants are the chlorinated solvents. Although considered immiscible, their solubilities in water are sufficient to produce dissolved phase concentrations which are several orders of magnitude above their current regulatory drinking water limits. The chlorinated solvents are typically more dense and less viscous than water and are therefore highly mobile as separate phase liquids in both saturated and unsaturated systems.

The movement of DNAPL through a porous medium is controlled by the wetting properties of the DNAPL / aquifer system, the interfacial tension and viscosity of the DNAPL, and gravity (Schwille, 1988). Following a finite volume release, a DNAPL will move through the aquifer until it exhausts itself in the form of isolated ganglia (often called "residual") and/or connected-phase pools. Pools are zones of DNAPL that have been immobilized by a capillary barrier, such as a zone of lower permeability. Capillary forces in a porous media system cause migrating DNAPLs to be quite sensitive to porous media heterogeneity. The final distribution of DNAPL will depend on several factors including: intrinsic permeability distribution; bedding structure of the aquifer; water content distribution; DNAPL fluid properties and the manner, rate and location at which

the DNAPL was introduced.

DNAPL movement has been examined in physical models by a number of researchers. Schwille (1988) used both homogeneous and layered porous media in idealized physical models to illustrate the basic principles governing the spreading of DNAPLs in the subsurface. He found that DNAPLs infiltrated into a dry porous media faster than water due to their lower viscosities. The capillary fringe obstructed entry of the DNAPL into the saturated zone until sufficient pressure developed to displace water. However, permeable aquifers (permeability [k] > 10^{-7} cm^2) were penetrated quickly when the infiltration rate was adequate, and spreading occurred on the bottom of the aquifer model.

Kueper *et al.* (1989) used four well sorted sands (permeabilities of 8.19 x 10^{-8} cm^2 to 5.04 x 10^{-6} cm^2) arranged in a block pattern in a parallel-plate cell to study the effects of porous media heterogeneity on the movement of tetrachloroethylene (PCE) through a water saturated system. PCE was found to flow laterally and cascade off lenses of higher fluid entry pressures. Pooling on the higher entry pressure media led to an increase in the non-wetting (DNAPL) phase saturation. Penetration of the lower permeability lens occurred only if the required capillary pressure was generated. PCE movement in their experiments was dominated by the structure of the sands. Considering the small differences in permeability and displacement pressure between the sands, it is evident that small differences in the capillary characteristics of a porous medium can bring about significant lateral flow of the non-wetting fluid.

Poulsen and Kueper (1992) conducted a study in which two releases of PCE into a naturally deposited unsaturated sandy aquifer were performed. The first release involved the infiltration of 6 L of liquid PCE under ponded conditions over a period of 90 sec, while the second involved a slow release of 6 L of PCE over 100 min. In both cases, migration was dominated primarily by capillary forces as evidenced by PCE migration parallel to the bedding structure of the sands. This was most pronounced in the slow-release where the migrating PCE followed exactly the shift in strike and dip of the strata. The slow-release was found to have migrated ~3.2 m deep. This was 1.2 m deeper than the ponded release. Detailed excavation and sampling of each release revealed an extremely heterogeneous distribution of residual PCE at the millimeter scale.

Detailed measurement of permeabilities and capillary pressure-saturation relationships revealed variations of these properties at the same scale, however, permeabilities of adjacent lamina differed on average by only a factor of 1.7.

In the research reported here, liquid-phase PCE was released into a large three-dimensional layered physical model. The model was composed of layers of clay, sand, and gravel. Movement of the PCE was tracked using a down-hole video camera and a neutron moisture probe (NP). The down-hole video camera enabled direct observation of the lateral and vertical extent of the pools as well as qualitative assessment of pore-scale distributions. The NP was calibrated for chlorine content allowing measurements from the physical model to be presented as %PCE content. Since both sampling techniques are non-destructive, the migration of the spill was tracked as a function of time. The final PCE distribution in the physical model was determined by the non-destructive techniques as well as confirmed with soil cores.

Characterization of the migration and final distribution of PCE are part of a larger project to examine the effectiveness of soil vapor extraction (SVE) of DNAPL-contaminated soils. The well-characterized structure of the model and the PCE distribution data reported here are ideally suited for controlled SVE experiments and simulation using numerical models (Allan and Johnson, 1995; Allan *et al.*, 1995).

MATERIALS AND METHODS

Physical Model

The physical model was constructed in an 8.4 x 8.4 x 2.9 m deep cell. The cell is made of an inner steel bunker with secondary containment provided by an outer concrete bunker. A 0.15 m annular space between the steel and concrete bunkers was filled with pea gravel. The water level in the annular space remained above the water level inside the model to create an inward hydraulic gradient in the event of failure of the inner steel bunker. Prior to filling the model a number of monitoring devices and wells (described below) were placed in the model.

The aquifer consists of complete layers of sand, pea gravel and clay, and a half-

layer of silica flour (Figure 2.1). The sand is washed medium Columbia river sand, with a porosity of 0.37 and k ~5 x 10^{-11} m^2. Grain size fractions are shown Table 2.1 (MacPherson, 1991). The capillary pressure-water saturation relationship for an air/water system are shown in Figure 2.2. The gravel is a uniform 5 mm pea gravel with a porosity of 0.36 and a k of ~2 x 10^{-7} m^2. The sand and gravel were placed into the model in shallow lifts and were manually smoothed before the next porous media type was overlaid. To maximize soil compaction, the water level was kept approximately 0.5 m below the porous medium surface while the model was being filled. The surfaces of the silica flour and clay were sloped slightly towards the center of the cell to prevent drainage of PCE towards the walls during the solvent release. Before the silica flour was overlaid with sand, the surface was watered with a fine mist to solidify the powder and create a more discrete interface with the overlying sand. The silica flour (Sil-Co-Sil, U.S. Silica, Ottawa, IL) and clay (C/S granular, American Colloid Company, Arlington Heights, IL) have low permeabilities ($k < 1 \times 10^{-13}$ m^2).

To contain vapors and reduce rainwater infiltration, the top sand layer was covered with a 0.37 mm vinyl sheet which was overlain with 0.1 m of sand. Twenty-four fully-screened wells were evenly spaced around the perimeter of the cell before the cell was filled. These provided access for monitoring and controlling the water level over the course of the study. Prior to initiation of the PCE spill, the aquifer was filled with water and drained to establish a water content profile under drainage conditions. The water level remained at the lower clay/sand interface for the duration of the study.

Solvent and Release Configuration

The tetrachloroethylene (PCE) used was industrial grade (99.0% min.) with a reported density of 1.62 kg/L (J.T. Baker, VWR Scientific), a solubility of 150 mg/l (Horvath, 1982), a vapor pressure of 2.48 kPa (MacKay and Shui, 1981) and a dynamic viscosity of 0.90 cP (Schwille, 1988). Prior to release, ~0.01 g/L of water-insoluble fluorescent dye (Coumarin 7, Eastman Kodak; Rochester, NY) was added to the PCE. This concentration enabled visual observation of PCE in the sand by a down-hole video camera (described in the next section).

A "source-zone" was created using a 0.1 m diameter tube inserted to a depth of 0.05m below the vinyl sheet (Figure 2.1). The tube was backfilled with sand to the level of the existing ground surface and PCE was delivered to the source zone through a 6 mm copper tube inserted just below the surface. A peristaltic pump supply PCE to the source zone at a nominal rate of 1 x 10^{-6} m^3/s. The duration of the spill was 50 hours, during which a total of 200 L of PCE was released. This rate was chosen so that several cycles of monitoring could be completed during the period of release and subsequent migration. This rate was similar to the slower release rate used by Poulsen and Kueper (1992).

Monitoring Equipment

During the solvent release and migration period, a down-hole video camera (Bartz Technology Co., Santa Barbara, CA) was used to directly observe PCE in the vicinity of the 10 observation tubes. Locations of the tubes are shown in Figure 2.3. Each observation tube was 2.3 m in length and fabricated from 0.05 m inside diameter (ID) PVC pipe with sections of 0.05 m ID glass tube inserted at specific depths where the PCE was expected to accumulate (Figure 2.1). The bottom 0.7 m of the observation tubes were glass and were sealed at the bottom. The tubes extended from the clay up through the lower sand layer to the gravel (Figure 2.1). In the observation tubes that penetrated the silica flour lens (observation tubes A, B and C) a second 0.5 m long glass section spanned the silica flour/sand interface. The glass and PVC tubes were connected by PVC couplings and sealed with a commercial grade silicon caulk. The tubes were placed into the model before it was filled with porous media to ensure that the soil was in contact with the glass.

The down-hole video-camera was equipped with both ultraviolet (UV) and incandescent light sources and has a resolution of approximately 50 microns. The viewing area of the camera was ~0.0125 x 0.02 m. The UV light source enabled visualization of the fluorescent dye added to the PCE and the incandescent light provided information on the structure of the porous media. During each monitoring period the camera was lowered to the bottom of the observation tube by an operator. A second operator observed and focused the camera using a video monitor. The video camera was

rotated 360° at each 0.0125 cm depth increment with alternating UV and incandescent light sources. Each session was recorded on video with audio commentary on location, depth and time.

Neutron Probe - Theory and Method

A CPN 503DR Hydroprobe (CPN Corp., Martinez, CA) (NP) was used to measure the water content profile before the spill, as well as PCE content during and after the spill. The NP consists of a source of fast (high energy) neutrons and a detector of slow neutrons. The neutron moderation process is dominated by neutron-hydrogen collisions. When a fast neutron collides with a relatively heavy soil atom, very little loss of velocity results; however, collisions with hydrogen atoms (of approximately equal mass) result in appreciable neutron slowing. Water is nearly always the greatest source of hydrogen in geological materials. Therefore, as dry soil is wetted, the detector will measure an increase in slowed neutrons.

Some atomic elements have the ability to absorb slowed neutrons. Of the elements present in soil systems chlorine and boron have the highest cross-sections for slowed neutrons absorption. Therefore, a high chlorine or boron content may result in reduced neutron counts at the detector. Schneider and Greenhouse (1992) reported a significant decrease in neutron counts resulting from the chlorine present in liquid PCE in a saturated groundwater system. Because the continuous normal approximation of a poisson distribution can be used to approximate the population from which neutron measurements were made (Kramer *et al.*, 1992), the significance of changes in neutron probe measurements (caused by the presence of chlorine in PCE) may be inferred from statistical analysis. The experimental design enabled monitoring of PCE migration and estimation of final PCE saturations using NP results.

Neutron probe measurements were made at 0.1 m intervals in the 10 glass/PVC observation tubes. Various well materials have a masking effect on the neutron measurements of the soil, the degree of masking varies depending on the type of well material (Keller *et al.*, 1990). To account for this difference, the measurements made in the PVC portions of the wells were adjusted by an independently determined calibration

factor. Although the zones of interest (*i.e.*, the zones of PCE accumulation) were in the depths spanned by glass, measurements made in the PVC sections were adjusted so that the results over the entire aquifer depth could be analyzed simultaneously.

Neutron Probe - Water Content Calibration

To calibrate the neutron probe for water content, a 0.6 m diameter by 3 m tall column was constructed. The column was filled with layers of clay, sand, gravel and silica flour in the same structured manner as the physical model. A 0.05 m diameter glass/PVC observation tube and 0.025 m drainage well (similar to those in the physical model) were placed in the column before it was packed with soil. The column was imbibed with water and drained, and the water level positioned at the clay/sand interface. NP measurements were made at 0.05 m intervals under saturated and drained conditions. Horizontal soil cores were collected at 0.07 m intervals along the length of the column under drainage conditions. The water content of the each sample was calculated from the original weight and dry weight (oven dried for 24 hours at 105 °C).

Calibration using the large column was complicated by the fact that the radius of influence (R_i) of the neutron probe was greater that the diameter of the column. Silvestri *et al.* (1991) summarized the findings of Nylan (1983) and determined that the measured R_i varied with water content as well as soil type. For sand, average R_i's of 0.22, 0.24, 0.21 and 0.14 m corresponded to volumetric water content of 4.6, 9.5, 12.7 and 32%. The R_i's of moist sand, moist clay and pure water were 0.15 m, 0.13 m, and 0.08 m respectively. The column design used in this study provided a 0.20 m radius of soil around the observation tube. Based on Silvestri *et al.* (1991) this size should have been sufficiently large for preventing the influence of the column walls on measurements. However, counts for saturated sand in the column were ~10% lower than measured counts for the sand in the physical model, indicating the possibility of wall effects.

Neutron Probe - Chlorine Calibration

Laboratory calibrations to determine the neutron response to chlorine were

performed in a 0.87 m x 0.57 m diameter (55-gallon) drum packed with sand. A glass access tube was placed in the center. The drum was slowly imbibed with water to minimize entrapped air, and water was recirculated up through the drum from a constant head reservoir. Chlorine (Cl) in the form of NaCl was dissolved in the reservoir and 5 pore volumes were recirculated through the calibration drum over a 24 hour period after each addition of NaCl. The Cl concentration was estimated from resistivity measurements in the recirculation reservoir using a resistivity meter (YSI Scientific, model 33, Yellow Springs, OH) calibrated for NaCl concentrations of 0 to 300 g/L. NaCl concentrations in water were converted to equivalent moles of Cl as PCE and reported as the equivalent volumetric fraction of PCE occupying the pore space. NP measurements were made in the calibration drum at 6 different Cl concentrations (Figure 2.4). A linear regression of the calibration results showed a good correlation ($R^2 = 0.97$) between the NP response and chlorine content. (The regression constant was equal to the neutron measurement without PCE.) The volume of PCE in the porous medium is estimated by multiplying the change in the NP counts from its background (uncontaminated) value by the calculated calibration factor (-0.0072).

PCE migration was tracked by changes in the NP measurements at the observation tubes. Background, pre-spill values were established from measurements on several consecutive days prior to the release. Detection of PCE was assumed to have occurred if the NP signal dropped by more than 100 counts below background. This criteria was chosen based on the fact that the estimated standard deviation for a poisson distribution is the square root of the mean value. Typical pre-spill neutron probe readings in the areas of later PCE accumulation were ~2500. Therefore, the estimated standard deviation is 50 (*i.e.*, $\sqrt{2500}$) and a 100 count change represents 2 standard deviations away from the background measurement.

Soil Coring and Analysis

Soil cores were collected using a modified version of the coring technique described by Starr and Ingleton (1992). The coring assembly consists of a 3 m long 0.05 m diameter stainless steel outer sleeve, 0.25 m long reusable sampling tubes, a drive head,

and a threaded inner tube connecting the sampling tube to the drive head (Figure 2.5). The outer sleeve is bolted to the drive head, such that the entire assembly is driven as a unit by pushing on the drive head. Cores are collected by advancing the assembly 0.25 m into the subsurface (the length of the sampling tube) using a jack hammer. The outer tube is left in place while the sampling tube is pulled up to the surface by the inner rod. To hold the soil in the sampling tube, a slight vacuum is pulled on the sampling tube while the assembly is lifted to the surface. The sampling tube is replaced with an empty sampling tube for the next sampling interval.

The sampling tubes are equipped with a "plunger mechanism" to extract the soil core from the sampling tube. The core was cut into 0.025 m samples as it was extruded from the tube. Approximately 4 ml from each soil core sample was put into a 40 ml vial with 20 ml of methanol for PCE analysis. The remainder of the sample was placed in a sealed jar for water content analysis. Methanol headspace standards were prepared from serial dilutions of a PCE-methanol stock solution in 45-ml vials equipped with Mininert valves. Analyses were performed using a Hewlett-Packard HP 5890 GC (Hewlett-Packard Co., Avondale, PA) equipped with electron capture and photoionization detectors.

RESULTS AND DISCUSSION

Water Content Profile

The calculated water content profile (from the NP) in the calibration column is presented along with the measured water content in Figure 2.6a. The sand layer above the silica flour and the gravel have drained to approximately residual water saturation and a higher water content capillary fringe is located above water table at the sand/bentonite interface. Because gravel does not provide as much capillary suction, the sand above the gravel did not fully drain to residual. A comparison of the calibrated and measured water content indicate consistent trends, however, the relationship does not remain linear over the entire profile. The deviation is most pronounced in zones with sharp contrasts in water content (i.e. near the tension saturated silica flour / sand interfaces). This is due to the poor vertical resolution of the NP, resulting in measurements being averaged over

low and high water content regions. Water saturation calculated from pre-spill neutron measurements in the physical model are presented in Figure 2.6b. Water saturation measurements from soil cores collected from the physical model are presented in Figure 2.6c. (Soil cores samples were not retained between the lower sand and silica flour.) Because of the difficulty with collecting vertical soil cores in high water content and saturated soil, there is scatter in the physical model soil core water content results. The agreement between NP measurements in the calibration column (Figure 2.6a) and the physical model (Figure 2.6b) support the assumption that the water content profile in the calibration column is an accurate representation of the water content and soil profile in the physical model.

PCE Arrival Time (video & neutron)

The rate and direction of the PCE migration was determined using the downhole video camera and the NP. The depths at which PCE pooled corresponded to the top of the silica flour and clay layers. The lateral extent of the pools as a function of time at those locations was determined from the video and NP data. The data from each observation tube (labelled A through J in Figure 2.7) are summarized for comparison in Table 2.2. Since sampling was not continuous, the time that PCE was first detected is listed first along with the previous sampling time (in parenthesis) at which it was not detected (the true arrival time being sometime between the two). Video and NP results showed very good agreement. The areal extent of the PCE at various times is shown in Figure 2.7.

Time-Series of Neutron Response

Time-series of the NP results at each observation tube are presented in Figure 2.8 (depth is shown on the y-axis and time from the start of spill on the x-axis). The symbols indicate the specific depths and times where measurements were made. The figures were created by interpolating between the data points using the kernel smoothing method (Spyglass, Inc., Champaign, IL). A white background indicates locations and times where

there has been no significant change in the NP data (i.e. no PCE); increasing darkness indicates a decrease in neutron response due to PCE.

At early time (<25h) PCE spread laterally at the silica flour interface (Figure 2.8 C, B and A; 0.7m depth) and ran over the edge of the silica flour. The observation tubes that do not span the silica flour half-layer do not show PCE accumulation at the 0.7m depth. At later time (>25h), PCE migrated downward to the clay interface (2.5m depth) and began spreading laterally. The PCE content at the tubes located closest to the center of the spill (Figure 2.8 C, E, F and G) was greatest and decreased with distance from the center (Figure 2.8 A, D, H and J). This was true at both the silica flour and clay interfaces. In general the PCE content at the clay interface was much greater than that at the silica flour interface.

The length of time between the initial detection of PCE above the clay (2.5 m) and maximum response increased with distance from the center (Figure 2.9). PCE content at the observation tubes closest to the center (tubes C and F) had reached maximum values within 30 hours of initial detection. At the perimeter tubes (A and J), the PCE content continued to increase for 70 to 100 hours following initial detection.

The data indicate that above the silica flour PCE drained to lower saturations after the source was stopped at 50 hours (Figure 2.9a). The highest percent bulk volume (%PCE) measurements at the silica flour interface (0.7 m) were 3.3%, 3.6% and 4.3% at tubes A, B and C respectively. At 360 h the %PCE measurements were 1.8%, 2.1% and 2.3% at the same locations. Neutron measurements at the clay interface (2.55 m) did not show this behavior and remained essentially constant once the maximum response had been reached (Figure 2.9b and 2.9c).

Final Distribution

Estimates of final PCE distribution (90 days after the start of the spill) were made by combining three approaches: the down-hole video camera, the NP and soil cores. Table 2.3 summarizes PCE thickness measured by the video camera at each observation tube and %PCE calculated from the neutron probe results. These results were used to generate thickness and %PCE contours (Figures 2.11 and 2.12).

Four soil cores were collected from below the gravel layer and analyzed for water content (Figure 2.6c) and PCE content (Figure 2.10). The specific volume of each core was calculated by summing the fraction of PCE (by volume) of each sample multiplied by the sample thickness. The average %PCE for each core was calculated by dividing the specific volume by 0.15 m. This adjustment was performed to present PCE content for each core in a manner which was independent of pool thickness. (A thickness of 0.15 m was chosen based on video measurements of pool thickness near the center.) Table 2.4 summarizes PCE thickness, specific volume and % PCE form the soil cores. Thickness and average %PCE data from the soil cores are shown in Figures 2.11 and 2.12.

PCE thickness from the soil cores were consistently higher than those observed by the down-hole video camera. This difference is believed to be due to smearing of PCE during coring. The %PCE data from the NP should be interpreted with caution because of the poor vertical resolution of the instrument. Near the center of the cell, cores and down-hole video results indicate the PCE thickness is 0.15 to 0.25 m. This is on the same order as the vertical resolution of the neutron measurements and should not result in significant averaging over contaminated and uncontaminated regions. The calculated %PCE at tubes C, F (the most centrally located tubes) are 7.8 and 7.3%. This agrees with the average %PCE of 6.8% in the soil core nearest the center (C4). At the tubes near the edges of the pool, where the thickness is as low as 0.025 m (tube A), the %PCE of 3.2 calculated from the NP data presumably represents an average over contaminated and uncontaminated regions.

A mass balance was performed based on knowledge of the pool thickness at each observation tubes from the video, and the average %PCE from the results from both the cores and the neutron probe results. The following assumptions were used to estimate the pool volume: the pool thickness was assumed to be zero at the four corners of the cell, and a thickness of 0.01 m was chosen for a 8.3 m diameter circle about the center of the cell. Using a 6.8% PCE by volume (the high end of the range measured in the cores), 196 L (or 98%) of the original 200 L of PCE was accounted for in the pool. Using 4.8 %PCE (the low end of the range measured in the cores), 90 L (or 55%) was the estimated to be pooled above the clay. The %PCE calculated from the neutron results near the center of the spill range from 5.95% to 7.5% bulk volume; which would result in 86 to

108% of the mass pooled above the clay.

Micro-scale Observations

Figure 2.13a - 2.13d are images taken by the down-hole video camera using ultraviolet light. Each figure represents a 0.0125 m x 0.02 m area of porous medium at the glass observation tube. The black background is uncontamined soil, the lighter zones show the fluorescing dye in the PCE. Figure 2.13a shows PCE pooled above the silica flour (observation tube C, depth ~0.7m, @ 1 hr); the PCE content from the NP measurements was ~3.5%. Figure 2.13b shows residual PCE above the silica flour after drainage had occurred (observation tube A, depth ~0.7m, @ 90 days); PCE content from neutron probe measurements in this observation tube was ~1.8%. Figure 2.13c shows PCE distributed in the tension saturated portion of the capillary fringe region above the clay (observation tube B, @ ~2.5m, @ 90 days). PCE content in this region was ~7.8%. Figure 2.13d shows a high saturation globule of PCE in the variably saturated zone above the clay (observation tube D, @ ~2.4 m, day 12). This type of distribution was commonly observed and is illustrative of the erratic behavior of PCE movement the sand.

At early times, differences in distribution and saturation in the sands above the clay and silica flour were a result of the differences in water content. Near the clay interface (where water content is high) PCE must displace water in order to spread, resulting in preferential flow of PCE into the larger pore spaces (often referred to as "fingering") (Figure 2.13d). Conversely, above the silica flour, where the water content was close to residual saturation, PCE spread laterally due to capillary forces. As a consequence, saturations were lower above the silica flour.

CONCLUSIONS

Two hundred liters of PCE were released into a 8.4 x 8.4 x 2.9 m deep physical model over a period of 50 hours. The model consisted of layers of well characterized sand, gravel, clay and silica flour. The bulk of the model was at residual water content, but included a water table and capillary fringe at the bottom of the model as well as a

tension saturated low permeability lens covering half of the model at a depth of 0.5 m below ground surface.

The migration and final distribution of PCE was monitored by a down-hole video camera and neutron probe. Soil cores were collected at the conclusion of the experiments. Observed movement of PCE during and after the release using the neutron probe and the down-hole video camera showed excellent agreement. PCE reached the bottom of the model within ~26 hours. Nearly all redistribution of PCE occurred within 200 hours. The relatively rapid downward movement has important implications for detecting and limiting DNAPL transport. The data suggests that, in many cases, significant downward migration of DNAPL will have occurred before any preventative action can be initiated.

Neutron data and soil cores showed average PCE saturations of ~7% by volume in the major pool located above the clay layer at the bottom of the model. The thickness of the pool ranged from 0.15 m at the center to 0.06 m at the perimeter observation tubes. Based on the areal PCE distribution, saturation and pool thickness, 80-90% of the mass reached the clay layer at the bottom of the model. Less than 2% of the soil in the physical model contained PCE. Under different conditions the PCE could have penetrated to a significantly greater depth and/or areal extent.

Both video and neutron results showed initial pooling above the tension saturated silica flour lens (3.3 to 4.3 %PCE) followed by drainage to residual saturation (1.8 to 2.3 %PCE) after the source was stopped. There was no evidence to suggest that PCE saturations above the clay decreased after the release was stopped.

Micro-scale down-hole video camera observations showed the distribution of PCE within the sand to be quite erratic. In areas of pooled PCE, many pores were free of PCE while others appeared completely saturated. PCE saturations in zones of lower water content were generally lower than in the capillary fringe, where the water content was high.

Pooling and lateral spreading on the clay layer occurred primarily in the tension saturated zone of the capillary fringe. This has significant implications for remediation by vapor extraction. Due to the high water content in this area, the majority of this pool is relatively inaccessible for volatilization.

These results have been used as initial conditions for a subsequent SVE remediation experiment (Allan and Johnson, 1995) and for numerical modeling of the spill and remediation (Allan *et al.*, 1995).

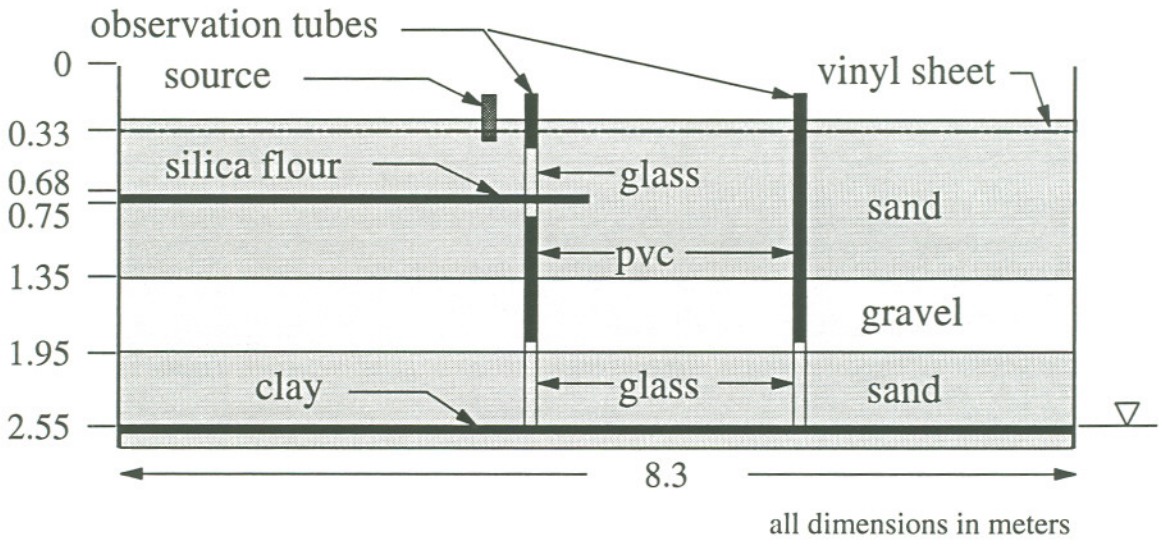

Figure 2.1 Schematic cross-section of the experimental aquifer.

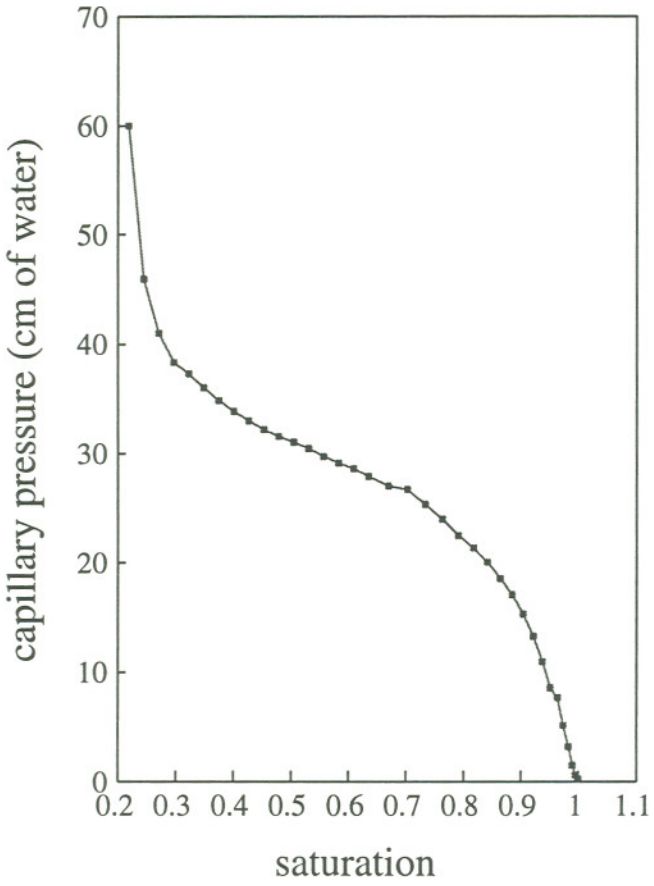

Figure 2.2 Measured air/water capillary pressure-saturation relationship for the sand.

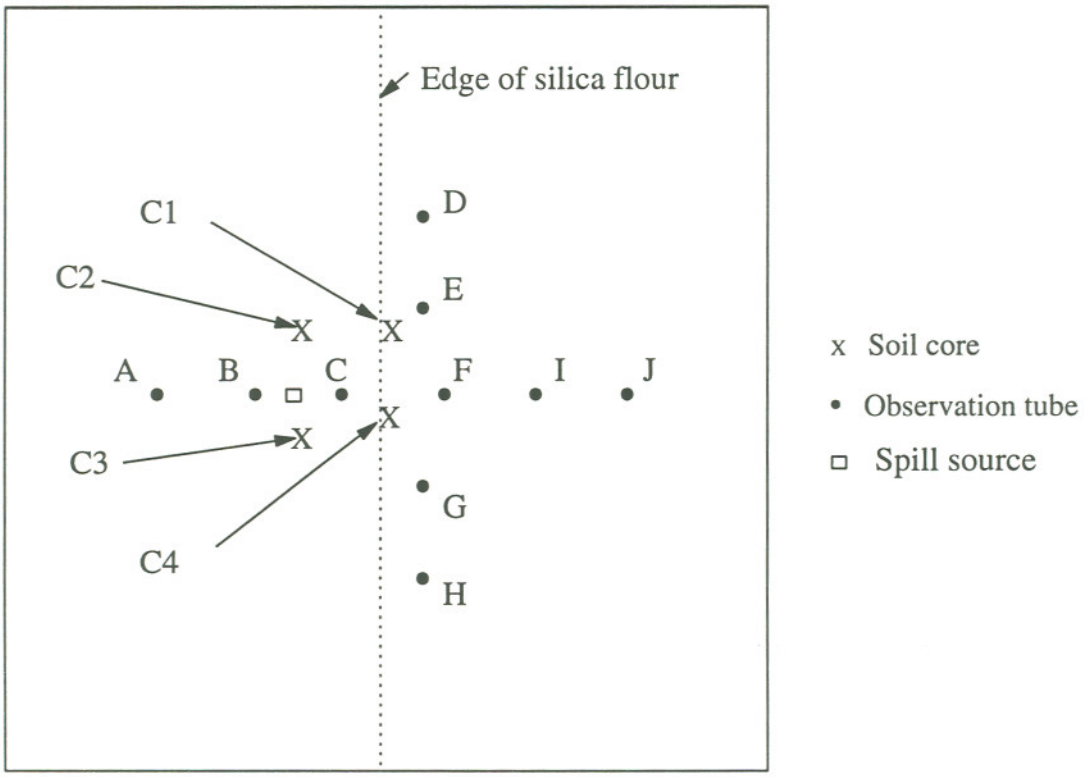

Figure 2.3 Schematic plan view of the physical model showing locations of cores, observation tubes and the spill source.

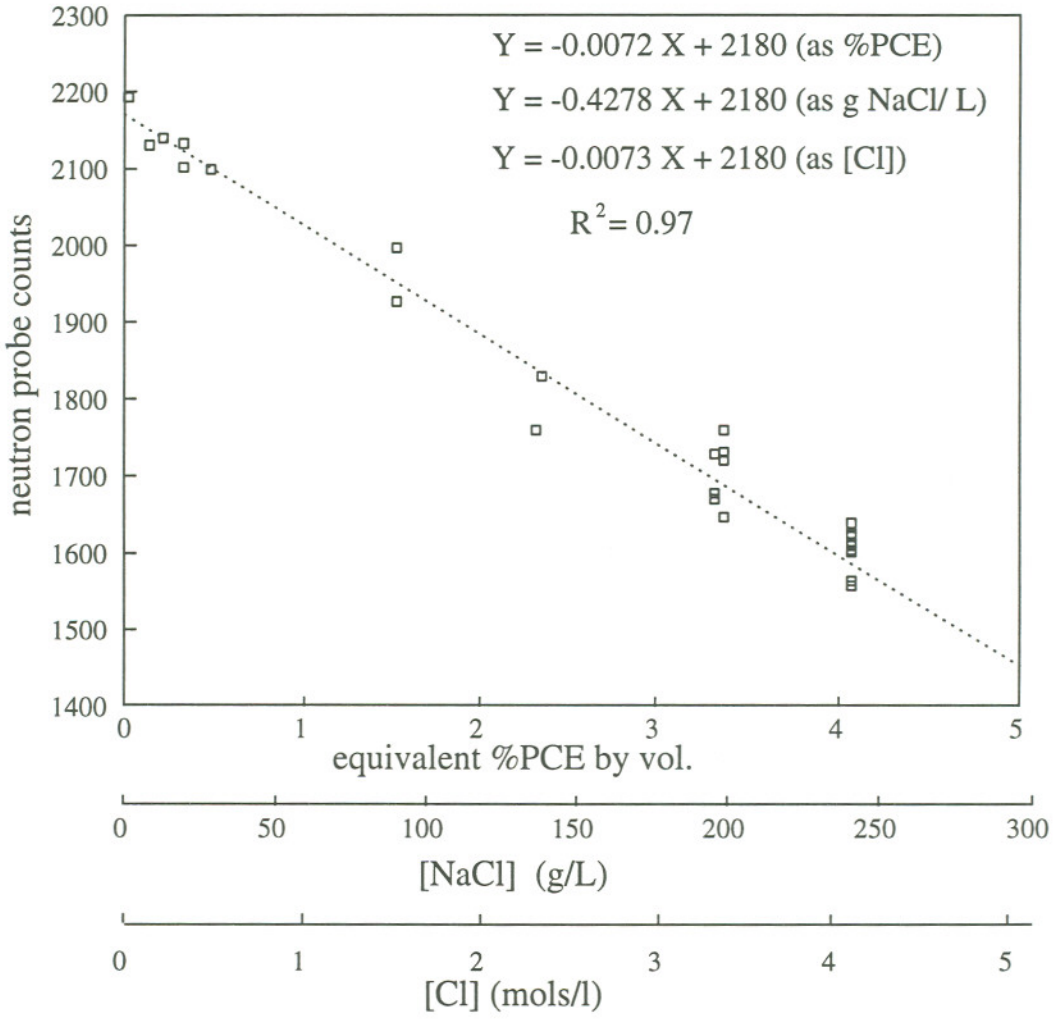

Figure 2.4 Neutron probe calibration curve for chlorine concentration in sand.

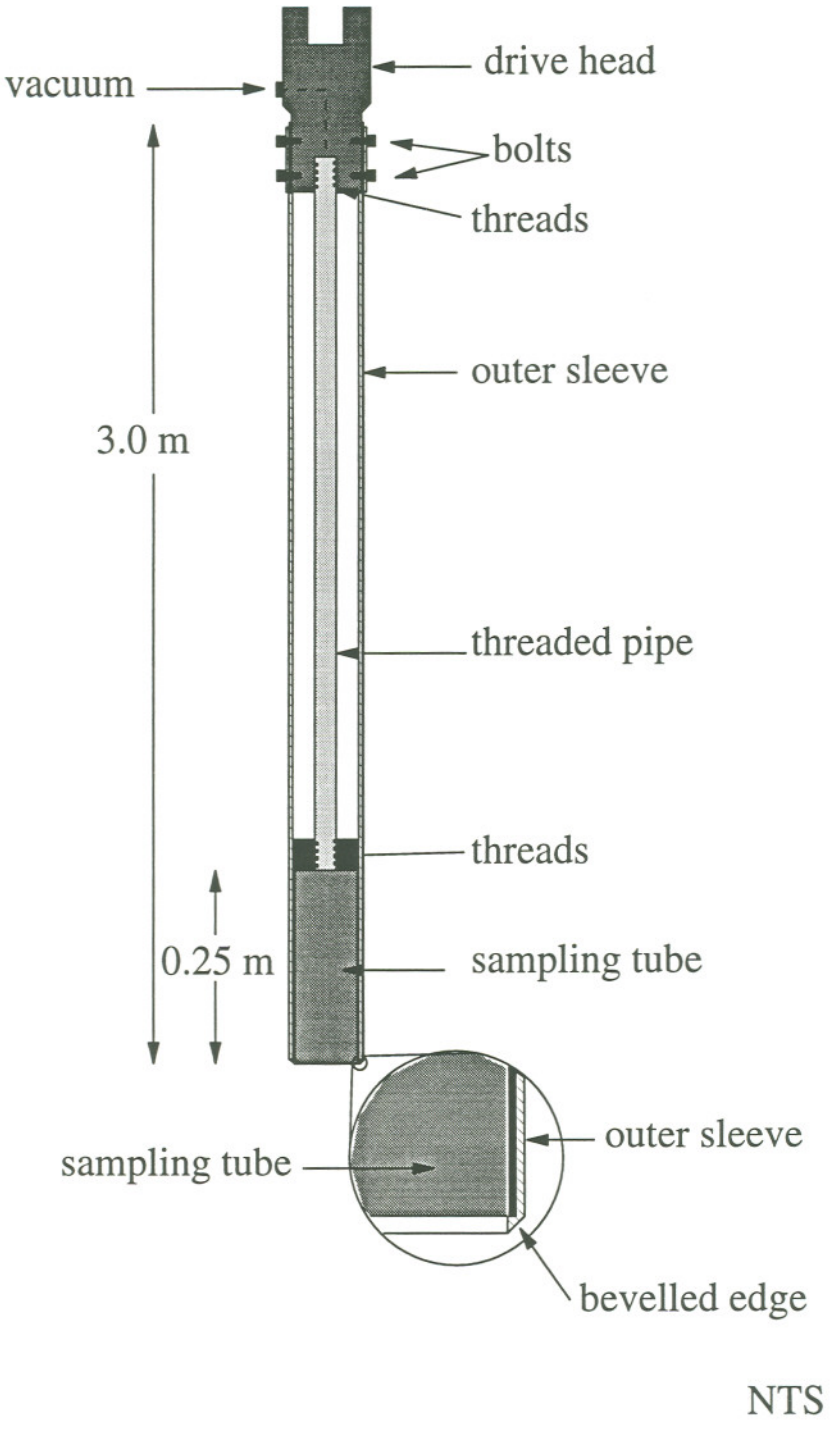

Figure 2.5 Schematic drawing of the apparatus used to collect soil cores.

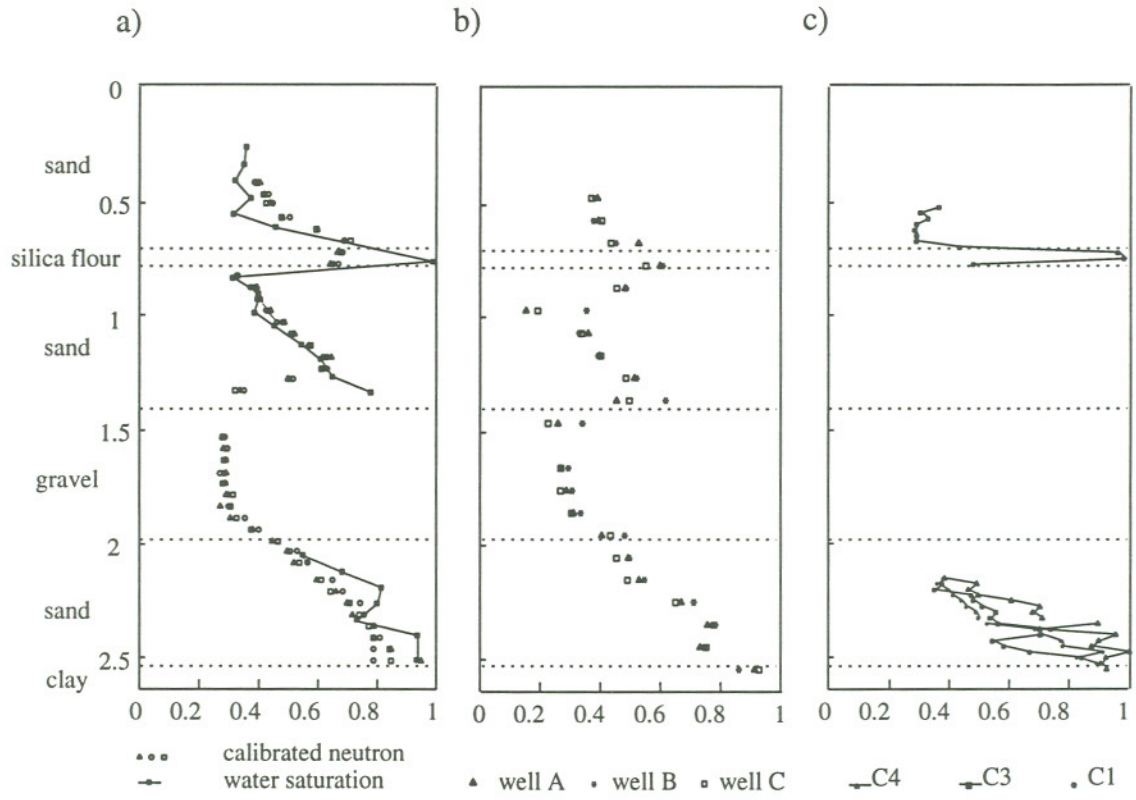

Figure 2.6 Water content profiles: a) calibration column: neutron probe and soil samples; b) physical model: neutron probe; c) physical model: soil cores.

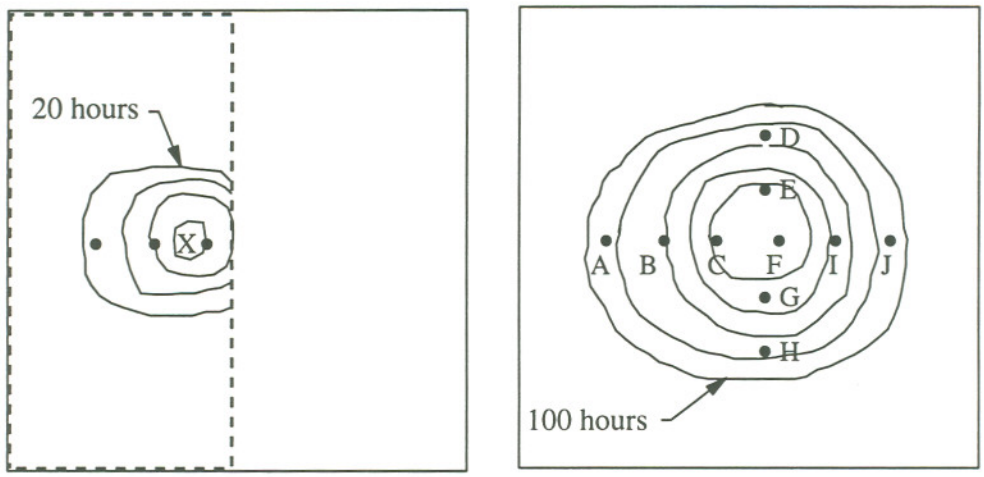

plan view - 0.7m depth
1, 2, 5 and 20 hours

plan view - 2.5m depth
30, 40, 50, 75 and 100 hours

silica flour half-layer

X source

• observation tube

Figure 2.7 Areal PCE distribution at various times as determined by neutron probe and down-hole video.

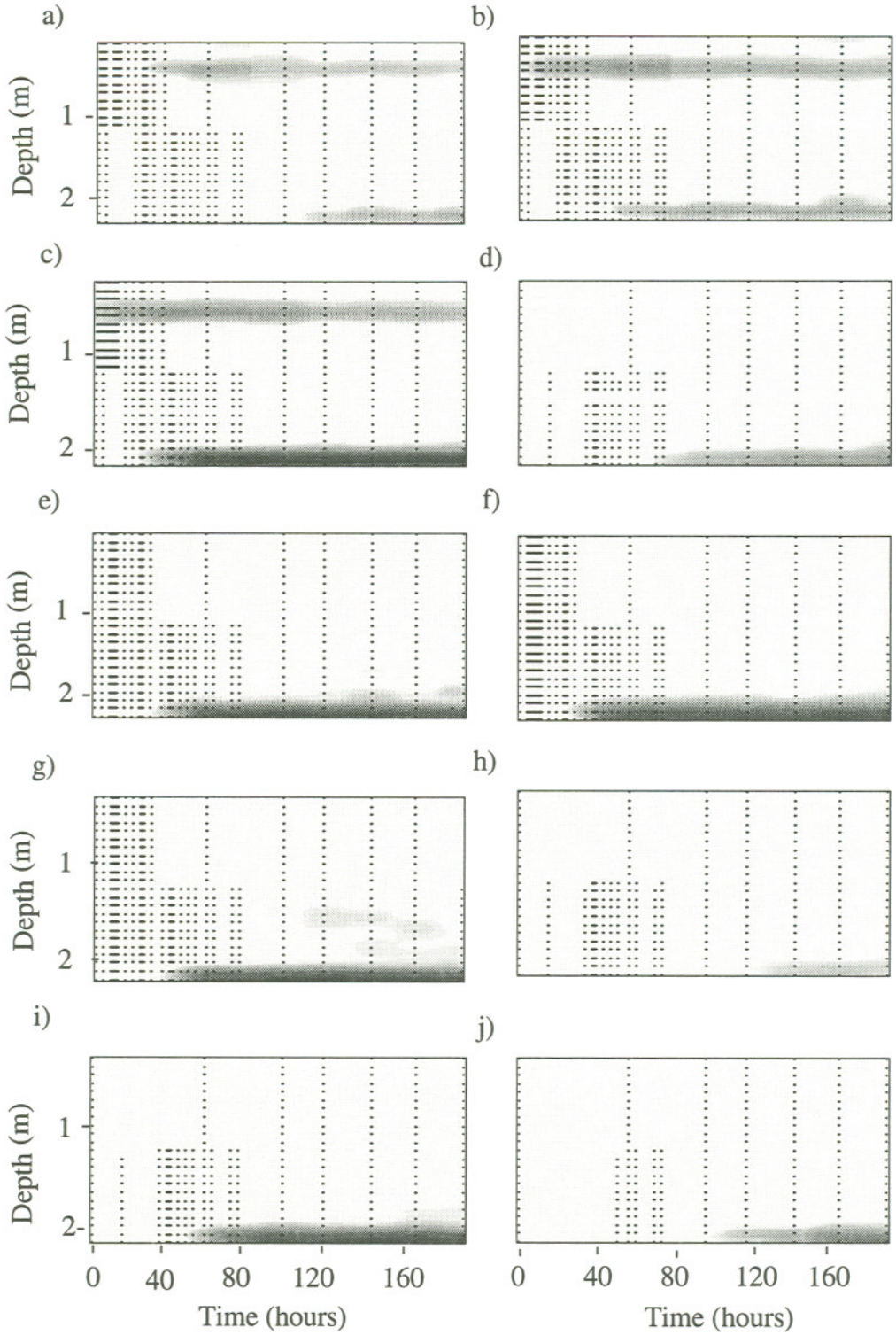

Figure 2.8 Time-series of change in neutron probe response at observation tubes A-J. (Darker shades indicate greater PCE concentrations.)

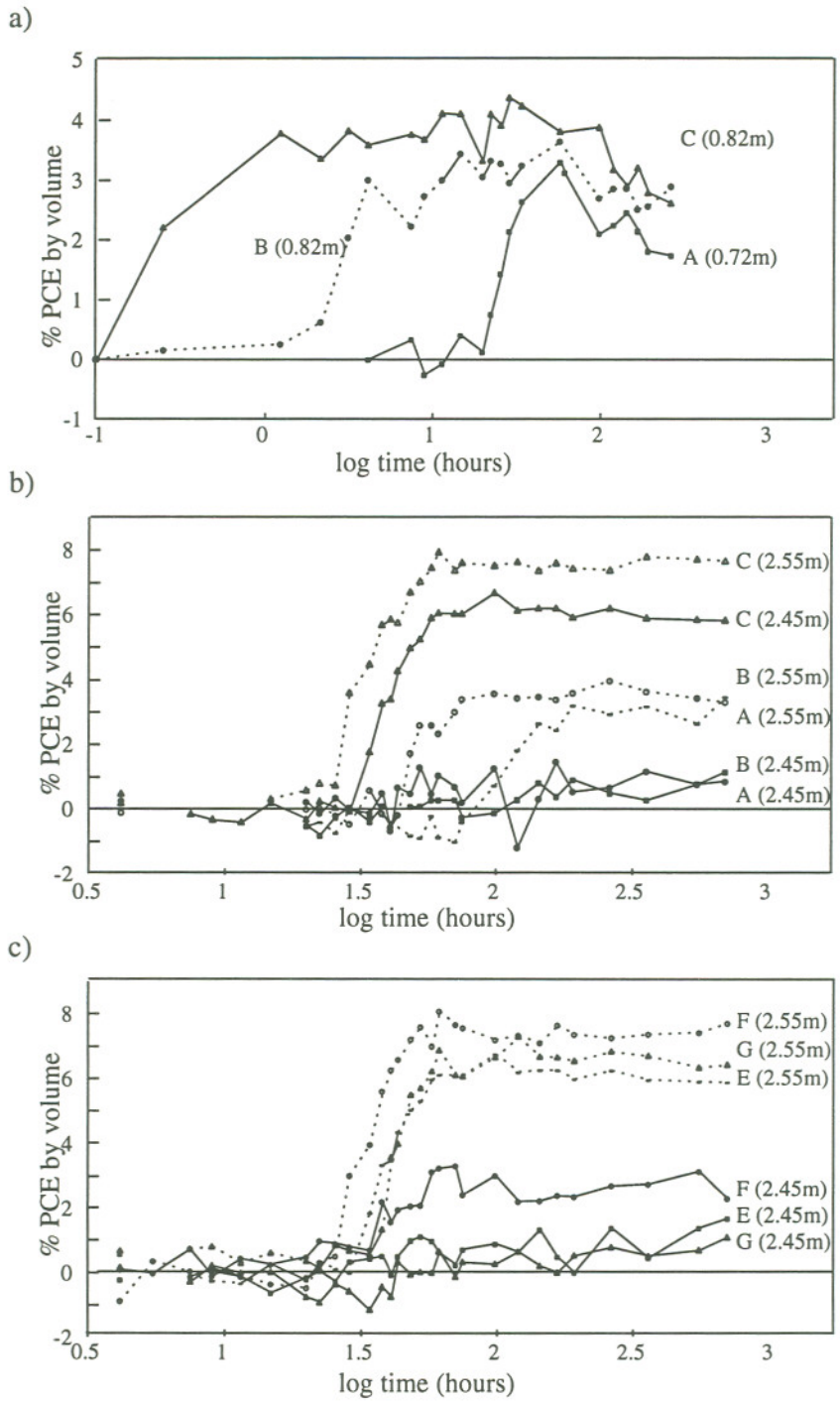

Figure 2.9 Neutron probe time-series data showing: a) pooling and draining off of the silica flour layer; b) and c) pooling and no subsequent draining above the bentonite.

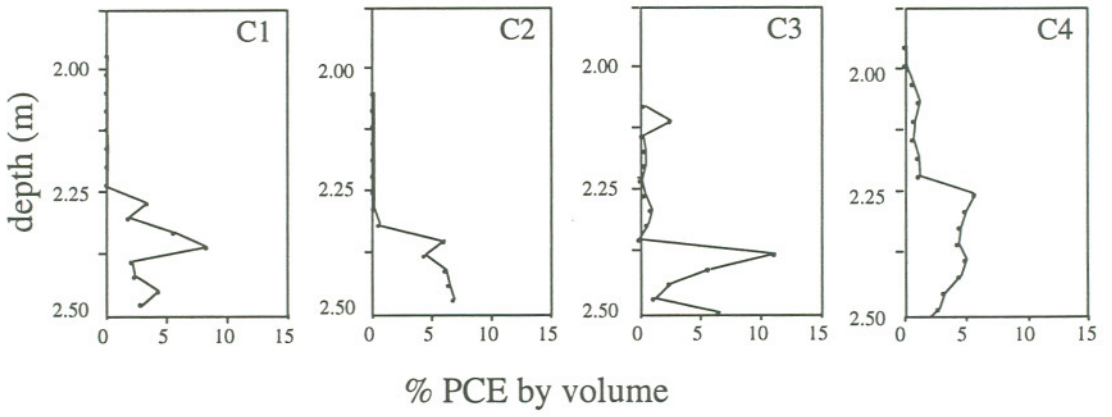

Figure 2.10 PCE content data measured in the soil cores.

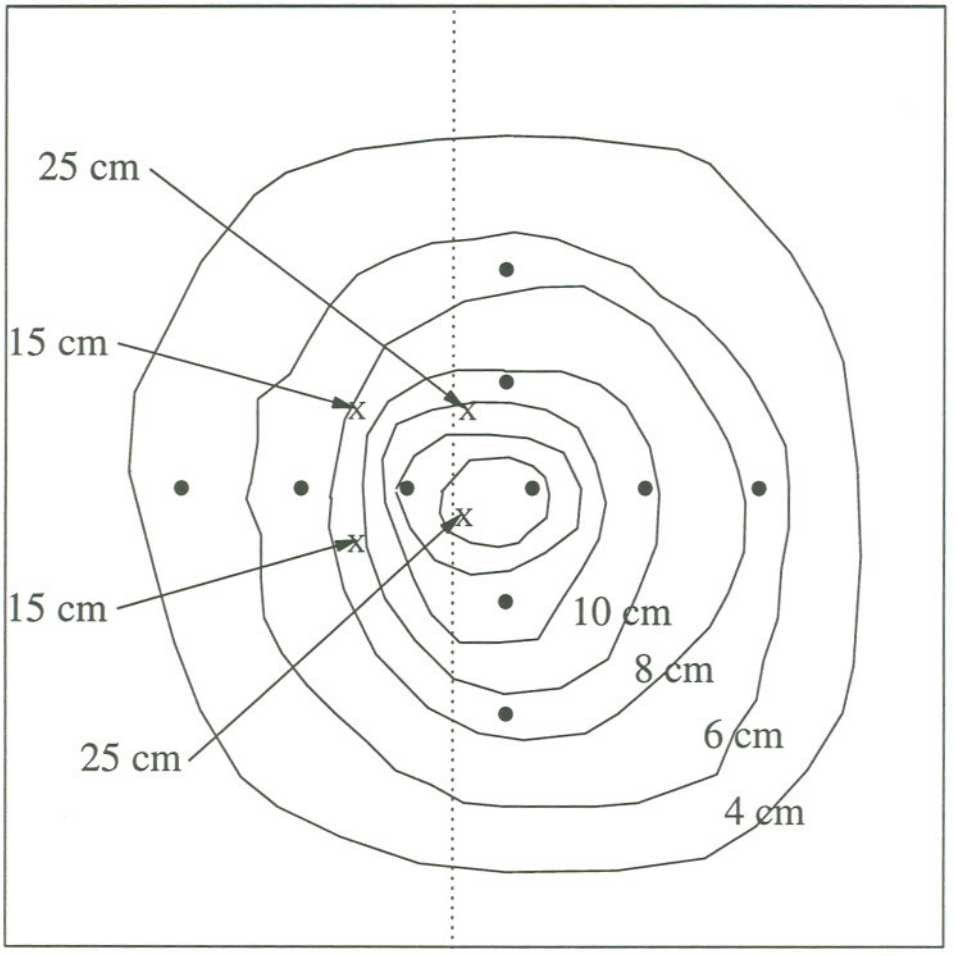

Figure 2.11 Observed PCE pool thickness from the down-hole video and soil cores.

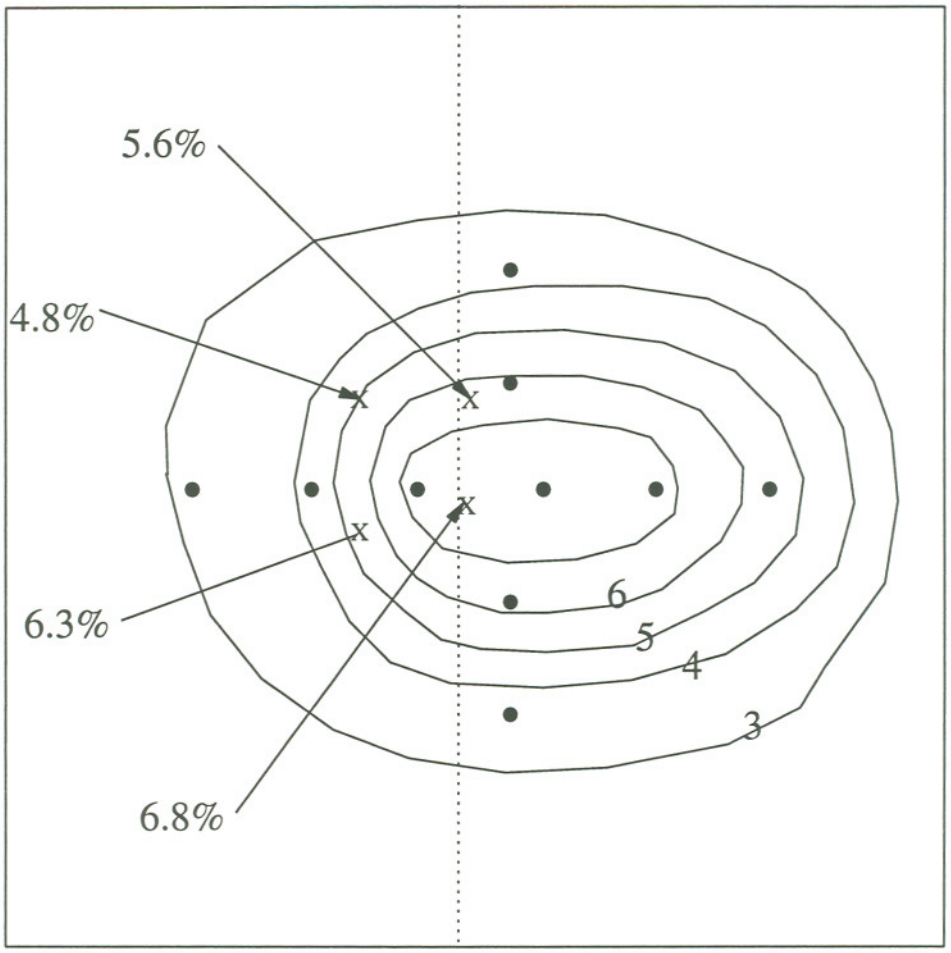

Figure 2.12 Observed PCE content (% bulk volume) from the neutron probe and soil cores.

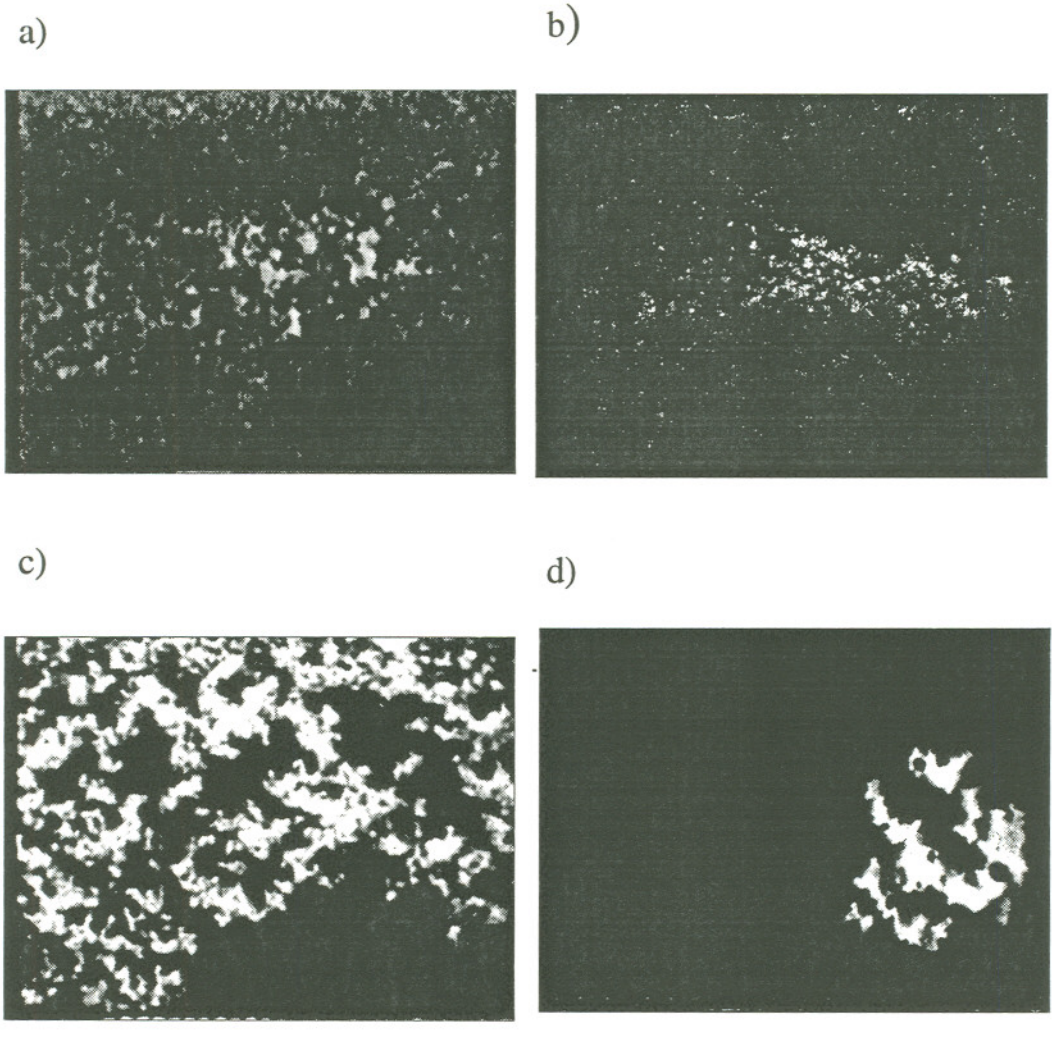

Figure 2.13 UV images showing PCE distribution at observation tubes; a) C; ~0.7m; 1 hour, b) C; ~0.7m; 90 days, c) B; ~2.5m; 90 days, d) D; ~2.4m; 90 days. Each figure represents an area of ~ 1.25 x 2 cm.

TABLE 2.1 - Grain size distribution of Columbia River sand

grain size (mm)	fraction[c]
> 4.00	4%
4.00 - 1.00	37%
1.00 - 0.71	8%
0.710 - 0.500	9%
0.500 - 0.246	26%
0.246 - 0.175	8%
0.175 - 0.043	7%
< 0.043	1%

[c] by weight (based on dry sieving for 3 minutes in triplicate)

TABLE 2.2 - Time interval during which PCE arrived at the observation tubes (hours)

OBSERVATION TUBE AND DEPTH	NEUTRON PROBE	VIDEO CAMERA
C - 0.07 m	0 - 0.25	0.7 - 1.0
B - 0.07 m	1.25 - 2.2	1.1 - 2.0
A - 0.07 m	20 - 22	13 - 18
C - 2.5 m	22 - 26	23 - 28
E - 2.5 m	26 - 29	24 - 28
F - 2.5 m	22 - 26	24 - 29
G - 2.5 m	34 - 38	32 - 39
B - 2.5 m	41 - 44	44 - 50
I - 2.5 m	44 - 48	39 - 54
D - 2.5 m	62 - 71	54 - 69
H - 2.5 m	71 - 75	73 - 96
J - 2.5 m	75 - 99	73 - 96
A - 2.5 m	75 - 99	69 - 73

TABLE 2.3 - PCE Pool Thickness (from video) and %PCE (from neutron) at 192 Hours

OBSERVATION TUBE AND DEPTH	POOL THICKNESS (cm)	PCE (% BY VOL.)
A - 0.07 m	-	1.8
B - 0.07 m	-	2.6
C - 0.07 m	-	2.8
A - 2.5 m	2.5	3.2
B - 2.5 m	7.5	3.7
C - 2.5 m	15	7.8
D - 2.5 m	7.5	3.7
E - 2.5 m	10	5.9
F - 2.5 m	18	7.3
G - 2.5 m	13	6.7
H - 2.5 m	10	3.2
I - 2.5 m	10	7.4
J - 2.5 m	7.5	6.0

TABLE 2.4 - Pool Thickness and Average PCE Content from soil cores

CORE LOCATION	POOL THICKNESS (cm)	SPECIFIC VOLUME (cm)	AVG PCE CONT. (% BY VOL)
C1	25	0.86	5.6
C2	15	0.73	4.8
C3	15	0.94	6.3
C4	30	1.02	6.8

REFERENCES

Allan, J.E. and R.L. Johnson, Solvent vapor extraction of DNAPL from a heterogeneous porous medium, to be submitted to *Water Resour. Res.* in 1995.

Allan, J.E., R.L. Johnson and N.R. Thomson, Numerical modeling of a DNAPL release into and SVE from a heterogeneous porous medium, to be submitted to *Water Resour. Res.* in 1995.

CPN Corporation, *Operator's manual, 503 Hydroprobe Moisture Depth Gauge*. Martinez. California, 1978.

Horvath, A.L., *Halogenated Hydrocarbons. Solubility-Miscibility with Water*. New York, Marcell Dekker, 1982.

Keller, B.R., L.G. Everett, and R.J. Marks, Effects of access tube material and grout on neutron probe measurements in the vadose zone, *Ground Water Monit. Rev., 10,* 96-100, 1990.

Kramer, J.H., S.J. Cullen and L.G. Everett, Vadose monitoring with the neutron moisture probe, *Ground Water Monit. Rev., 12,* 177-187, 1992.

Kueper, B.H., Abbott, W and G. Farquhar, Experimental observations of multiphase flow in heterogeneous porous media. *J. Contam. Hydrol., 5*, 83-95, 1989.

MacKay, D. and W.Y. Shui, A Critical Review of Henry's Law Constants for Chemicals of Environmental Interest. *Journal of Physical and Chemical Reference Data 10(4)*, 1175-1199, 1981.

MacPherson, J.R., *Gas Phase Diffusion of Organic Compounds in Porous Media: Physical and Numerical Modelling*, Ph.D. Dissertation, Dep. of Environ. Sci. and Eng.,

Oregon Graduate Institute, Beaverton, Oregon, 1991.

Nyhan, J.W., B.J. Drennon, J.C. Rodgers and W.V. Abeele, *Spatial Resolution of Soil Water Content Measurement by Three Neutron Moisture Gauges*, Report No. LA-83-2863, Los Alamos National Laboratory, 1983.

Poulsen, M.M. and B.H. Kueper, A Field Experiment to Study the Behavior of Tetrachloroethylene in Unsaturated Porous Media, *Environ. Sci. Technol., 26(5)*, pp. 889-895, 1992.

Schneider, G.W., and J.P. Greenhouse, Geophysical detection of perchloroethylene in a sandy aquifer using resistivity and nuclear logging techniques. In *Proceedings of the Symposium on the Application of Geophysics to Engineering and Environmental Problems*, Oakbrook, Illinois, 619-628, 1992.

Schwille, F., *Dense Chlorinated Solvents in Porous and Fractured Media*, Chelsea, MI, Lewis, 1988.

Silvestri, V., G. Srakis, N. Bekkouche, M. Soulie, and C. Tabib, Laboratory and Field Calibration of a Neutron Depth Moisture Gauge for Use in High Water Content Soils, *Geotechnical Testing Journal, 14(1)*, 64-70, 1991.

Starr, R.C. and Ingleton, R.A., A new method for collecting core samples without a drilling rig, *Groundwater Monit. Rev., 12(1)*, 91-95, 1992.

CHAPTER 3

SOIL VAPOR EXTRACTION OF DNAPL FROM A HETEROGENEOUS POROUS MEDIUM

INTRODUCTION

Widespread use of hydrocarbon fuels and chlorinated solvents has made these non-aqueous phase liquids (NAPLs) among the most commonly found contaminants in groundwater. These chemicals are particularly problematic because, even though they are immiscible with water, their solubilities are commonly orders of magnitude greater than established drinking water limits. Even if NAPLs do not reach the water table, aqueous and gas phase transport to groundwater can result in concentrations significantly higher than the drinking water limits. For this reason, remediation of a NAPL site to comply with drinking water standards often means removing essentially all of the contaminants.

Soil vapor extraction (SVE) has become a popular means for removal of NAPL's from the vadose zone. There are a number of reasons for the popularity of SVE, including: it is straight forward to implement, the cost is generally modest, large mass removal can usually be achieved and soil concentrations are often significantly reduced. The SVE technique is based on simple physical/chemical principles: by applying a vacuum to the soil, contaminated air is extracted and replaced by clean atmospheric air. This exchange perturbs the local chemical equilibrium, causing transfer of contaminant into the soil gas and subsequent removal from the subsurface. In theory this will eventually lead to complete cleanup. However, in practice mass removal rates may become mass transfer limited due to media heterogeneities and high water content.

At least three stages in effluent concentration may be observed during operation

of an SVE system for removing NAPL (McClellan, 1991; Armstrong *et al.*, 1994; Buscheck and Peargin, 1991). The first stage is characterized by high effluent concentrations with all phases in the system are at or near equilibrium. The duration of this high mass removal rate phase varies from one site to another. The second stage is a transition from equilibrium to non-equilibrium behavior. The third stage is characterized by very low effluent concentrations because the system is far from physical and chemical equilibrium and mass removal is limited by mass transfer from zones without significant air flow. This third stage can result in very long clean-up times.

A number of laboratory studies have examined the mechanisms involved in the mass transfer processes. In a study of uniformly distributed NAPL in a homogeneous porous media (McClellan, 1991), effluent concentrations were initially saturated (equilibrium between the NAPL and all the moving air phase) followed by a rapid decrease and long period during which concentrations were low and fairly steady. McClellan suggested that once the NAPL phase had been removed, mass removal rates were limited by diffusion from the aqueous and sorbed phases or mass transfer kinetics from the aqueous to the gas phase.

Benson (1990) also found that, with uniformly distributed NAPL in a homogeneous porous medium, effluent concentrations were initially saturated. However, when a portion of the air flow cross-section was uncontaminated, effluent concentrations were only a fraction of saturation. The ratio of contaminated to total air flow cross-section was equal to the ratio of the effluent concentration to the saturated concentration. In this case, diffusion into the uncontaminated zone was negligible. These data indicate that concentrations decreased as the fraction of extraction air by-passing contaminated zones increased.

Ho and Udell (1992) examined effluent concentrations from NAPL trapped in low permeability layers adjacent to higher permeability layers (no water phase was present in either layer). They found that for permeability ratios of up to 1:10 sufficient air flowed through the contaminant zone and removal rates were dominated by the volumetric flux of air flowing in the vicinity of the contaminant. However, for permeabilities ratios greater than 100, removal rates were limited by diffusion from low-permeability zones to high-permeability zones. As the zone of contamination receded further into the low

permeability zone, the effluent concentrations decreased due to increased diffusion length.

Gierke *et al.* (1992) performed experiments on toluene vapor transport in columns of sand and aggregated porous media under dry and moist conditions. They developed a dual-porosity model where advection was the primary transport mechanism in the mobile zone and diffusion was the dominant process in the immobile zones. Under moist conditions in sand they found that vapor transport was near equilibrium. However, vapor removal from aggregated soil was not at equilibrium, due to intraagregate (liquid) diffusion. Under dry conditions transport in both soil types was influenced by gas advection and diffusion. They suggested that behavior in aggregated soils was analogous to that in heterogeneous soils, where the lower permeability zones act as immobile zones.

Brusseau (1991) developed a parametric model using a dual-porosity concept to describe structured or heterogeneous porous media. The parameters used in his model were all obtained from independent sources. Results showed increasing deviation from the local equilibrium assumption (LEA) as the degree of heterogeneity increased. Brusseau concluded that, even under laboratory conditions using homogeneously packed columns, physical heterogeneity contributes to non-ideal behavior.

Most of the studies discussed above were based on results from uniformly distributed NAPL in homogeneous sand and examined only the processes limiting removal at the pore scale. Because of the design of these experiments, essentially all of the air flow passed directly through the residual zone. In natural systems this is not like to occur for several reasons, including: 1) NAPL distribution may be highly non-uniform; 2) porous media permeability contrasts result in non-uniform air flow, and 3) zones of higher water content will have lower relative permeabilities and therefore less air flow.

NAPL movement in the subsurface is controlled by the wetting properties of the NAPL/soil system and differences in interfacial tension. Even subtle variations in porous media properties result in a heterogeneous distribution of NAPL. "Pools" are formed when migrating NAPL encounter a capillary barrier such that downward migration cannot be sustained (Kueper *et al.*, 1993). In the unsaturated zone these barriers may be a result of lower permeability and/or higher water content strata. Infiltrating water may also become trapped by these capillary barriers, resulting in zones of high NAPL and water content. If the NAPL is more dense than water (a DNAPL) then it can penetrate into

high water content zones and become encapsulated by the water.

Intrinsic permeability contrasts and water content variation may also result in a non-uniform vapor extraction air flow field. Air flow can partially or completely bypass low permeability zones, particularly when they have high NAPL and water saturations. Mass recovery from these zones will be limited by diffusion into higher permeability zones where the air is flowing. Surface leakage is another factor controlling air flow. Many SVE models (Johnson *et al.*, 1990a and 1990b; Baehr *et al.*, 1989) assume confined flow conditions in the unsaturated zone due to an impermeable surface boundary. However, recent controlled field studies (Flynn, 1994; Beckett *et al.*, 1994) indicate that confined vapor flow conditions are not common in field applications, despite the presence of surface covers. Beckett *et al.* (1994) were able to fit data from a number of field sites using a Hantush-Jacob leaky flow analytical model (Hantush and Jacob, 1955). Their data indicated that both surface leakage and subsurface geology can have a significant influence on subsurface air flow. Surface leakage can also significantly affect the effective "radius of influence" of the SVE system (Benson *et al.*, 1990). The amount of atmospheric air that leaks into the subsurface during SVE operations is a function of the vacuum induced in the subsurface (e.g. the amount of leakage is greatest near the vapor extraction well). This has the effect of increasing the rate of contaminant removal from soil located near vapor extraction wells and decreasing the radius over which air is being drawn to the SVE well.

While numerous SVE case studies have been reported (e.g., Hutlzer *et al.*, 1989), very few have been sufficiently instrumented to draw conclusions about limitations on SVE performance. Buscheck and Peargin (1991) conducted a nation-wide study of 143 operating vapor extraction systems in order to generate two distinct databases: an operational database and a performance database. The majority of the SVE sites were not adequately monitored for quality performance data, and as a result only 15 of the 143 sites were used. Regression analyses on SVE removal rates at 15 sites identified two categories of sites which appear to correlate with hydrogeologic conditions and SVE air flow rates. Mass removal from sites in the first category was limited by volatilization and advection, at later time mass removal rates approached zero. These sites are generally described as medium- to coarse-grained, high permeability sediments. Mass removal from

sites in the second category was initially limited by evaporation and advection, but became diffusion-limited as characterized by non-zero asymptotic mass removal rates. These sites are dominated by fine-grained, low permeability sediments.

From the previously discussed laboratory and field studies it is evident that non-equilibrium processes control mass removal in even moderately heterogeneous systems. Mass removal of DNAPLs by SVE is particularly problematic because of the manner in which DNAPLs become distributed in the unsaturated zone as a result of permeability and water content distributions. Although there have been numerous laboratory studies examining microscale transport processes during SVE (Brusseau, 1991; Gierke *et al.*, 1992), there have been few field-scale SVE studies for which information on DNAPL distribution and transport properties of the porous media were available (Baehr *et al.*, 1989; Buscheck and Peargin, 1991). Therefore, detailed large-scale SVE experiments are needed to examine the processes controlling the performance at the field scale.

The research reported here describes the second phase of a study in which a large physical model contaminated with PCE was remediated using SVE. The first phase (Allan and Johnson, 1995) described PCE migration and characterization of the spatial distribution of PCE within the model. These results defined initial conditions for the SVE phase of the study. Mass removal by conventional SVE (i.e. low vacuum, high flow) was examined intitally. Subsequently, mass recovery using enhanced SVE (high-vacuum extraction from drive points and air injection into drive points) was examined. Air flow rates were examined using tracer tests and numerical modeling. Mass transfer limitations due to diffusion were evaluated using a one-dimensional diffusion model. These results will be compared to a 3-dimensional, 3-phase numerical model in a subsequent paper (Allan *et al.*, 1995).

MATERIALS AND METHODS

Physical Model

The experimental aquifer was constructed in an 8.4 x 8.4 x 2.9 m deep cell. The aquifer consists of complete layers of sand, pea gravel and clay, and a half-layer of

silica flour (Figure 3.1). The sand is washed medium Columbia river sand with a porosity of 0.37 and an intrinsic permeability (k) of ~$5x10^{-11}m^2$. The gravel is a uniform 5mm pea gravel with a porosity of 0.36 and a k of ~$2x10^{-9}m^2$. The silica flour (Sil-Co-Sil, U.S. Silica, Ottawa, IL) and clay (C/S granular, American Colloid Company, Arlington Heights, IL) have very low permeabilities. A more detailed description of the physical model can be found in Allan and Johnson (1995).

A three-dimensional sampling network was installed before the cell was filled to ensure that soil in contact with the sampling points was undisturbed (Figure 3.1 and 2). Twelve sampling bundles consisting of 1/8" stainless steel tubes attached to a 1/2" support post were installed in the aquifer. All of the bundles consisted of 12 lengths of tube, each of which terminated at a specific depth, providing 20cm vertical resolution. The opening at the lower end of each tube was wrapped with 100 mesh stainless steel screen to prevent soil particles from blocking the inlet. The top of each sampling tube was fitted with a threaded nut. These sampling tubes were used to measure both PCE concentrations in the soil gas and vacuum produced by the extraction system. They were also used as injection points for the gas-phase tracer tests discussed below.

Twenty-four 2 inch diameter PVC wells were evenly spaced around the perimeter of the cell before the cell was filled (Figure 3.2). The wells were screened from the bottom of the porous medium (2.55 m below datum) to the vapor barrier (0.3 m below datum). These served as extraction and inlet wells for the SVE system and provided access for monitoring and controlling water levels over the course of the study. Inflatable packers were placed in each of the wells during the SVE phase.

The surface of the aquifer was covered with a 0.015" vinyl vapor barrier to contain vapors, reduce rainwater infiltration and help seal the surface of the cell (Figure 3.1). To reduce air leakage, the joints between the vinyl liner and the cell walls, sampling bundles and other monitoring equipment were sealed with silica flour. The entire vapor barrier surface was then covered with 0.1m of sand for protection and to improve surface seal. The cell was covered by a movable deck to reduce rainwater infiltration and protect the instrumentation.

Prior to initiating the PCE release, the water level was raised to the top of the model and lowered down to the clay layer. The system was allowed to drain for a period

of ~1 month. The approximate water saturation profile in the physical model is shown in Figure 3.3a. Water contents were estimated from neutron moisture probe measurements prior to the PCE release (Allan and Johnson, 1995).

The DNAPL release was created by delivering 200 L of PCE to a source zone at a constant rate of ~4 L/hr through a 3mm tube inserted just below the vapor barrier. The source zone consisted of a 0.1 m diamter tube extending from the surface to a depth of 0.05 m below the vapor barrier. The PCE moved downward through the sand and spread laterally over the low permeability silica flour. The PCE spilled off of the silica flour and moved down through the sand and gravel to the clay (Figure 3.3b). Prior to SVE start up, 80-90% of the PCE was pooled on the clay layer near the bottom of the model, the remainder was above the silica flour (~10%) or trapped as residual in the sand and gravel between the silica flour and clay. Product distribution before SVE start-up was determined by extensive monitoring using a neutron moisture probe and a down-hole video camera (Allan and Johnson, 1995).

Two air flow configurations were chosen to optimize air flow near the zones containing liquid phase PCE. The first flow configuration was designed to optimize flow through the sand above the silica flour half-layer. Under ideal conditions, air entered only through the portion of the inlet wells above the silica flour. Extraction air was withdrawn over the full vertical extent of the system (Figure 3.4a). The second flow configuration was designed to optimize flow through the sand above the clay layer, near the water table. The top portion of both the inlet and extraction wells was packed off such that air entered and exited only through the lower sand layer (Figure 3.4b).

The extraction wells and vacuum blower (EG&G Rotron) were connected using 2" (0.05 m) diameter Schedule 40 PVC pipe. The six extraction wells were connected by a manifold to the blower inlet (Figure 3.5a). A portion of the blower effluent was piped directly to a Hewlett-Packard HP 5890 gas chromatograph (GC) (Hewlett-Packard Co., Avondale, PA) through 2.54 cm O.D. stainless tubing. A fresh air intake valve at the influent end of the blower provided make-up air flow to the blower. The extraction flow rate from the model and the total flow (extraction plus make-up flow) were measured using in-line flowmeters (Figure 3.5b). Nominal extraction flow rates from the SVE system were 25-50 scfm.

Air Velocity Tracer Tests

In order to characterize air flow in the cell and quantify surface leakage, gas phase tracer tests were performed. To conduct a test, a conservative gas phase tracer (SF_6) was injected into a sampling port (Figure 3.1) and effluent concentrations from the SVE system were monitored using a GC equipped with an electron capture detector (ECD). Breakthrough curves from the tests were used to determine residence times. Gas phase velocities were estimated in the different zones of the aquifer under the two flow configurations (Figures 3.4a and 3.4b). Gas phase vacuums at the sampling ports were measured using a magnehelic gauge. These data were compared to numerical model results using the permeability and water contents ditributions measured in the physical model.

Extraction air and soil gas sampling and analysis

Extraction air was analyzed using a GC equipped with an electron capture detector (ECD) and a photoionization detector (PID). The ECD was used to measure concentrations between 6×10^{-7} and 8×10^{-5} kg/m^3, and the PID for the 8×10^{-5} to 9×10^{-3} kg/m^3 concentration range. Samples were drawn from the effluent line using an automated 10-port gas sampling valve. Gas-phase standards were prepared in 0.8 L stainless-steel canisters equipped with stainless-steel bellows valves (Whitey Co., Highland Heights, OH). A known volume of PCE was injected into the clean canister, and the canister was pressurized with nitrogen gas to obtain the appropriate PCE concentration.

Prior to SVE start-up, the performance of the extraction and analysis systems were evaluated by pumping liquid PCE into the extraction line at a known rate using a syringe pump. A mass balance was performed using the effluent concentration measured by the GC and the total air flow. This test confirmed that mass was not lost from the system and that the GC and flowmeters were operating properly. The test was repeated including an internal standard (vinyledine chloride (VC)). The internal standard was also used during the initial stages of operation of the SVE system and periodically while the system

was in operation.

At various times during the extraction process, soil gas samples were collected from the sampling ports for analysis of gas phase PCE concentrations. Sample collection was performed with the extraction system turned off. Before each sample was collected, 75ml of air was withdrawn using a hand vacuum pump to purge the sampling tube. A 10 ml air sample was collected in a precision ground glass syringe (Hamilton Company, Reno, Nevada). The sample was immediately injected directly into the sampling loop of the heated gas sampling valve injector of a GC.

Enhanced SVE operations

Following conventional SVE operation, a positive-displacement pump (Air Components Engineering, Grand Forks, MI) was used for high vacuum extraction/injection from drive points placed in the PCE/water zone above the clay. Two injection/extraction drive points were fabricated from 2.4m of 2.54 cm OD stainless steel (SS) tube, a 5cm length of wire wrapped SS well screen, and a SS drive tip. The three sections were welded together and driven into the physical model with a jack hammer (Figures 3.1 and 3.2). The drive point was connected to the pump by 2" (5 cm) PVC pipe and fittings. Two air/water separators were installed between the drive point and the pump. The extraction vacuum (measured at the blower) was constant at ~40 kPa (10 inches of Hg) and the air extraction rate was ~3.8 scfm, dilution air was introduced at the blower. The drive points were also used for active air injection into the PCE/high-water-content zone. Air injection was coupled with the existing conventional vapor extraction system. Air was injected using an oil-less compressor with an air flow rate of ~5 scfm and a pressure of ~140 kPa (measured at the compressor). The SVE system operated at a vacuum of ~8 kPa and a flow rate of 65 scfm.

RESULTS AND DISCUSSION

Flow Characterization

Measured pressure fields for the two air flow configurations are shown in Figures 3.6a and 3.7a. These contours were generated from pressures measured at the 72 sampling ports located in the cross section parallel to the direction of air flow. Errors associated with these measurements are ± 25 Pa. Simulations of the two air flow configurations were conducted using a two-dimensional, two-phase flow model (Thomson, 1995). Air flow from the screened portion of the extraction wells was set equal to extraction air flow rates measured in the physical model (50 scfm for flow configuration A and 25scfm for flow configuration B). Under ideal conditions, "no flow" boundaries were prescribed over the "packed-off" regions of the wells and at the surface boundary (these are shown in Figure 3.4a and b). The simulated pressure field contours and velocity vector profiles under ideal boundary conditions (no surface leakage) are presented for flow configuration A (Figure 3.6b and c), and for configuration B (Figure 3.7b and c). The velocity vectors are on a log scale. The figures show that simulations of the ideal scenario do not describe the measured pressure fields and that surface leakage has a significant effect on air flow in the physical model under both air flow configurations A and B. Therefore, a "leaking surface" boundary was created by specifying a low permeability layer, between the top of the physical model domain and an ambient pressure boundary. The pressure field contours and velocity vector profiles simulated for flow configurations A and B under leaking surface conditions and shown in Figure 3.6d and 3.6e, and 3.7d and 3.7e respectively. The pressure gradients simulated under leaking surface conditions more closely resemble those observed in the physical model.

Tracer tests were performed to provide a more direct measurement of air velocities within the different zones of the physical model. Figure 3.8a presents the residence times of tracer injected at several sampling ports under flow configuration B. The residence time is defined here as the length of time between tracer injection at the sampling port and maximum concentration on the extraction breakthrough curve. Simulated tracer tests were also performed using the leaking flow model for configuration B (Figure 3.7d and

7e), and are presented for comparison in Figure 3.8b. No attempts were made to adjust model input parameters to improve the matches between the tracer test and model data. Both the measured and calculated tracer test results show that travel times vary substantially within the model. As expected, the tracer released into the gravel travelled very quickly through the system. Transport from the lower sand layer into the overlying gravel involved initial transport mainly by diffusion to the overlaying gravel and advection in the gravel to the extraction well. As the distance into the sand from the gravel layer increased, transport became limited due to gas and/or aqueous phase diffusion through the high water content zone, and the residence time increased significantly. Movement of tracers released into the sand above the gravel on the side without silica flour traveled quickly, due to air flow from the leaky surface to the extraction well. Simulated tracer tests from between the gravel and silica flour overestimated travel times. This is likely due to leakage around the perimeter wells and monitoring devices in the physical model.

The normalized measured and simulated breakthrough curves from tracer injection at sampling ports C2, C3, C7 and C11 are presented in Figure 3.9a and 3.9b (injection locations are shown in Figure 3.8a). The shapes of the tracer breakthrough curves varied significantly depending on injection location. Breakthrough for the injections above the gravel (C7 and C11) was fairly symmetrical, while tracers injected into the high water content sand below the gravel (C2 and C3) tailed significantly. This is observed in both the measured and simulated breakthrough curves. The differences in shape were due to the differences in porous media properties through which the tracers travel. For example, the tracer injected at C11 was advected through sand and gravel at residual moisture content whereas tracer injected at C3 travelled through a high water content zone where advective flow was small and diffusion played a significant role in transport. In general, the degree of asymmetry increased as a function of the water content at the injection point. Mass balance for the injections into C2, C3, C7 and C11 in the physical model were 94, 98, 78 and 110% respectively.

Tracer test residence times were used to quantify surface leakage. Under ideal conditions using flow configuration B, ~100% of the flow should travel through the gravel. Actual air velocities within portions of the gravel were estimated by dividing the

distance between two sampling points by the difference between tracer residence times injected into those points. The data indicated that ~50% of the total extraction flow travelled through the gravel. Similar calculations between sampling points above the gravel indicated that ~50% of the extraction flow leaked from the surface with ~10% of that leakage originating in the immediate vicinity of the extraction well.

SVE mass removal performance

The SVE system was in essentially constant operation for 270 days. Extraction concentrations (kg/m^3) and mass removal rates (kg/day) are presented in Figure 3.10 along with a summary of any changes in operating variables. During the first 166 days the SVE system operated with packer configuration A in order to optimize flow above the silica flour. Extraction concentrations were initially as high as $1x10^{-2}$ kg/m^3 (~10% of saturated values) at 25 scfm. Within 20 days concentrations had dropped by an order of magnitude, and within 50 days concentrations had decreased by two orders of magnitude. After 100 days of operation the extraction concentration was below $1x10^{-5}$ kg/m^3 ($1x10^{-2}$ kg/d). Initially the water level was ~0.2 m above the sand/clay interface. Over the first 95 days of operation the water level had increased by ~0.3 m due to rainwater infiltration. The water level was lowered to the clay/sand interface by pumping (days 95 to 120). Extraction concentrations increased from ~10^{-5} to ~$4x10^{-5}$ kg/m^3 as the water level was lowered indicating that the most of the mass removed by the extraction system during that period was from near the clay layer. Transport from this lower zone was limited to aqueous diffusion through the water saturated sand above the clay.

At day ~170 the packers were changed to flow configuration B (extraction flow rate remained at 25 scfm). There was no significant change in the PCE mass removal rate, indicating that mass removal was limited by diffusion through the sand into the high air flow gravel layer and the change in air flow pattern had not resulted in any significant increase in flow through the contaminated region. With the water level at the sand/clay interface the mass removal rate was ~$6x10^{-2}$ kg/d ($6x10^{-5}$ kg/m^3). At ~220 days the extraction air flow was increased to ~50 scfm. The effluent concentration decreased slightly and the mass removal rate increased marginally to ~$8x10^{-2}$ kg/d ($4x10^{-5}$ kg/m^3).

Within 20 days at 50 scfm the mass removal rate returned to ~6 x 10^{-2} kg/d ($3x10^{-5}$ kg/m^3).

During the 270 days of operation the extraction system was stopped several times for periods of up to 3 days. Each time the system was restarted the extraction air concentration would rebound by approximately an order of magnitude then decreased rapidly to the concentration prior to system shut down (eg. days 130 and 182). This once again indicates that mass removal from the system was mass transfer limited.

Diffusion model

The rate of PCE diffusion from the high PCE/water content zone above the clay to the high permeability gravel was estimated using a one dimensional, air/water phase diffusion model (McCarthy and Johnson, 1993) and compared to the experimentally-observed mass removal rate. To accomplish this the PCE pool above the clay was divided into 15 concentric zones with pool thickness ranging from 1 to 18cm, these were estimated from the results of the pool thickness and areal extent described in Allan and Johnson (1995). The diffusion model assumed that the concentration at the top of the PCE pool was saturated and the concentration at the sand gravel interface was $5x10^{-4}$ kg/m^3 (this was the approximate concentration of PCE observed in the gravel zone of the physical model). (Diffusion simulations with a 0 kg/m^3 concentration boundary at the sand/gravel interface produced nearly the same flux rates.) The mass flux rate (kg/m^2/d) from the pool to the gravel layer was calculated for each zone. A summary of the surface area, calculated flux rate and flux for each concentric zone is provided in Table 3.1. The calculated flux rate was 0.09 kg/d. This compares well with the observed rate of removal ~0.06 kg/d. Simulated concentration profiles from a point located at the perimeter of the pool (1 cm thick pool) and a point near the center of the pool (18cm thick pool) are shown in Figure 3.11. The difference in the profiles is due to the increasing thickness of the layer of water overlying the PCE as the pooled thickness decreases. Average concentrations as a function of depth for all the sampling bundles (A-F, Figure 3.1), as well as the average concentrations of two perimeter sampling bundles (A and F) and two central sampling bundles (C and D) are presented in Figure 3.11. The soil gas

concentration profile at the perimeter sampling bundles approach the calculated profiles for diffusion from a 1cm pool. The measured soil gas profile near the center of is close to the calculated profile for diffusion from a 18 cm pool.

Enhanced SVE

Conventional SVE was terminated on day 270. Of the 320 kg released into the model only ~30 kg had been removed by SVE. Soil core analysis and neutron probe results indicated that the sand above the silica flour was clean, but the mass of PCE above the clay was essentially unchanged. In order to overcome the mass transfer limitation in this region, two modes of enhanced SVE operation were investigated: high vacuum extraction from a drive point and air injection into a drive point coupled with conventional vapor extraction. For 19 days the system operated under high vacuum extraction from drive point 1 (DP1) (Figure 3.2). Initial concentrations were less than 0.01 kg/m^3 until the water level in the air/water separator was regulated (day 10) and air flow could be maintained at 3.8 scfm. (Reduced flow through the seperator meant increased makeup air and resulted in lower concentrations). When the water level in the separator was reduced, the PCE concentration immediately increased to ~0.1 kg/m^3. Subsequent changes in offgas concentration in Figure 3.12a were related to changes in water level in the air/water separator and resulting changes in air flow rate.

On day 21 of enhanced SVE, the system was reconfigured for conventional SVE under flow configuration B with extraction flow of ~69 scfm. Extraction concentrations were initially high as mass was removed from the zones of high air flow, then decreased rapidly (Figure 3.12b). On day 24 the mass removal rate was ~0.08 kg/d (*i.e.*, close the removal rate by SVE described in the previous section), and air injection into the second drive point (DP2) was initiated. Between days 24 and 26 air flow through the drive point was constricted and flow rates were erratic. The contriction in the drive point was cleared and between day 27 and 42 air was injected into DP2 continuously at a nominal rate of 5 scfm. Extraction concentrations decreased steadily but more slowly than for SVE alone. The injection was turned off at day 42 at which time extraction concentrations had decreased to ~6 x 10^{-5} kg/m^3 (0.15 kg/d). The SVE system alone was operated between

days 46 and 48 and mass removal dropped quickly to ~0.08 kg/d (3 x 10^{-5} kg/m^3) showing that combining injection into the drive point with conventional SVE resulted in an approximate doubling of the mass removal rate in the "tailing portion" of the mass removal curve. However, mass removal rates were still quite low.

On day 48 high vacuum extraction from DP2 was initiated. Mass removal rates were more than an order of magnitude lower than for high vacuum extraction from DP1, with very little water and no pure phase PCE recovered in the air/water seperator. The low mass removal rates from extraction at DP2 suggested that prior air injection at that point may have pushed PCE and water away from the drive point. This hypothesis was tested by injecting air into DP1 followed by high vacuum extraction from DP1. Mass removal during this second extraction from DP1 showed an order of magnitude decrease over "pre-injection" extraction removal rates (data are not shown), supporting the hypothesis that the air injection had reduced the performance of high vacuum extraction from DP2.

The cumulative mass recovery for SVE and enhanced SVE are shown in Figure 3.13. Mass recovery rates were only ~0.06 kg/d when the conventional SVE was terminated. Enhanced SVE by high vacuum extraction at DP1 removed ~650 l of water (~1.3 kg of dissolved phase PCE), ~16kg as pure phase PCE and ~45 kg of gas-phase PCE in the extraction air over a period of 20 days. At the time the extraction was turned off, water recovery was very low and there was no pure phase PCE recovery. However, PCE recovery was still greater than 1 kg/d. Soil gas pressure measurements at the vapor sampling ports indicate that the zone of vacuum surrounding the extraction drive point is less than 1 m. Air injection at DP2 coupled with SVE recovered 8 kg of mass over 20 days, with a mass removal rate of ~0.16 kg/d at the time the system was shut down.

CONCLUSIONS

Experimental data from the large physical model demonstrated that SVE air flow varied significantly within the model. The data indicated that air flow was very low in the portion of the porous medium which contained most of the PCE. This was due to both the presence of an overlying high permeability zone (*i.e.*, gravel) and a low air filled

porosity in the contaminated zone. Tracer tests were utilized to determine travel times from various locations throughout the physical model and to estimate surface leakage. These tests indicated that approximately half the air flow leaked through the surface cap. Mathematical modeling of air flow and tracer transport showed good agreement with the experimental data.

A total of 320 kg of PCE was released into the physical model. Of that amount, only ~30 kg was recovered by conventional vapor extraction over a period of 270 days. The primary limitation to recovery was that nearly all of the PCE mass was located at the bottom of the model below a high-permeability gravel layer and was retained within a high-water-content sand zone above a clay layer. The process of diffusion of the PCE through the capillary fringe up to the gravel layer was modeled using a one-dimensional diffusion model. The model simulated mass flux from pools of various thicknesses based on the distribution of PCE above the clay. The overall integrated mass flux agreed well with mass removal rates from the physical model.

Mass removal from the high NAPL and water content zone above the clay was substantially increased over conventional SVE when high-vacuum extraction was initiated from a drive point placed just above the clay layer. A total of ~65 kg of PCE (in the vapor and aqueous phases, as well as pure phase PCE) were removed in a 20-day period. Mass removal by air injection into a second drive point, coupled with conventional SVE, resulted in some increase in mass removal over conventional SVE alone, however it appears that the injection process drove PCE and water away from the drive point and prevented sustained high mass recovery.

The physical and mathematical modeling data reported here demonstrate the impact that aquifer heterogeneity can have on PCE distribution and subsequent mass recovery by SVE. The results point to the potential importance of understanding the distribution of a DNAPL and air flow in the subsurface. The tracer test procedure used to characterize air flow distribution coupled with other field data on DNAPL distribution (e.g. neutron probe and soil core data) provide practical tools which can be used at contaminated field sites to better optimize SVE performance.

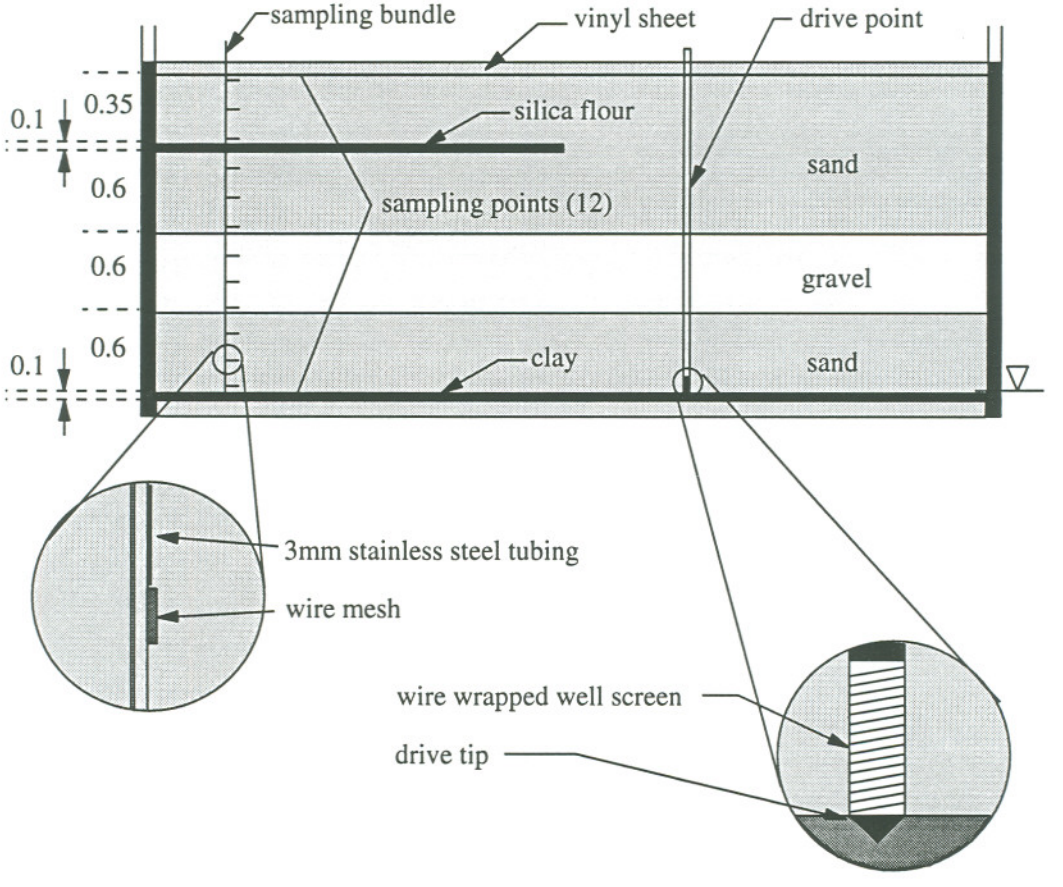

Figure 3.1 Schematic cross-section of experimental aquifer

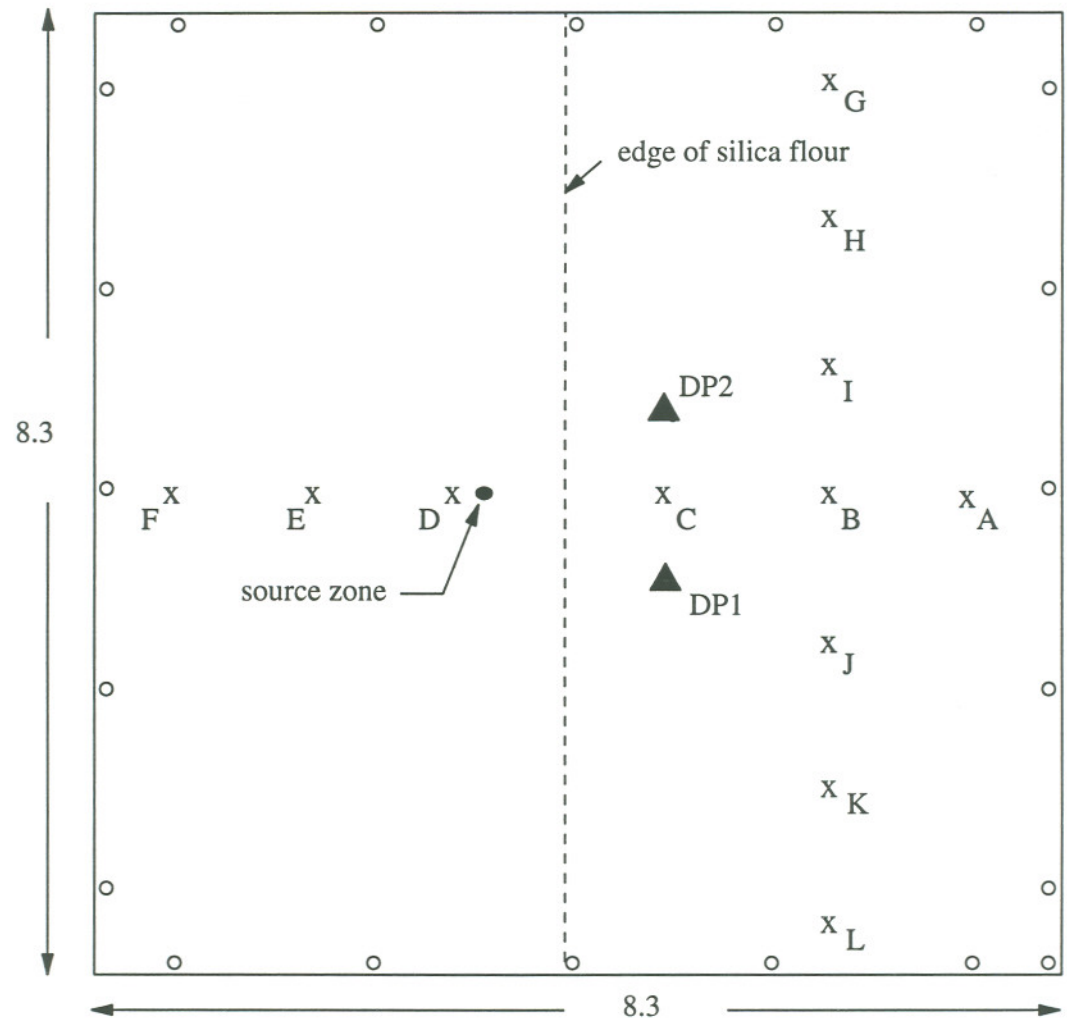

Figure 3.2 Plan view of experimental aquifer showing location of source (•), multi-level sampling bundles (X), SVE wells (o), and drive points (▲).

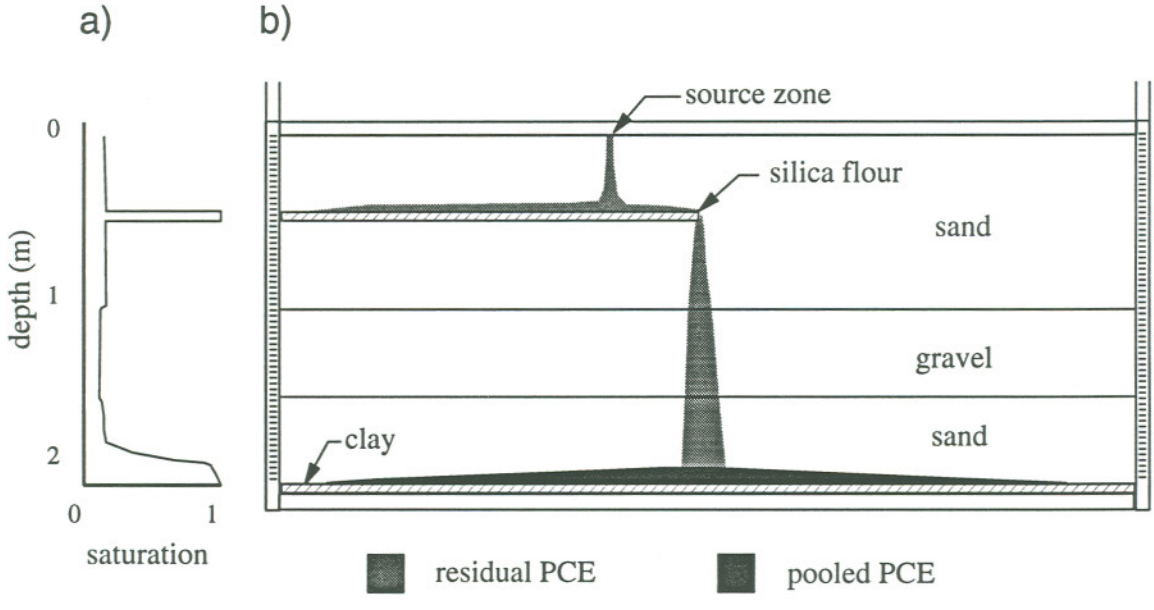

Figure 3.3 Cross-section of experimental aquifer showing a) approximate water saturation profile and b) PCE distribution.

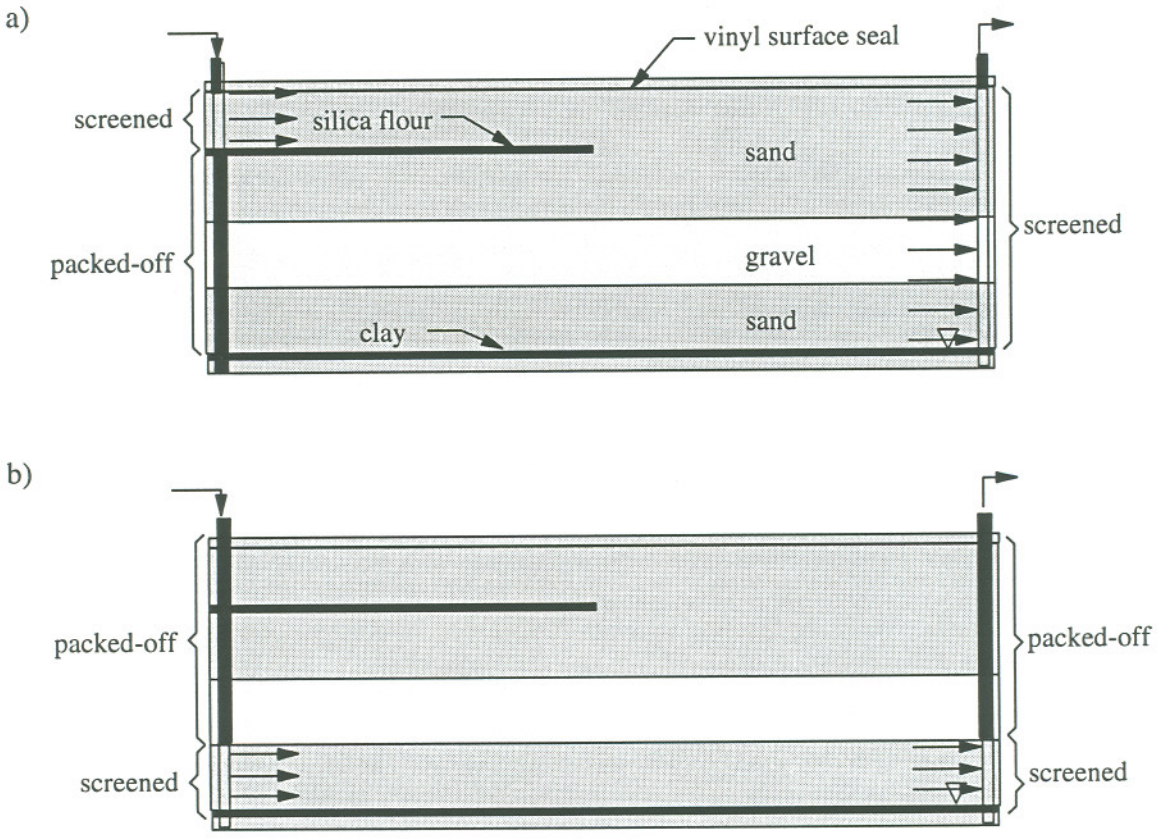

Figure 3.4 Schematic showing air flow configurations (A and B) used during conventional SVE.

a)

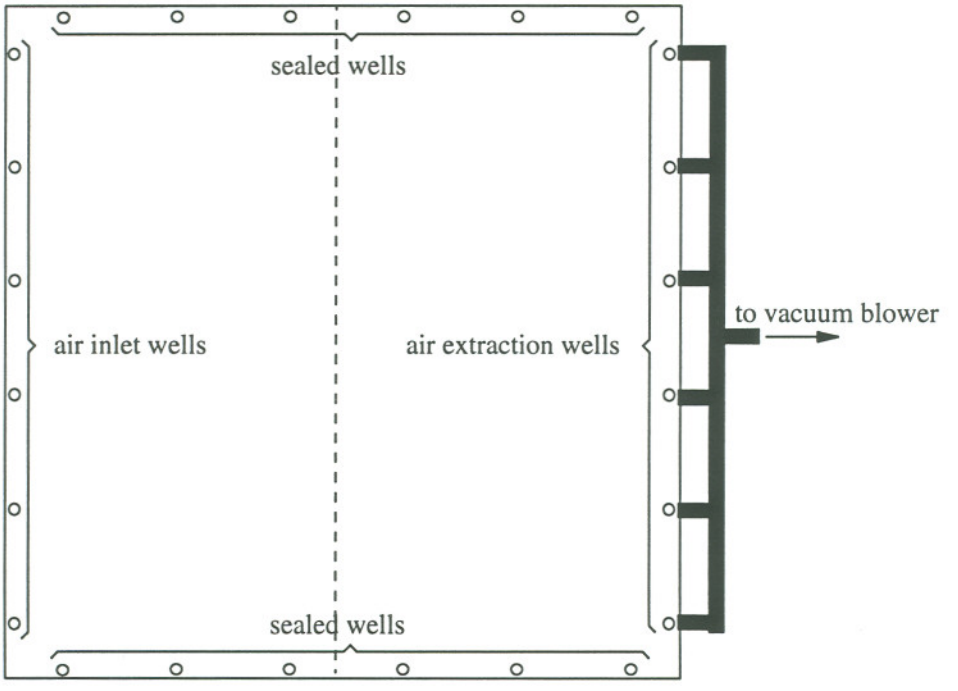

b)

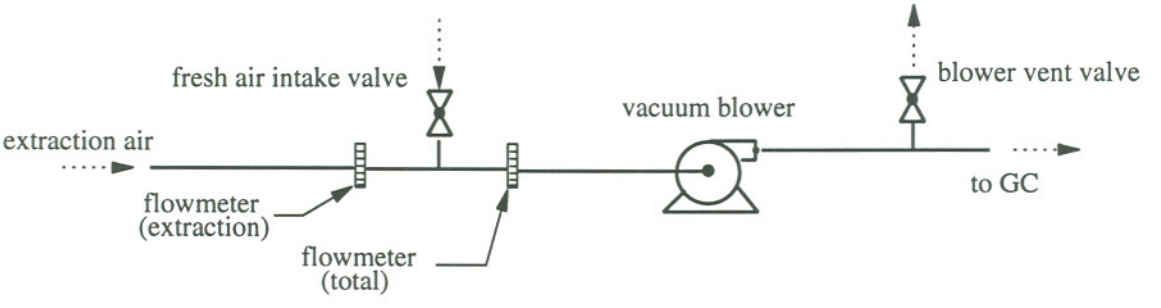

Figure 3.5 a) plan view showing extraction, inlet and sealed wells, and extraction manifold.

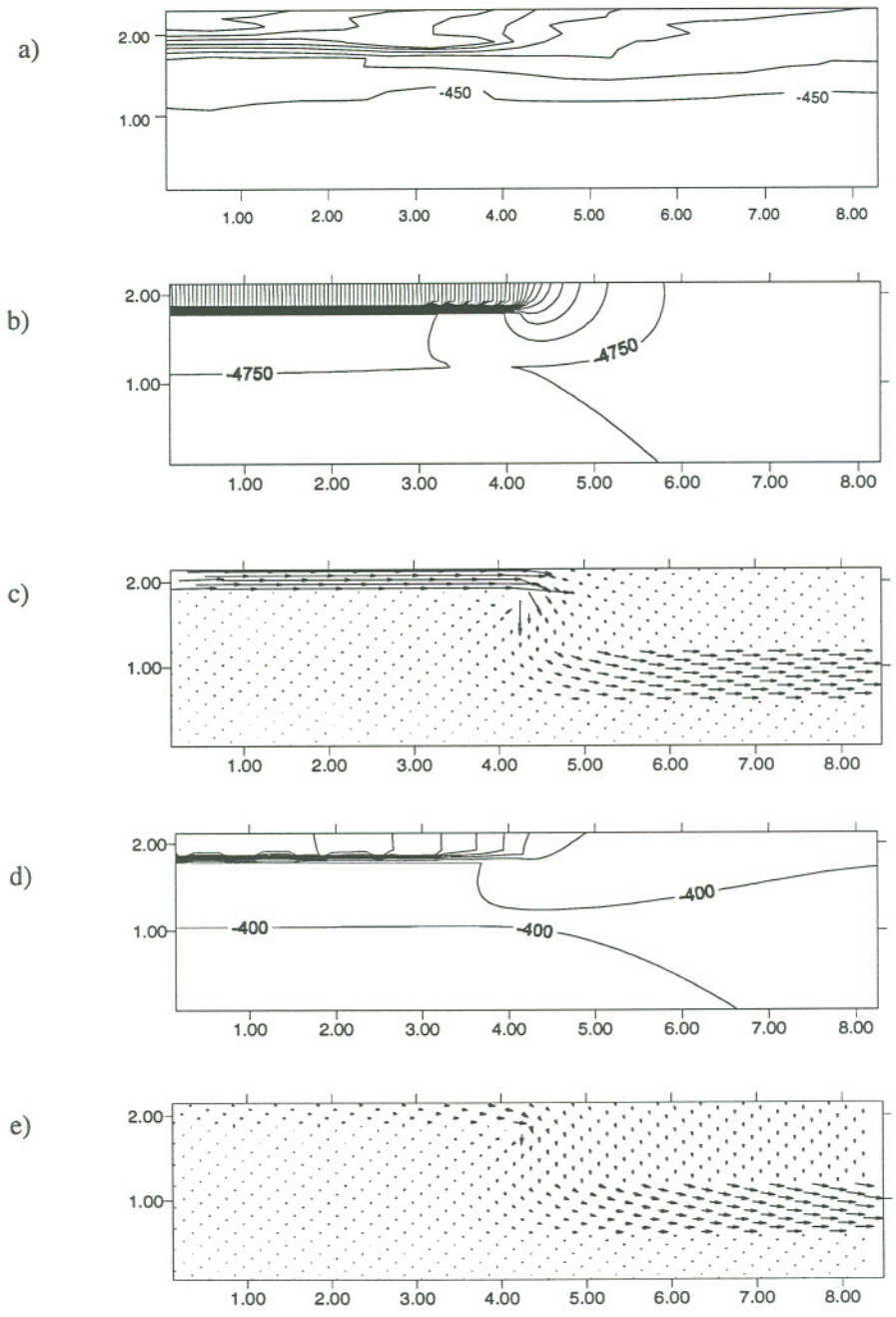

Figure 3.6 Flow configuration A: pressure fields a) measured b) simulated without surface leakage and d) simulated with surface leakage; velocity vector profile c) simulated without surface leakage and e) simulated with surface leakage.

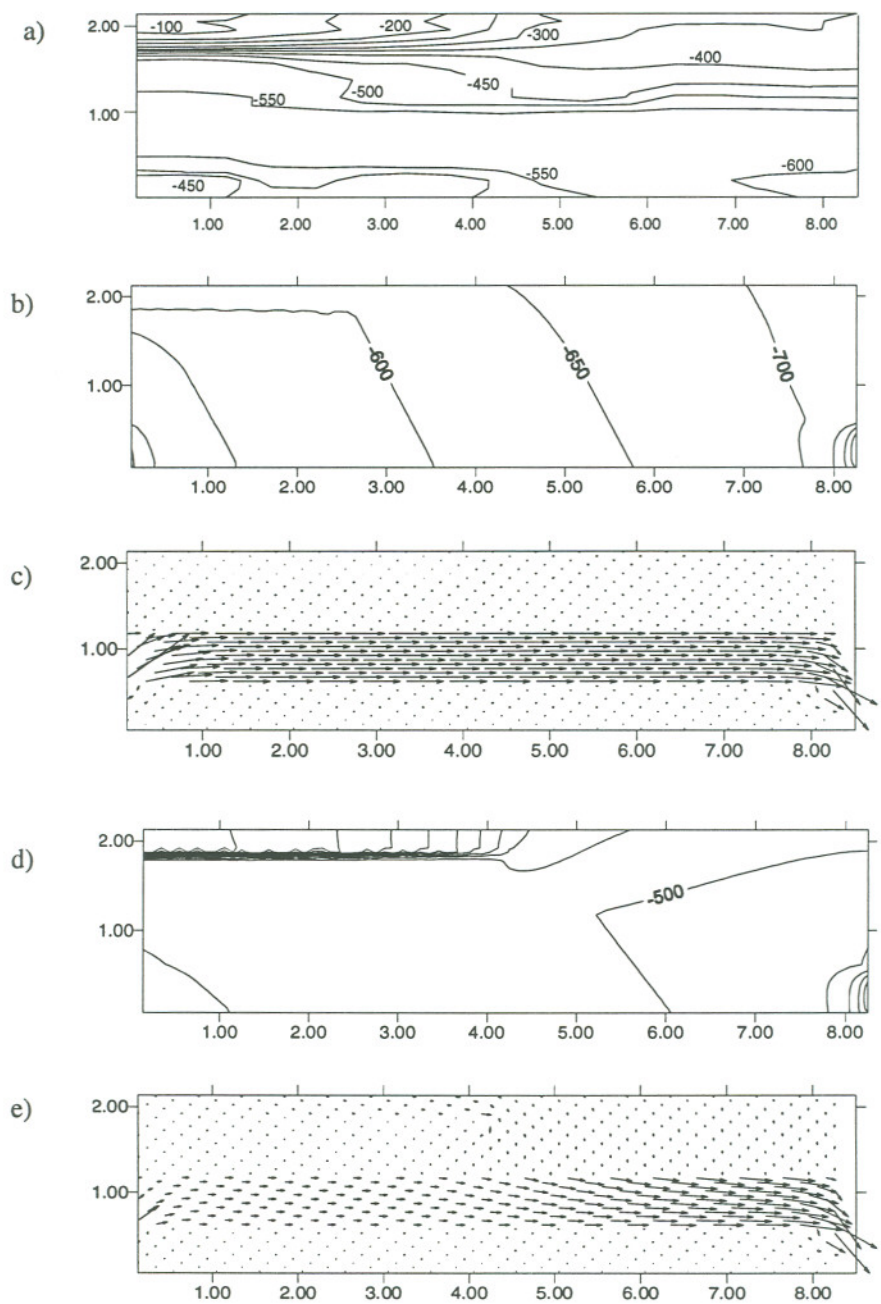

Figure 3.7 Flow configuration B: pressure fields a) measured, b) simulated without surface leakage, and d) simulated with surface leakage; velocity vectors c) simulated without surface leakage and e) simulated with surface leakage.

a)

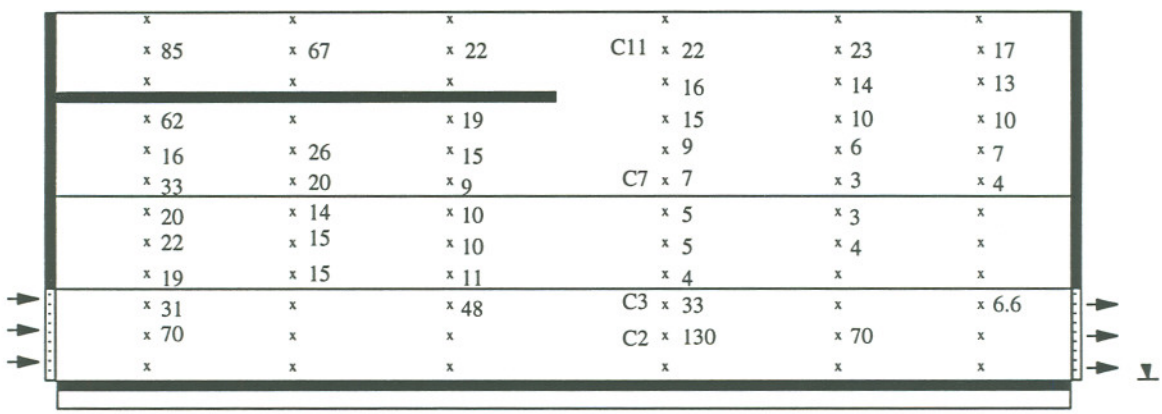

b)

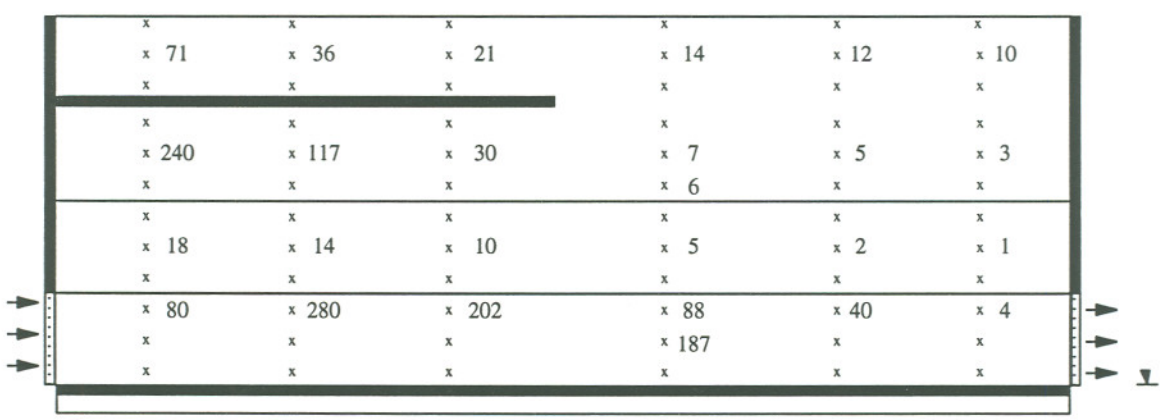

Figure 3.8 Tracer test residence times (minutes) for air flow configuration B, a) experimental values and b) model values.

a)

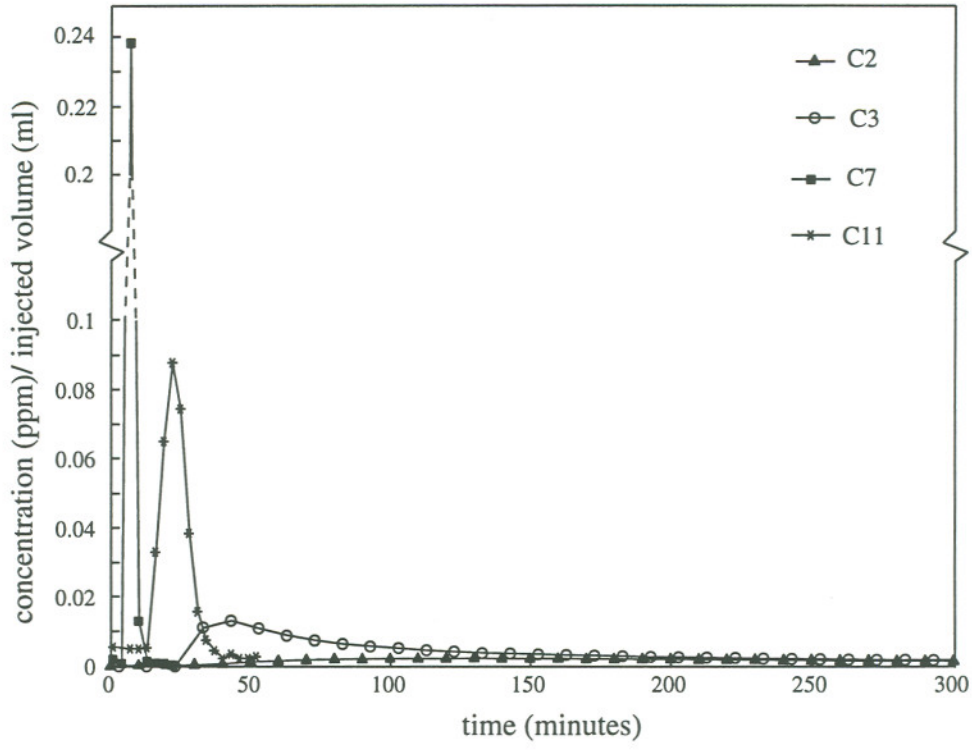

b)

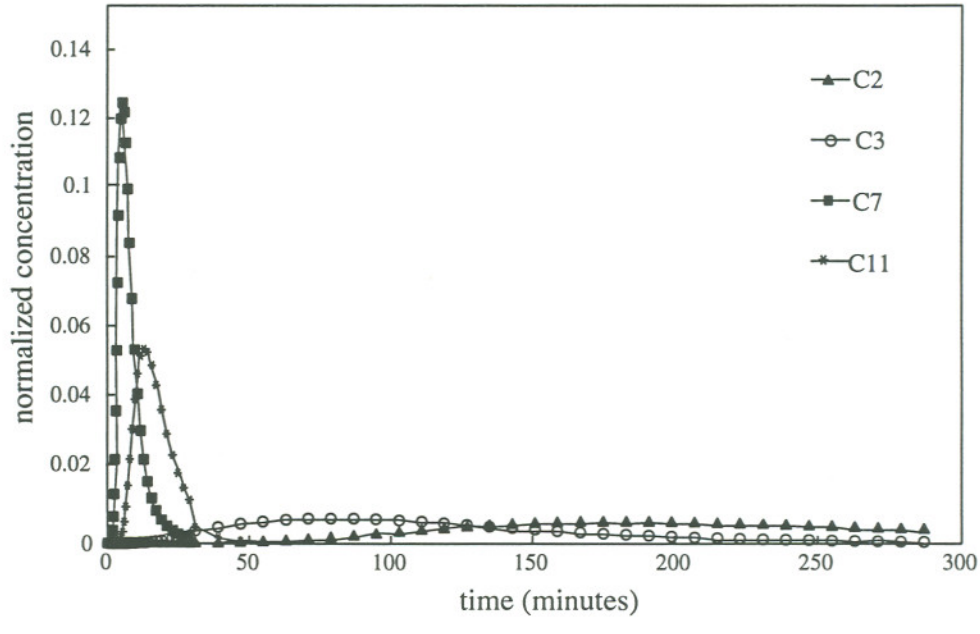

Figure 3.9 Tracer test breakthrough curves a) measured and b) simulated

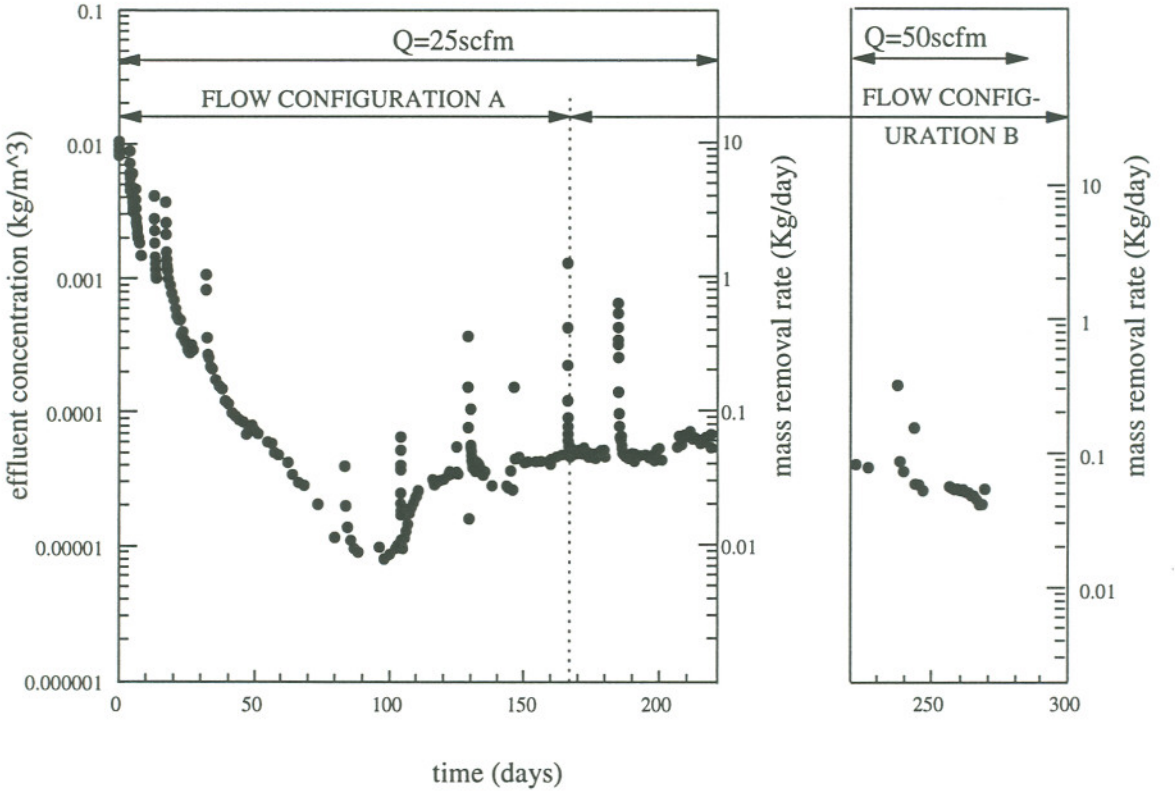

Figure 3.10 Mass removal during conventional SVE.

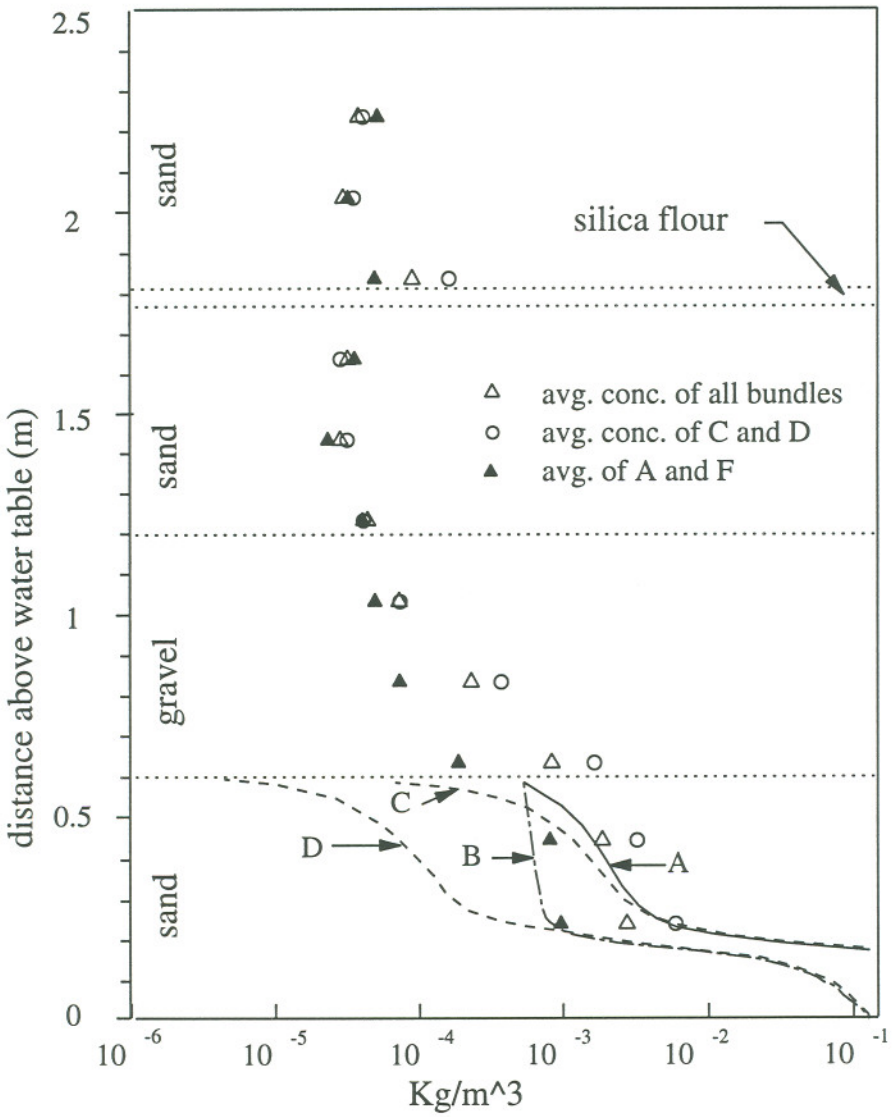

Figure 3.11 Measured (symbols) and simulated (lines) vapor concentrations; diffusion from a 18cm (A & C) and 1cm (B & D) pool using c=0 (C & D) and $c=0.5x10^{-4}$ kg/m^3 (A & B) at the sand/gravel interface.

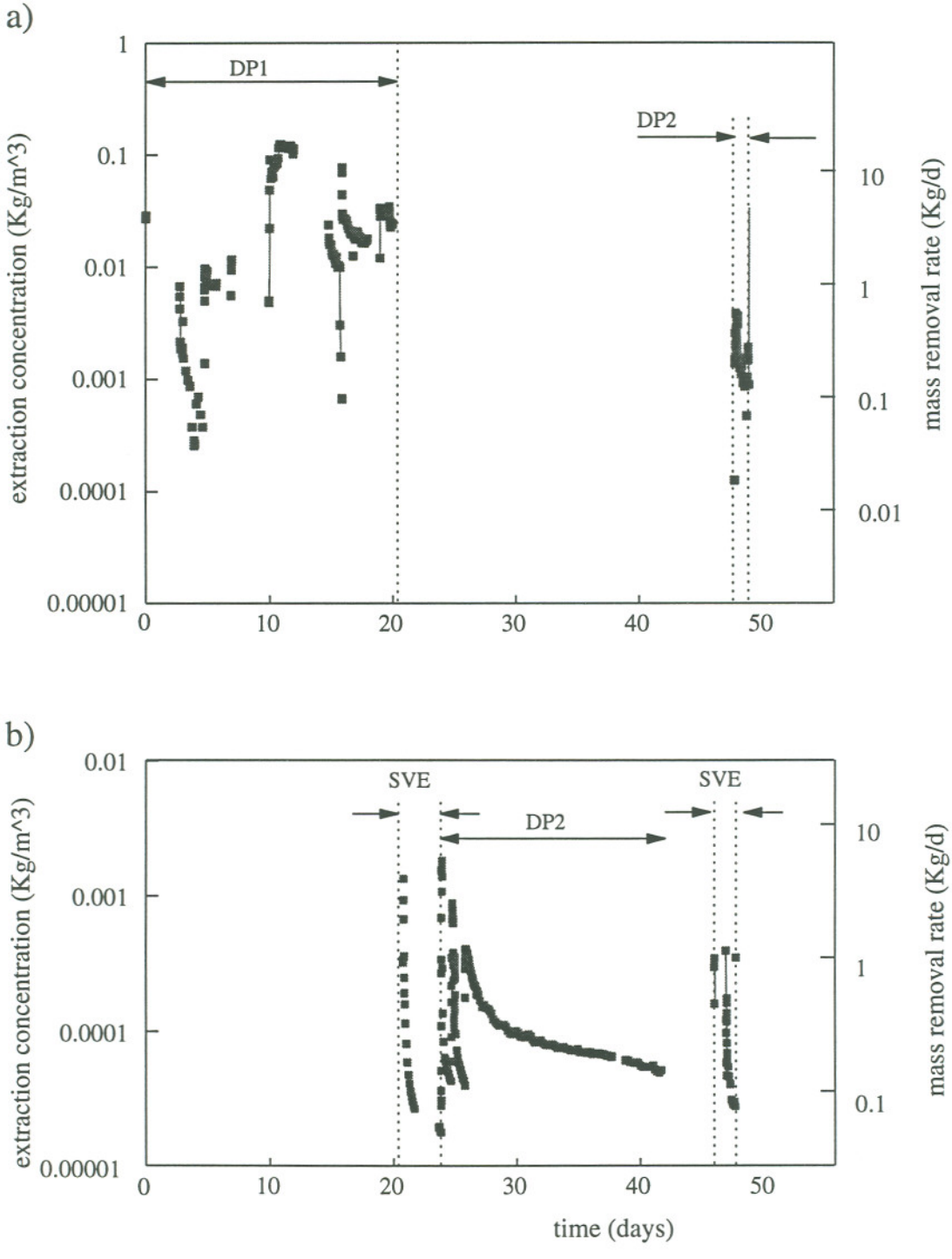

Figure 3.12 Mass removal during enhanced SVE using drive points a) high vacuum extraction and b) air injection with conventional SVE.

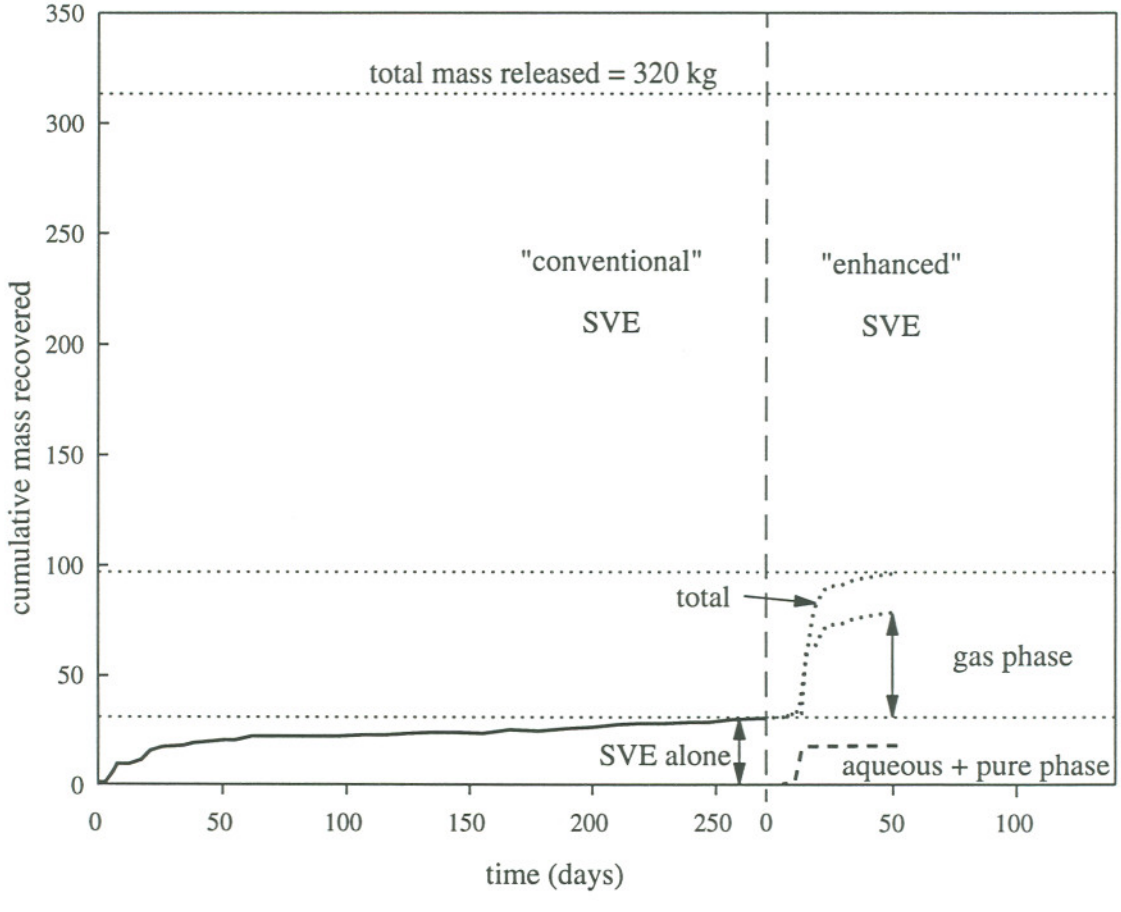

Figure 3.13 Cumulative mass removal under conventional and enhanced SVE.

TABLE 3.1 - Calculated mass flux by diffusion

"zone" name	surface area	pool thickness	flux rate	flux
	m^2	cm	$kg/m^2/d$	kg/d
1	0.2	18	0.0215	0.0042
2	0.6	16	0.0079	0.0047
3	1.0	14	0.0047	0.0046
4	1.4	12	0.0034	0.0047
5	1.8	11	0.0030	0.0052
6	2.2	10	0.0026	0.0057
7	2.6	9	0.0024	0.0060
8	2.9	8	0.0022	0.0063
9	3.3	7	0.0020	0.0063
10	3.7	6	0.0018	0.0065
11	4.1	5	0.0017	0.0069
12	4.5	4	0.0016	0.0071
13	4.9	3	0.0015	0.0072
14	5.3	2	0.0014	0.0073
15	5.7	1	0.0013	0.0073
totals	44.2			0.0901
total area	68.9			

REFERENCES

Allan, J.E. and R.L. Johnson, Characterization of a DNAPL release into a heterogeneous porous medium; in preparation for submission to *Water Resour. Res.* in 1995.

Allan, J.E. and R.L. Johnson, and N.R. Thomson, Numerical model of DNAPL release into and SVE from a heterogeneous porous medium; in preparation for submission to *Water Resour. Res.* in 1995.

Armstrong, J.E., E.O Frind and R.D. McClellan, Non-equilibrium mass transfer between the vapor, aqueous and solid phases in unsaturated soils during vapor extraction, *Water Resour. Res., 30(4)*, 355-368, 1994.

Baehr, A.L., G.E. Hoag and M.C. Marley, Removing volatile contaminants from the unsaturated zone by inducing advective air-phase transport, *J. Contam. Hydrol., 4(1)*, 1-26, 1989.

Beckett, G.D., D. Huntley, Characterization of flow parameters controlling soil vapor extraction, *Ground Water, 32(2)*, 239-247, 1994.

Benson, B., *Experiments with removal of volatile contaminants from soil by forced air venting*. M.A.Sc. Thesis, Depart. of Civ. Eng., Univ. of Waterloo, Waterloo, Ont., Canada, 1990.

Benson, D.A., D. Huntley and P.C. Johnson, Modelling vapor extraction and general transport in the presence of NAPL mixtures and nonideal conditions. *Ground Water, 31(3),* 437-445, 1993.

Buscheck, T.E. and T.R. Peargin, Summary of a nation-wide vapor extraction system performance study. In *Proceedings of the Third National Outdoor Action Conference on Aquifer Restoration, Ground Water Monitoring and Geophysical Methods*, 575-589, 1991.

Brusseau, M.L., Transport of organic chemicals by gas advection in structured or heterogeneous porous media: development of model and application to column experiments, *Water Resour. Res., 27(12)*, 3189-3199, 1991.

Flynn, D.J., *Soil vacuum extraction to remove residual and pools of perchloroethylene from a heterogeneous sand aquifer: a field trial.* M.A.Sc. Thesis, Dep. of Civ. Eng., Univ. of Waterloo, Waterloo, Ont., Canada, 1994.

Gierke, J.S., N.J. Hutzler, D.B. McKenzie, Vapor transport in unsaturated columns: implications for vapor extraction, *Water Resour. Res., 28(2)*, 323-335, 1992.

Hantush, M.S. and C.E. Jacob, Non-steady radial flow in an infinite leaky aquifer, *Trans. American Geophysical Union, 36(1)*, 95-112, 1955.

Ho, C.K. and K.S. Udell, Air venting of volatile liquid hydrocarbon mixtures, *J. Contam. Hydrol., 11*, 291-316, 1992.

Hutzler, N.J., B.E. Murphy, J.S. Gierke, *State of Technology Review: Soil Vapor Extraction Systems*, U.S. EPA, CR-814319-01-1, 1989.

Johnson, P.C., M.W. Kemblowski and J.D. Colthart, Quantitative analysis for cleanup of hydrocarbon-contaminated soil by in-situ soil venting, *Ground Water, 28(3)*, 413-429, 1990.

Kueper, B.H., D. Redman, R.C. Starr, S. Reitsma and M.Mah, A field experiment to study the behavior of tetrachloroethylene below the water table: spatial distribution of residual and pooled DNAPL, *Ground Water, 31(5)*, 756-766, 1993.

McCarthy, K.A. and R.L. Johnson, Transport of volatile organic compounds across the capillary fringe, *Water Resour. Res., 29(6)*, 1675-1683, 1993.

McClellan, R.D., *Vapor extraction of trichloroethylene under controlled field conditions.* M.Sc. Thesis, Dep. Earth Sci., Univ. of Waterloo, Waterloo, Ont., Canada, 1991.

Thomson, N.R., *Documentation for 3D3PT: a three-dimensional, three-phase, flow and transport model*, Dep. of Civ. Eng., Univ. of Waterloo, 1995.

CHAPTER 4

NUMERICAL MODELING OF DNAPL MOVEMENT AND SUBSEQUENT REMOVAL BY SOIL VAPOR EXTRACTION

INTRODUCTION

DNAPL Spill

The movement and final distribution of PCE in the large physical model discussed in Chapter 2 represents only one of many release scenarios. The most practical approach to generalizing the observed physical model results to other scenarios is to use numerical modeling. A number of researchers have developed numerical codes to predict the movement and distribution of a non-aqueous phase liquid (NAPL) in the subsurface. Faust (1985) was the first to include a static air phase to allow for the simulation of NAPL movement in the unsaturated zone. Abriola and Pinder (1985) further extended the model of Faust (1985) to include phase changes (ie. volatilization, dissolution). The current state-of-the-art models are three-dimensional (3-D) with three-phase flow and transport and may include fully hysteretic capillary pressure-saturation solution (Van Geel and Sykes, 1994), multi-component capabilities (Sleep and Sykes, 1993) and a variety of chemical reactions.

Because of the difficulties associated with the collection of the data necessary to test multiphase flow and transport models, the evaluation of these has, in general, lagged behind the development of the numerical techniques themselves. As a result, the use of multiphase flow models has been mainly limited to conceptual studies (Mercer and Cohen, 1990; Sleep and Sykes, 1993; Faust *et al.*, 1989) and simulations of one and two-

dimensional laboratory experiments (Lenhard *et al.*, 1988; Kueper and Frind, 1991). Kueper and Frind (1991) compared their numerical model to a 2-D, 2-phase parallel-plate laboratory experiment involving the infiltration of tetrachloroethylene into a heterogeneous sand pack, and saw good agreement between the two.

Illangasekara *et al.* (1993) evaluated a multiphase flow model using data from an LNAPL (NAPL with a density less than water) release into a large 2-dimensional structured, water-table physical model. They found that the model performed adequately under idealized homogeneous conditions. However, the diffusive behavior of the fronts as predicted by the model did not adequately allow for sharp variations of the material properties encountered at interfaces between heterogeneities. The physical model showed ponding between coarse and fine layers that the numerical model unable to reproduce.

Essaid *et al.* (1993) used a 2-D multiphase cross-sectional flow model to simulated the movement of oil and water at a spill site. Model predictions were compared to detailed field data collected 10 years after the spill. The authors found that the large scale features of the observed oil body were reproduced only when hysteresis with oil entrapment was incorporated into the model. The small-scale features of the observed oil distribution were not reproduced in the simulations. The discrepancy in the observed and simulated oil distributions was attributed to the considerable uncertainty in the model parameter estimates.

Because of the lack of experimental data related to immiscible flow in soils, the general validity of the assumptions used in the derivation of the immiscible flow and transport models have not been adequately demonstrated, particularly for three-dimensional (3-D), immiscible liquid movement in the unsaturated zone. The research presented here represents the first large-scale effort to perform such an evaluation.

Remediation by SVE

Mathematical models can play an important role in the design and optimization of soil vapor extraction (SVE) systems. Current SVE models can be broadly divided into 2 groups: 1) "screening" models studies investigate hypothetical SVE remediation scenarios under somewhat simplified conditions to illustrate specific aspects of the

technology (e.g. Johnson *et al*, 1990); and 2) laboratory-scale "process-oriented" models examine the important mechanisms controlling mass removal under various conditions (Armstrong *et al.*, 1994; Gierke *et al.*, 1992; Rathfelder *et al.*, 1991).

Johnson *et al.* (1990) presented several models to be used as screening tools to determine whether SVE is viable at a given site. The models assumed equilibrium partitioning between the vapor, free-liquid, sorbed and dissolved phases. Simulations under optimal conditions used uniformly distributed contaminant in homogeneous soil. A vapor-phase diffusion-limited model simulated mass removal when vapor flowed around, but not through the zone of contaminated soil (*i.e.,* mass trapped in a low-permeability layer or as a layer of free product). Comparison of the two cases illustrated the potential inefficiency of SVE in heterogeneous systems.

Gierke *et al.* (1992) compared simulated results to observations from a one-dimensional column experiment to distinguish between the impacts of different physical non-equilibrium mechanisms on organic vapor transport through sand and aggregated porous soil material (APSM). They examined the effects of gas diffusion, gas-water partitioning, liquid diffusion, and sorption on the transport of toluene vapor. Experiments were performed to measure these processes for dry and moist conditions in two homogeneous soil materials, a sand and a porous aggregate. They concluded that gas phase advection and diffusion had the greatest impact in the dry and moist sand and the dry APSM, but non-equilibrium conditions (due to intra-aggregate liquid diffusion) had to be considered in the moist APSM column. The authors suggested that these results apply to remediation of homogeneous soil contaminated with low levels of volatile organic compounds (VOC's) and that the results for APSM apply qualitatively to layered soil systems. Gas-water mass transfer was not found to be important at the low velocities used in their column studies.

Armstrong *et al.* (1994), simulated the extraction of VOC's controlled by non-equilibrium phase partitioning. In a homogeneous porous medium with high air velocities and in the absence of pure phase NAPL, they found that air-water mass transfer was the limiting process. A first-order approximation of the mass transfer process was found to be appropriate over the short duration of the simulations. They determined that, since kinetic coefficients depend on particular site conditions, model calibration is the best

means for estimating the coefficients. Their numerical experiments showed that, under mass transfer limited conditions, an optimum air flow rate exists above which mass removal rate stays constant. These experiments also showed that, although pulsed pumping may increase energy efficiency, mass removal during continuous pumping is greater since the concentration gradients are maximized at all times.

Rathfelder *et al.* (1991) developed a numerical model for the field-scale prediction of the soil vapor extraction process. Application of the model is restricted to scenarios with low moisture content and interphase mass transfer is described by either equilibrium or kinetically-controlled phase partitioning (*i.e.*, water/solid and water/gas). Sensitivity studies and laboratory evidence suggest that, at the field scale, equilibrium vapor concentrations from organic liquid volatilization are established in relatively short travel distances. Consequently, the local equilibrium assumption provides and adequate description of organic liquid volatilization in modelling field-scale venting operations. Sensitivity studies also showed non-equilibrium desorption and contaminant volatilization from the water phase could potentially reduce venting efficiency. Simulations of hypothetical field scale problems demonstrated that the efficiency of SVE operations was highly sensitive to the magnitude and distribution of soil permeability.

Benson *et al.* (1993) presented model results for remediation of a hypothetical fuel hydrocarbon spill by SVE. They illustrated how mass removal under non-ideal conditions (e.g., inhomogeneous soil permeability, leakage from the surface and irregular contaminant distribution) could be significantly lower than expected based on simplified conditions.

Although there have been a few highly monitored SVE field sites (Crow *et al.*, 1987) there are currently no published reports comparing numerical model results with field observations which incorporate non-uniform NAPL distribution and non-uniform air flow. The work reported here takes advantage of a highly monitored SVE operation in a well-characterized porous medium with a known initial NAPL distribution (described in Chapters 2 and 3) to model mass removal by SVE under highly heterogeneous conditions.

NUMERICAL MODEL AND GOVERNING EQUATIONS

The numerical model used for the PCE spill and subsequent SVE is capable of simulating the flow of three fluid phases (gas, non-aqueous phase liquid, and water), and the transport of one chemical component in both the aqueous and gaseous phases in three spatial dimensions. All three fluid components are active and at no time is a passive gas phase employed; hence, capillary and gravitational forces act on all three phases. Transport in the gaseous and aqueous phases considers the processes of advection, diffusion, dispersion, non-equilibrium volatilization, non-equilibrium dissolution, non-equilibrium gas/water mass transfer, and non-equilibrium sorption.

A control volume numerical approach is used in the model to approximate the governing equations. To reduce the computational burden, a sequential approach is used to simulate flow and transport components within the model. The resulting set of highly non-linear equations are solved using a full Jacobian iterative approach in conjunction with pre-conditioned orthomin solver at each time step.

The governing equations considered in this model to represent three-phase flow are (Bear, 1972):

$$\frac{\partial (\phi \rho_\beta S_\beta)}{\partial t} = + \frac{\partial}{\partial x_i} \left[\frac{\rho_\beta k_{ij} k_{r\beta}}{\mu_\beta} \left(\frac{\partial P_\beta}{\partial x_j} + \rho_\beta g e_j \right) \right] + \Gamma_\beta \qquad i,j = 1,2,3 \quad (1)$$

where β represents either the water (w), napl (n), or gas (g) phases; ϕ is the porosity, ρ_β is the phase density, S_β is the phase saturation, k_{ij} is the intrinsic permeability field, $k_{r\beta}$ is the relative permeability, μ_β is the absolute viscosity, P_β is the pressure, g is the gravitational acceleration, e_j are the components of a unit vector in the positive z-coordinate direction <0,0,1>, and Γ_β is a fluid sink or source.

The density of both the water and the NAPL phases are assumed to be constant, while compressibility of the gas phase is considered through the following relationship

$$\rho_g = \rho_g^o + c_g P_g \quad (2)$$

where ρ_g is the gas density at $P_g = 0$ (zero gauge pressure), and c_g is the gas phase

compressibility determined from the ideal gas law.

Associated with (1) are the following constraints :

$$\sum S_\beta = 1 \tag{3}$$

$$P_{cnw} = P_n - P_w \tag{4}$$

$$P_{cgw} = P_g - P_w \tag{5}$$

$$P_{cgn} = P_g - P_n \tag{6}$$

where P_{cnw}, P_{cgw} and P_{cgn} is the capillary pressure between NAPL and water, gas and water, and gas and NAPL phases respectively. It is assumed in this model that phase wettability decreases in the order water to NAPL to gas. The capillary pressure-saturation relationships developed by Parker *et al.* (1987) are employed. In these relationships it is assumed that the water-NAPL capillary pressure is a function of water saturation, while the NAPL-gas capillary pressure is a function of total liquid saturation (water and NAPL). Using this approach, the following relationships were derived:

$$\begin{aligned} \overline{S_w} &= [\ 1 + (\alpha\beta_{nw}P_{cnw})^N\ ]^{-M} ; \quad P_{cnw} > 0 \\ \overline{S_w} &= 1.0 ; \quad P_{cnw} \le 0 \end{aligned} \tag{7}$$

$$\begin{aligned} \overline{S_t} &= [1 + (\alpha\beta_{gn}P_{cgn})^N\ ]^{-M} ; \quad P_{cgn} > 0 \\ \overline{S_t} &= 1.0 ; \quad P_{cgn} \le 0 \end{aligned} \tag{8}$$

given:

$$\beta_{gw} P_{cgw} = \beta_{nw} P_{cnw} = \beta_{gn} P_{cgn} \tag{9}$$

$$\beta_{gw} = 1 \tag{10}$$

$$\beta_{nw} = \frac{\sigma_{gw}}{\sigma_{nw}} \tag{11}$$

$$\beta_{gn} = \frac{\sigma_{gw}}{\sigma_{gn}} \tag{12}$$

and

$$\overline{S_w} = \frac{S_w - S_r}{1 - S_r} \tag{13}$$

$$\overline{S_t} = \frac{S_w + S_n - S_r}{1 - S_r} \tag{14}$$

where β_{nw} and β_{gn} are scaling parameters used to extend the two-phase data to three phase systems; σ_{gw}, σ_{nw}, and σ_{gn} are the interfacial tensions for an air-water, NAPL-water, and air-NAPL system respectively. S_w and S_n are the water and NAPL saturations; $\bar{S}_w$ and $\bar{S}_t$ are the effective water and total liquid saturations; S_r is the irreducible liquid saturation; and M, N and α are capillary pressure-saturation curve fitting parameters (van Genutchen, 1980).

The relative permeabilities for each fluid phase are given by (Parker *et al.*, 1987):

$$k_{rw} = \overline{S_w}^{1/2} \left[1 - \left(1 - \overline{S_w}^{1/M}\right)^M \right]^2 \tag{15}$$

$$k_{rg} = (1 - \overline{S_w})^{1/2} \, (1 - \overline{S_T}^{1/M})^{2M} \tag{16}$$

$$k_{rn} = (\overline{S_t} - \overline{S_w})^{1/2} \, [\, (1-\overline{S_w}^{1/M})^{M} - (1-\overline{S_T}^{1/M})^{M} \,]^{2} \tag{17}$$

The source or sink term Γ_β can be defined for each phase as:

$$\Gamma_w = Q_w \tag{18}$$

$$\Gamma_g = Q_g + Q_{leak} \tag{19}$$

$$\Gamma_n = Q_n - \gamma_{n,w} - \gamma_{n,g} \tag{20}$$

where Q_w, Q_g and Q_n are inflow/outflow of water, gas and NAPL due to the presence of wells; Q_{leak} is inflow from surface leakage; and $\gamma_{n,w}$ and $\gamma_{n,g}$ are mass transfer from the NAPL phase by dissolution and volatilization.

Mass transport in the aqueous and gaseous phases is assumed to follow the nonlinear advective-dispersive conservation equations given by (Bear, 1977):

$$\frac{\partial(\phi S_\beta C_\beta)}{\partial t} = \frac{\partial}{\partial x_i}\left(\phi S_\beta D_{\beta ij} \frac{\partial C_\beta}{\partial x_j}\right) - \frac{\partial}{\partial x_i}(q_{\beta i} C_\beta) + \gamma_{\beta,\alpha} + Q_\beta C_\beta^* \tag{21}$$

with

$$D_{\beta ij} = \phi S_\beta D_{\beta ij} = \alpha_T |q_\beta| \delta_{ij} + (\alpha_L - \alpha_T) \frac{q_{\beta i} q_{\beta j}}{|q_\beta|} + \phi S_\beta D_\beta{}^m \tau_\beta \delta_{ij} \tag{22}$$

$$\tau_\beta = \frac{(\phi S_\beta)^{7/3}}{\phi^2} \tag{23}$$

where C_β is the mass concentration in phase β; α_T and α_L are the transverse and longitudinal dispersivity coefficients; $q_{\beta i}$ is the darcy flux; D^m_β is the free solution molecular diffusion coefficient; τ_β is the tortuosity factor; δ_{ij} is the Kronecker delta and $Q_\beta C_\beta{}^*$ is the mass leaving or entering the system from the wells ($C^*_\beta = C_\beta$ for mass withdrawn and $C^*_\beta = C_{\beta inj}$ for mass injected)

Mass transfer between phases is described by the following equations:

$$\gamma_{w,n} = \phi S_w \lambda_D (C_w^{\max} - C_w) \tag{24}$$

$$\gamma_{w,g} = -\gamma_{g,w} = \phi S_g \lambda_H (C_g - HC_w) \tag{25}$$

$$\gamma_{g,n} = \phi S_g \lambda_v (C_g^{\max} - C_g) \tag{26}$$

where λ_D, λ_H and λ_V are the mass transfer rate coefficients for dissolution, air-water transfer, and volatilization; H is the Henry's constant; $C_g{}^{max}$ is the maximum gas phase concentration and $C_w{}^{max}$ is the aqueous phase solubility. A provision in the model allows for a constant λ_D and/or λ_V, or for the mass transfer coefficient to vary as a function of the NAPL saturation as defined by:

$$\lambda_i = S_n^a \quad ; \qquad i = D,V \tag{27}$$

where a is an empirical constant.

METHOD

Numerical simulations (Thomson, 1995) of a 200 L release of PCE into a 3-D heterogenous domain (Figure 4.1a) was performed using porous media properties measured in the laboratory (Table 4.1). A schematic drawing of the 3-D grid used for the simulation is shown in Figure 4.1b. As was the case for the corresponding physical model experiment (Chapter 2) the water table in the numerical model was at the interface

between the sand and the impermeable clay layer. Initial water saturations throughout the model were defined by capillary pressure-saturation relationships using zero gauge pressure for the water phase at the water table. The experimental set-up is symmetrical about an xz plane through the source. Therefore, to reduce the number of control volumes without affecting the accuracy of model results, a grid was constructed with only half of the domain and half the experimental PCE release rate (Figure 4.1b). Physical model results indicated that PCE did not reach the walls of the model, therefore to further reduce computational expense 1.15m was cut off the sides of the grid. These steps reduced the 3-D grid from 8.3x8.3x2.2m to 6.0x3.0x2.2m and reduced the number of control volumes by almost a factor of 3. PCE was released into the system from the surface for the first 50 hours of simulation then allowed to redistribute for 150 hours.

Because of the time required for the 3-D simulations, sensitivity analyses were performed using a 2-D grid (Figure 4.1c). Since the PCE release-rate in the physical model can not be converted to an equivalent 2-D release-rate, simulations using a range of release rates were compared to observed time-series PCE saturations at several locations in the domain (Figure 4.1d) to determine an appropriate rate. Model sensitivity to discretization, air-water capillary pressure saturation relationship for sand, sand permeability and beta factors (describing PCE/water and PCE/air capillary pressure-saturation relationships) were examined using parameters listed in Table 4.2.

Mass removal by soil vapor extraction (SVE) was also simulated using a 2-dimensional grid (Figure 4.1e). Initial water and PCE distributions were obtained from PCE release simulation results after 58 days of redistribution. Initial concentrations of the air and water phases were saturated with PCE over the entire domain. The assumption of chemical equilbrium between all phases was chosen because the time between the NAPL release into the physical model and SVE start-up was approximately 8 months.

Air pressures in the model during SVE were constant and defined by the pressure distribution generated using the leaking surface boundary condition described in Chapter 3. During SVE simulations only the air and water phases were mobile, and the effect of the NAPL-phase on air relative permeability was not considered. All model parameters used to define flow and transport are listed in Table 4.3. The affects of sorption were

assumed to be negligible because of the large quantity of NAPL in the system and the slow rate at which concentrations change in the system. Numerical model results were compared to mass removal performance in the physical model. Model sensitivity to the parameters describing mass transfer between phases was evaluated using the parameters listed in Table 4.4.

RESULTS

PCE Release Simulations

Two- and three-dimensional numerical simulations were compared to observed PCE saturations from the calibrated neutron probe (NP) measurements discussed in Chapter 2. In order to compare NP and numerical results it is necessary to know the vertical thickness over which the NP measurements were integrated. If the spatial discretization used in the numerical model is smaller than the zone of measurement of the NP and saturations vary sharply over the zone of measurement, then the model results may appear to overpredict saturations. Since the zone of measurement of the neutron probe was not known, a mass balance was performed to estimate the vertical averaging thickness. It was assumed that lateral averaging did not significantly influence measurements because the PCE saturation within the pools did not vary sharply in the lateral directions near the measurement locations. Two seperate calculations were made using distributions at early times when all the PCE was pooled above the silica flour. The following information was used for the mass balance calculations: the areal extent of the PCE pool at 2 and 5 hours (Figure 2.7), %PCE saturations based on the NP measurements above the silica flour at 2 and 5 hours (Figure 2.9a); and the volume of PCE released (0.008 m^3 at 2 hours and 0.02 m^3 at 5 hours). The pool area above the silica flour at 2 hours was divided into 2 concentric zones. For each zone the surface area was calculated and the average %PCE saturation was estimated from the NP measurements at 2 hours. The averaging thickness of NP measurements was calculated by dividing the volume of PCE released at 2 hours (m^3) by the sum of the areas (m^2) multiplied by the %PCE for each zone. This calculation was repeated for the distribution

at 5 hours. The calculated averaging thickness was 0.21±0.03 m.

Three-Dimensional Simulation

Vertical (XZ) cross-sections showing PCE saturation contours from the 3-D grid simulation at 20, 50 and 100 hours are presented in Figures 4.2a through 4.2c respectively. Observed PCE saturations (defined as the fraction of the pore space occupied by PCE) at 25, 50 and 100 hours are shown in Figures 4.3a through 4.3c, respectively. The general features from the physical model, including pooling, lateral spreading and drainage off the edge of the above the silica flour, as well as pooling on the clay were reproduced in the numerical model simulations. Model results also showed some horizontal spreading as the PCE moved downward through the sand and gravel. Because the spatial sampling interval of NP measurements was ~1m in the lateral direction, horizontal spreading of PCE during the downward migration was not detected by the NP. Simulated PCE saturations above the silica flour were higher and showed more lateral spreading toward the wall. Possible reasons for this difference will be addressed in the discussions that follow.

Time-series results of observed and simulated PCE saturations a 6 locations in the domain (Figure 4.1d) are shown in Figures 4.4a and 4.4b. Above the silica flour, simulated arrival times at the observation tubes locations were close to those observed in the physical model (Figure 4.4a), however, simulated peak saturations were much higher. In addition, simulated PCE saturations increased for a much longer period of time than observed in the physical model. When the source was discontinued at 50 hours, numerical model saturations decreased rapidly while physical model results showed a slow decrease.

Above the clay, simulated arrival times at the observation tubes were almost two times greater than observed in the physical model (Figure 4.4b). There are two possible explanations for these discrepencies: 1) the silica flour layer had a slight slope (~2% towards the center) in the physical model and this resulted in less pooling and earlier flow off the silica flour; and 2) the permeability of the sand in the physical model could be higher than the value measured in the laboratory. These will be examined below in the

discussion on sensitivity analysis.

Two-Dimensional Simulations

Vertical cross-sections showing PCE saturation contours from the 2-D grid simulation at 20, 50 and 100 hours are presented in Figure 4.5a through 4.5c. As with the 3-D simulation (Figure 4.2) the general features of the 2-D simulations are the same as those observed in the physical model (Figure 4.3), and also include horizontal spreading as PCE moved downward. The 2-D simulations show earlier arrival time at the clay bottom and higher saturations than the 3-D simulations. However, these results may be influenced by finer discretization for the 2-D grid (as well the lack of a third dimension).

Time-series PCE saturations above the silica flour and above the clay for the 2-D base case simulation are presented in Figures 4.6a and 4.6b along with the observed PCE saturations from the physical model. Simulated arrival times above the silica flour are close to those observed in the physical model. Above the clay, simulated arrival time at a central location (C, Figure 4.1d) is later than observed in the physical model, while at the perimeter location (A) an earlier arrival time is observed. Earlier arrival at the perimeter location is expected for the simulations because spreading the 2-D simulation is limited to the lateral direction whereas spreading in the 3-D physical model is radial. Simulated saturations both above the silica flour and clay are much higher than observed saturations. Differences in observed and simulated saturation may be the result of several factors, including: 1) observed PCE saturations from the NP results represent average %PCE values over a 0.2m thickness while model grid blocks are 0.1m thick; and 2) PCE may accumulate to higher saturations and pool thicknesses in a 2-D system than in the 3-D system because the 2-D system does not allow radial spreading. As with the 3-D simulation, the overall trend in PCE content with time indicated that drainage off of the silica flour began earlier in the physical model (*i.e.*, the simulations showed a longer period of accumulation after initial arrival at A above the silica flour and later arrival at the lower clay layer).

Sensitivity Analysis

Permeability:

Time-series PCE saturations from simulations using a range of sand permeabilities are presented for four locations in the domain (Figure 4.7a through 4.7d). Model sensitivity to permeability was evaluated by examining the changes which resulted from increasing the permeability (k) by factors of 2 and 5 and decreasing the permeability by a factor of 2. Above the silica flour the simulated arrival time at C was not significantly affected by k because of its proximity to the source, however for two-fold k increase, the arrival time at A was reduced by ~25%. Peak saturations at both locations were influenced by the permeability increase (~10% decrease at A and ~17% decrease at C). Above the clay simulated arrival times at A and C increased by 25% when k was doubled. Peak saturations after 200 hours (150 hours after source was stopped) increased with increasing k (~10% increase at both observation points) because less PCE was being held above the silica flour.

Silica Flour Layer Slope:

In both the 3-D grid and the 2-D base case grid, the silica flour layer is represented as being horizontal. However, in the physical model the silica flour layer was sloped ~2% towards the center. To approximate the sloping silica flour layer, a 2-D grid was created with stepping silica flour layers (6 steps: dz=0.01m, dx=0.5m). Time series PCE saturations for simulations with a sloping and non-sloping silca flour are shown in Figure 4.8a through 4.8d. Above the silica flour arrival time at C was insentive to the silica flour slope (again, because of the proximity of the well to the source location, Figure 4.8a). Peak saturation at C was not significantly influenced by the slope of the silica flour, however, the saturations decreased more rapidly saturation when the silica flour layer is represented as sloped. The measure arrival time at A above the silica flour in the pysical model was in between that simulated and using the sloping and non-sloping silica flour (Figure 4.8b). In addition peak saturation at A was much lower for the

sloping case and saturations did not decrease significantly after the source was discontinued. Above the clay, arrival times at A and C were earlier for the sloped case (Figures 4.8c and 4.8d); with the arrival at C now close to the observed data. As with all the 2-D simulations, the PCE saturations at A and C are overpredicted.

van Genutchen α parameter:

Two capillary pressure-saturation curves for air/water in the sand were measured in the laboratory, the best-fit for the α parameter were $3.7x10^{-4}$ (used for base case simualtions) and $3.0x10^{-4}$ m^{-1}. Simulation results for both values of α show that model sensitivity is small within this range (Figure 4.9a through 4.9d).

Beta Factors:

Beta factors for scaling the capillary pressure-saturation curves were estimated using two methods described by Lenhard and Parker (1987). The first method defines the beta factors as the ratios of the interfacial tensions of the two liquids, these values were used for the base case. The second method of estimation used the laboratory measured capillary pressure-saturation for PCE/water and air/water. The beta factors were calculated from the ratio of the alpha parameters of the best fit van Genutchen curves. The laboratory measured beta factors were very close to those estimated from the interfacial tension (Table 2) and results from simulations using both sets of beta factors were essentially the same.

Discretization:

Model sensitivity to grid size is difficult to interpret using time-series of saturations at specific grid blocks in the domain because the sizes of the grid blocks are different. An alternate method of examining the influence of grid size on PCE movement is to compare the PCE saturation distribution over the entire domain a different times during the PCE release and redistribution. Simulations for the base case (0.2m wide *

0.1m deep), with a coarser grid (0.4 * 0.2m), and with a finer grid (0.1 * 0.05m) were performed and the saturations at 20, 50 and 100 hours are shown in Figures 4.5, 4.10 and 4.11. The base case (Figure 4.5) and finer grid case (Figure 4.10) are very similar at the three times shown. The finer grid simulations showed a somewhat larger lateral PCE spreading above the silica flour (at 20 hours) and above the clay (at 50 hours) than base case results. Simulations using the coarse grid showed significantly slower PCE movement (Figure 4.11). In the coarse grid case, PCE was distributed over the entire depth of the layer above the silica flour before mass spilled over the edge of the silica flour and a larger fraction of the mass was retained above the silica flour resulting in lower saturations above the clay. The coarse (0.2m deep) discretization is probably too coarse for these simulations because the capillary pressure saturation relationships vary sharply over dimensions of ~0.1m.

Soil Vapor Extraction Simulations

Comparison of numerical model and observed mass removal performance

Mass removal results from the numerical simulations were compared to the data from SVE in the physical model. There were several differences between the physical and numerical model conditions that must be considered before comparing the results. Initial PCE saturations generated by 2-D simulations were higher than those observed in the physical model and the amount of mass retained above the sililca flour was also higher in the 2-D simulations. However, the general features from the 2-D vertical section through the center of the physical model are captured by the numerical model (*e.g.* a fraction of the PCE was present as residual saturation in the high air saturation zone and most of the mass was pooled above the bentonite in a high water saturation zone).

Air flow in the physical model is essentially 2-D, however, observed extraction concentrations in the physical model are expected to be lower than the numerical simulation because air flowing through the center of the physical model is mixed with air flowing through the porous media along the walls where PCE saturations, and therefore

concentrations are lower. Transport by diffusion and dispersion in the third dimension is also not accounted for in the 2-D simulations, however these are not expected to be significant processes. As a result of these limitations, comparison of 2-D SVE simulations with SVE the results observed in the physical model are based only on: 1) trends in extraction concentration with time and 2) distribution of remaining mass when the extraction was stopped.

Physical model SVE results are presented along with numerical simulations under mass transfer conditions which approach equilibrium using high values for the mass transfer coefficients ($\lambda_D = \lambda_V = \lambda_H = 100\ s^{-1}$) (Figures 4.12a through 4.12b). Both observed and simulated results show rapid decreases in extraction concentrations within 10 days of system start-up. Following the rapid decrease, the simulation showed prolonged tailing at extraction concentrations slightly lower than observed in the physical model. Simulated and observed cumulative mass removed follow the same general trend, however, the total mass of PCE removed is higher for the simulated results, presumably because the amount of accescible PCE in the high air flow zone above the silica flour is greater.

The mass of PCE remaining and mass removal rates above and below the sand gravel interface over the duration of the extraction simulations are shown in Figures 4.13a and 4.13b. During the first 75 days of extraction, the model indicates that most of the mass was removed from above the interface. The rate of removal was initially high but decreased rapidly as the residual NAPL source decreased. At 68 days almost all of the mass above the interface had been removed and removal rates became very low until 80 days when all the mass was removed. Simulated mass removal rates from below the interface also decreased with time as the concentration profile between the PCE pool at the bottom and the lower sand/gravel interface shifted from the initial conditions (saturated aqueous and gas phases concentrations) to a concentration profile fixed by low concentrations at the sand/gravel interface and high PCE saturations above the clay. The final mass removal rate from below the interface is limited by aqueous diffusion from the PCE pooled in the tension saturated portion of the capillary fringe.

Contours of PCE saturations before initiation of SVE, after 10 days, 15 days and 100 days of extraction are presented in Figure 4.14. The distribution of the remaining PCE after 100 days is similar to that observed in the physical model. Soil cores collected

after 270 days of SVE showed no PCE in or above the silica flour. Core data from above the clay showed PCE saturations of 0.13 to 0.26 in an ~0.2m thick pool.

Model sensitivity to mass transfer parameters

Mass transfer coefficients (λ) vary in space and time, depending upon environmental factors including flow rate, capillarity, temperature and diffusivities (Rathfelder, 1989). Non-equilibrium mass transfer between phases is a function of the concentration gradient and λ. The numerical simulations which was compared with experimental SVE results in the previous section used high values of λ approximating chemical equilibrium between all phases. Since there was no means to measure λ directly and sensitivity to these parameters will depend on site conditions, a range values for λ were used to illustrate sensitivity for the given scenerio. Two formulations were used to define λ. The first assumes that λ is a constant. The second, for mass transfer from NAPL to water and NAPL to gas, assumes that λ is a function of the NAPL saturation: $\lambda = S_n^a$ (where S_n is the NAPL saturation and a is an empirical constant). The second formulation assumes that the rate of mass transfer from the NAPL phase is a function of the surface area of the NAPL which is related to the saturation. Guiger (1994) fit mass transfer coefficients between NAPL and water from a plume developed from an emplaced source in the Borden aquifer. The relationship: $\lambda_{n,w} = S_n^{1.6}$ best fit the observed results.

Figure 4.15 shows mass remaining above and below the lower sand/gravel interface using mass transfer coefficients ranging from 0.001 to 100 s^{-1}. Mass removal from below the interface was only slightly influenced by changes in the mass transfer coefficients. However, mass removal from above the interface was very sensitive to these parameters. As the mass transfer coefficients decreased the amount of mass still retained when tailing began increased. The mass remaining above the interface was contained within the low permeability/high water content silica flour, and between the gravel and silica flour layers where there was little advective air flow. Both zones had very low PCE saturations (< 0.005). (Analysis of cores collected in the physical model after SVE and the video results collected during the spill indicated that PCE did not penetrate into the silica flour (Chapter 2)). The NAPL trapped in the silica flour was removed through

dissolution into the aqueous phase (controlled by λ_D) and mass transfer into the gas phase above by air-water transfer (controlled by λ_H). Rate limited mass transfer appeared to reduce mass removal of NAPL from within the silica flour and the zone of very low air flow between the gravel and silica flour. Figure 4.16 shows a similar trend in the sensitivity of mass removal from above the interface to mass transfer coefficients defined as a function of NAPL saturation.

CONCLUSIONS

Numerical simulations of PCE released into a heterogeneous porous medium reproduced trends in the migration and final distribution observed in the physical model. Both the 3-D and 2-D grid simulations showed a longer period of accumulation before PCE spilled of the edge of the silica flour. This resulted in higher simulated saturations above the silica flour as well as later arrival and lower saturations above the clay layer at the bottom for the 3-D simulation. PCE saturations for the 2-D simulations both above the silica flour and above the clay were higher than 3-D simulations and the observed because spreading in the 2-D system is limited to one lateral direction.

Sensitivity anlysis showed that PCE saturation above the silca flour and the time to reach the clay bottom were sensitive to the sand permeability as well as the slope of the silica flour layer (the silica flour in the physical model was sloped ~2% towards the center). PCE saturations were not particularly sensitive to the capillary pressure-saturation relationship for an air-water system or the scaling factors for PCE-water and PCE-air within the range of laboratory measurements.

Soil vapor extraction simulations were performed using an initial PCE distribution from a 2-D PCE release simulation and air flow with a leaking surface boundary condition. Simulations under equilibrium-like conditions (ie. using high mass transfer coefficients) showed the same trends in the mass removal rate as were observed in the physical model. However, because of the differences between SVE from a system with 2-D PCE distributions and the 3-D distributions in the physical model, the results could not be compared directly. Distribution of the PCE remaining in the soil when simulated mass removal rates became very low matched soil cores collected from the physical

model. Both showed that essentially all the mass from above the silica flour was removed and high PCE saturation remained in the capillary fringe above the clay. Simulated mass removal rates and the mass of remaining PCE were evaluated seperately for the lower portion (the lower sand layer in which most of the mass was pooled in the capillary fringe) and the upper portion (where a smaller fraction of the PCE was left as residual above the silica flour). Mass removal rates from the upper portion were initially high and decreased until all the mass was removed. Mass removal from the lower portion remained low during the entire extraction period.

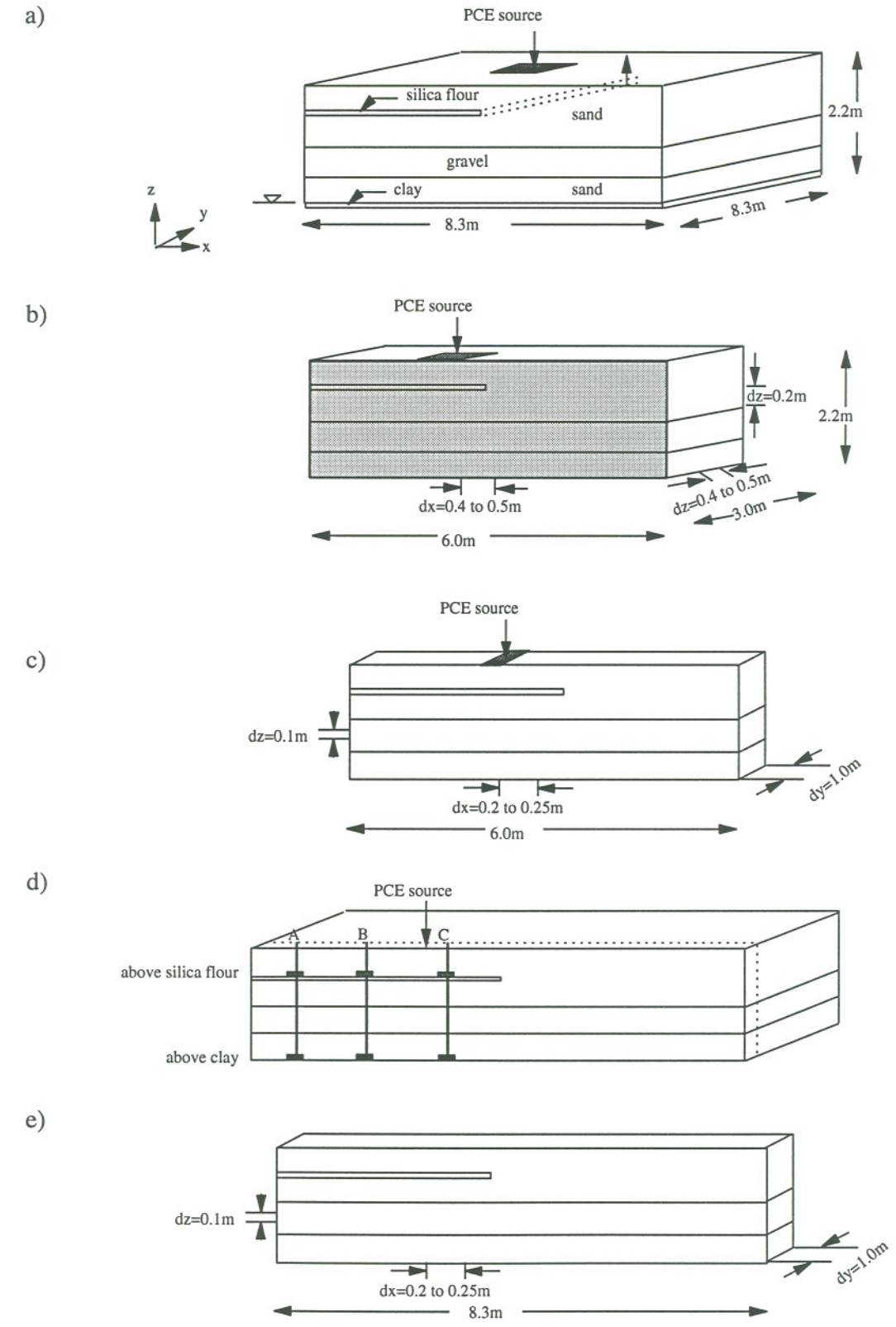

Figure 4.1 Schematic drawing of a) physical model, b) 3-D grid and c) 2-D grid for PCE release simulations, d) observation points and d) 2-D grid for SVE simulations.

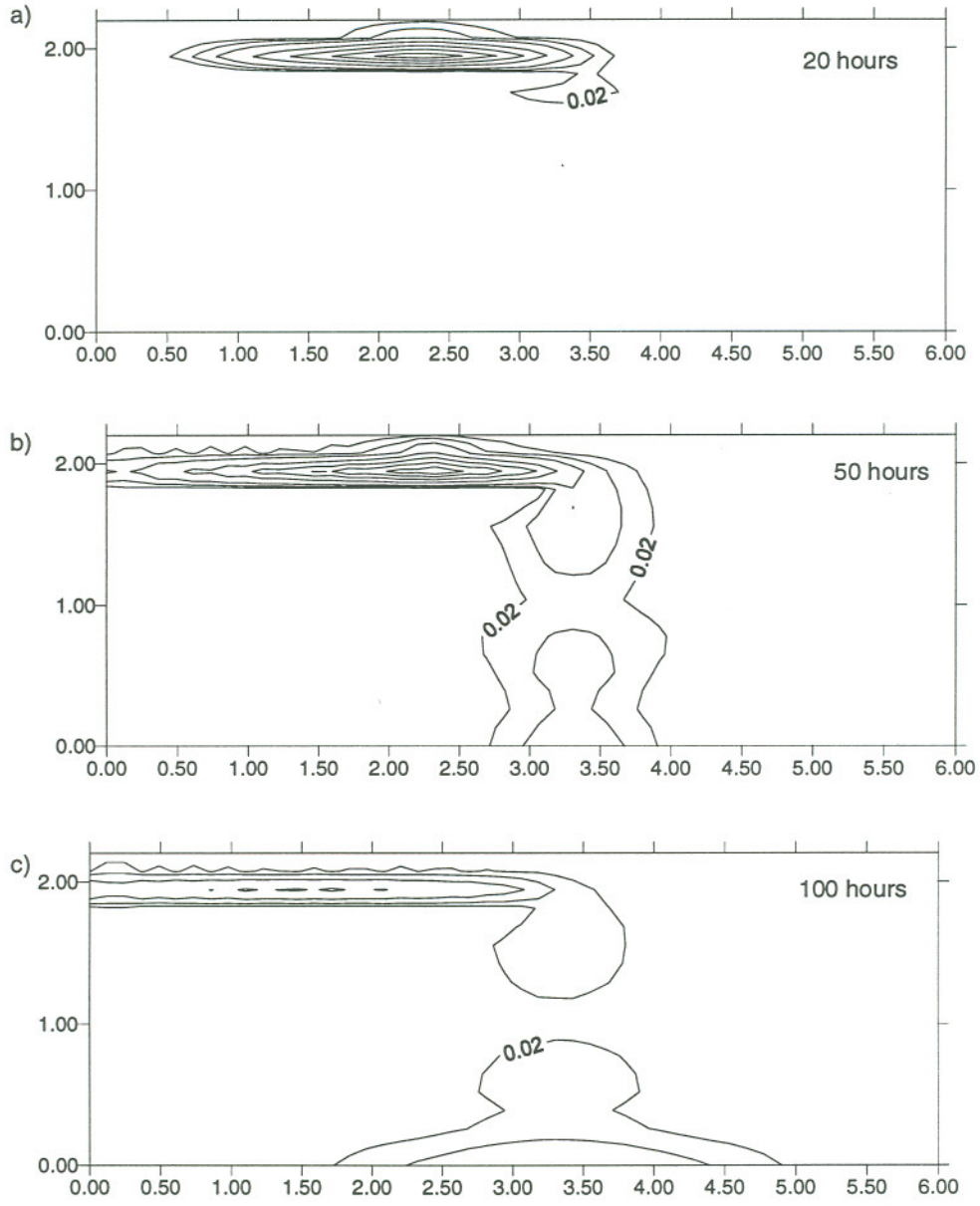

Figure 4.2 PCE saturation contours (0.02, 0.05, 0.1 ... @0.1) for 3-D simulations at a) 20 hours, b) 50 hours, and c) 100 hours.

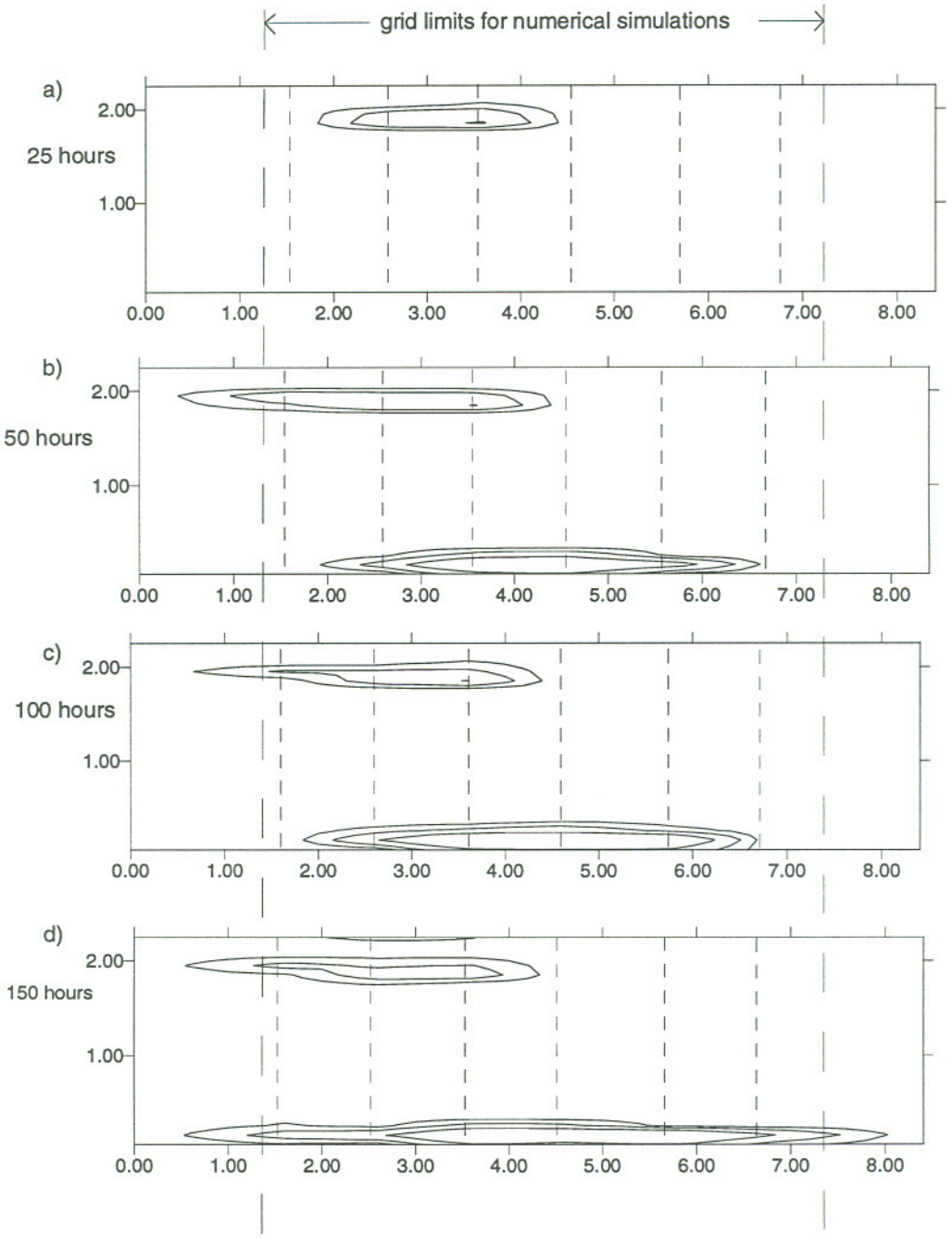

Figure 4.3 PCE saturation contours (0.02, 0.05, 0.1) from NP measurements in the physical model at a) 25 hours, b) 50 hours, c) 100 hours and d) 150 hours.

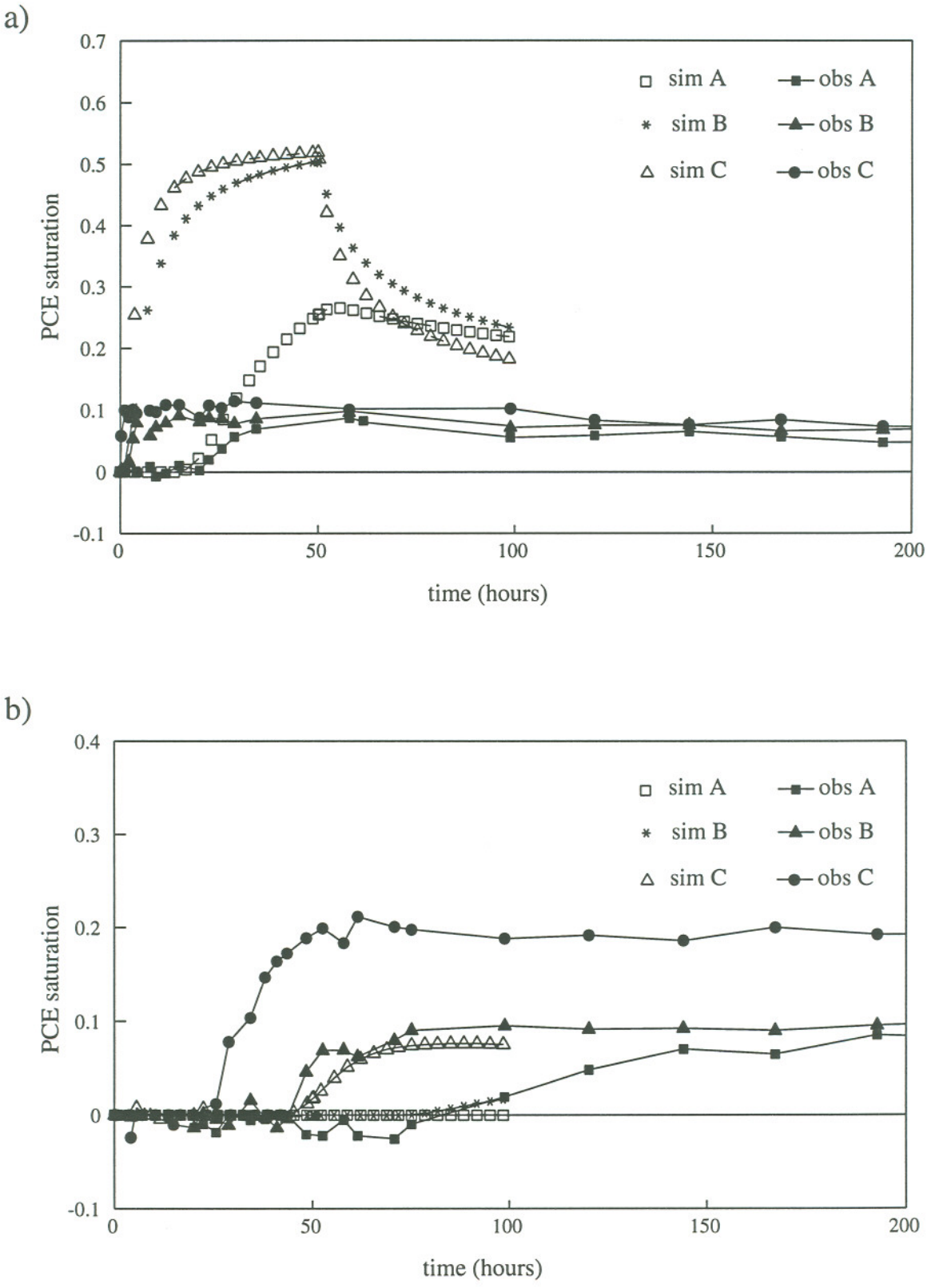

Figure 4.4 Physical model and 3-D simulation PCE saturations at observation points a) above the silica flour and b) above the clay.

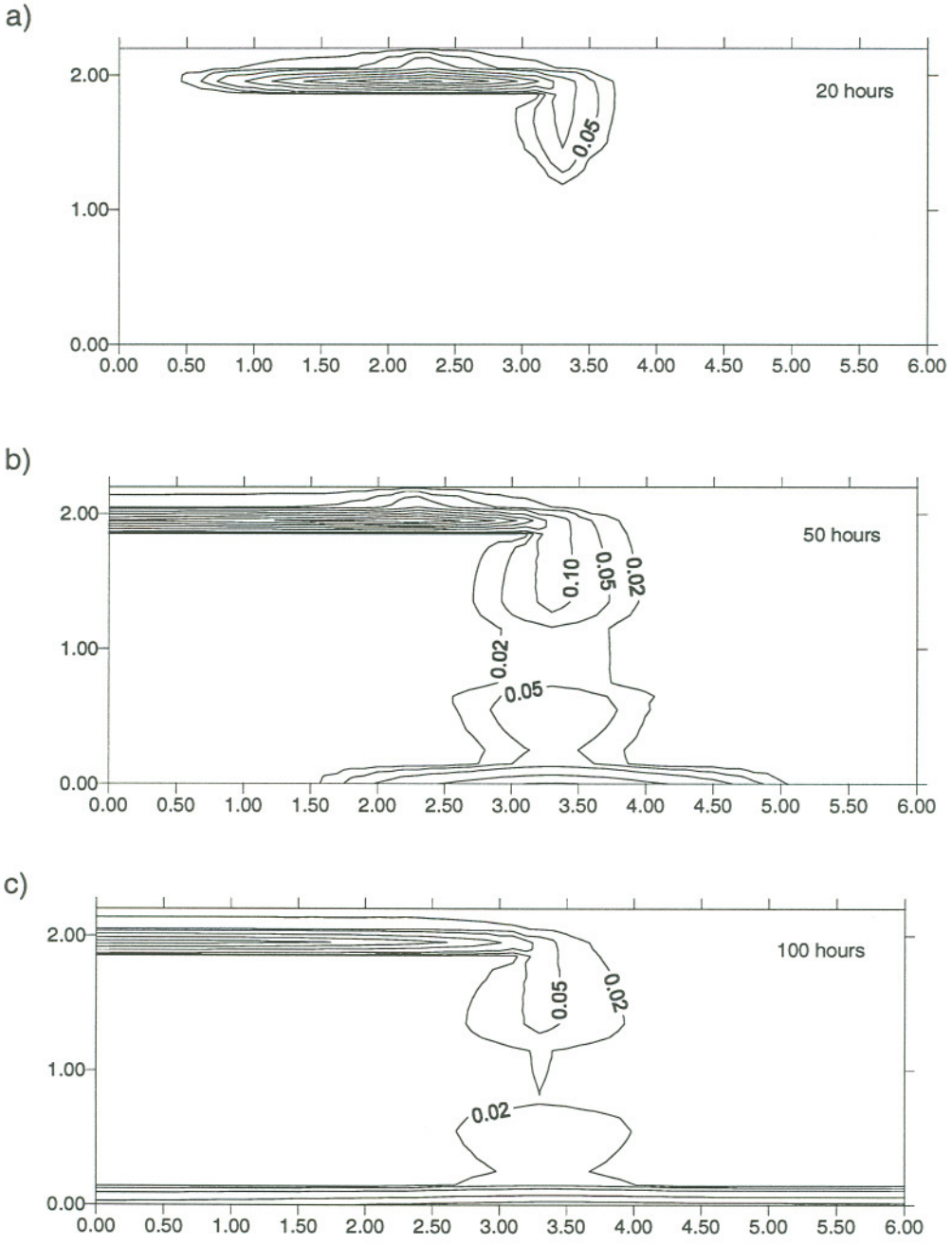

Figure 5.5 PCE saturation contours (0.02, 0.05, 0.1 ... @ 0.1 intervals) for 2D simulation at a) 20 hours, b) 50 hours, and c) 100 hours.

a)

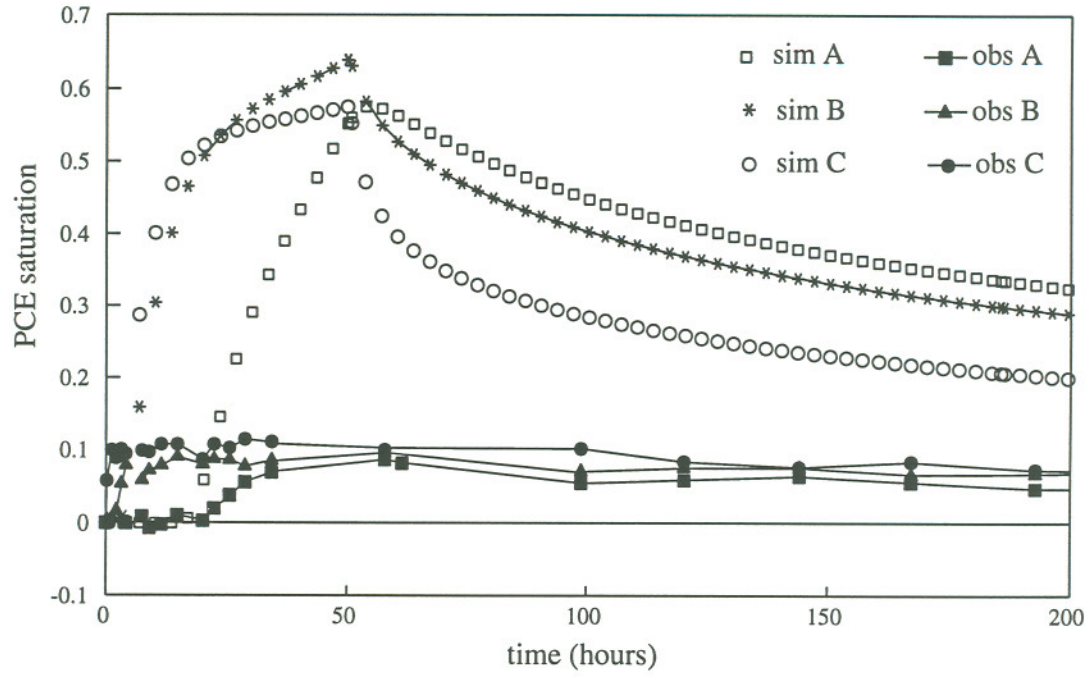

b)

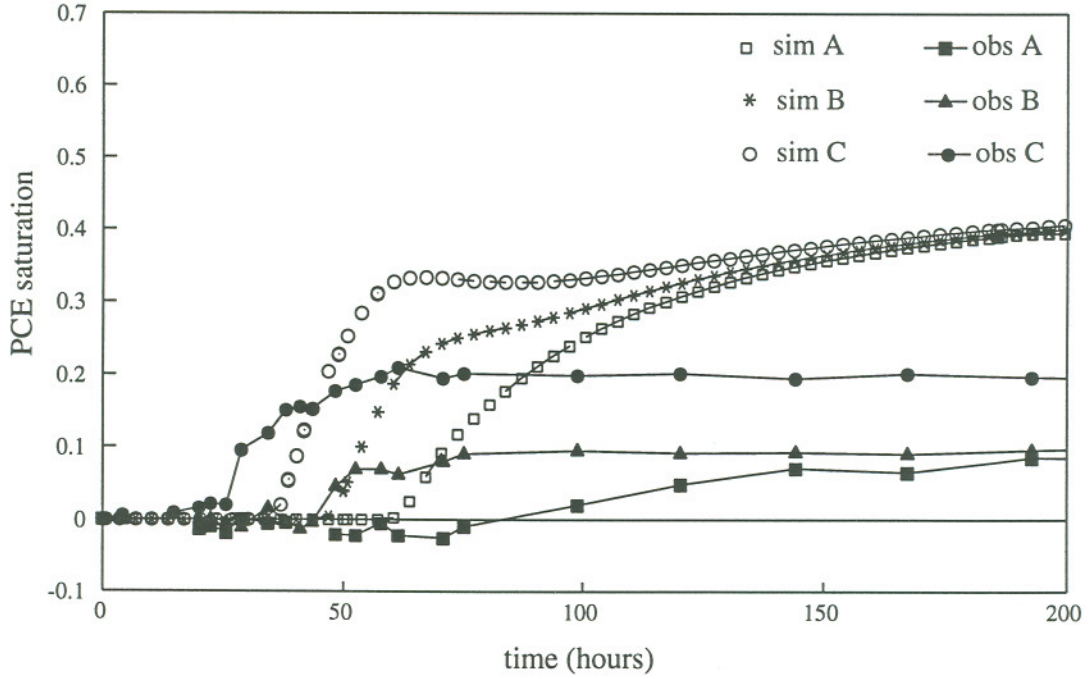

Figure 4.6 Physical model data (obs) and 2-D simulation results (sim) PCE saturations at observation points a) above the silica flour and b) above the clay.

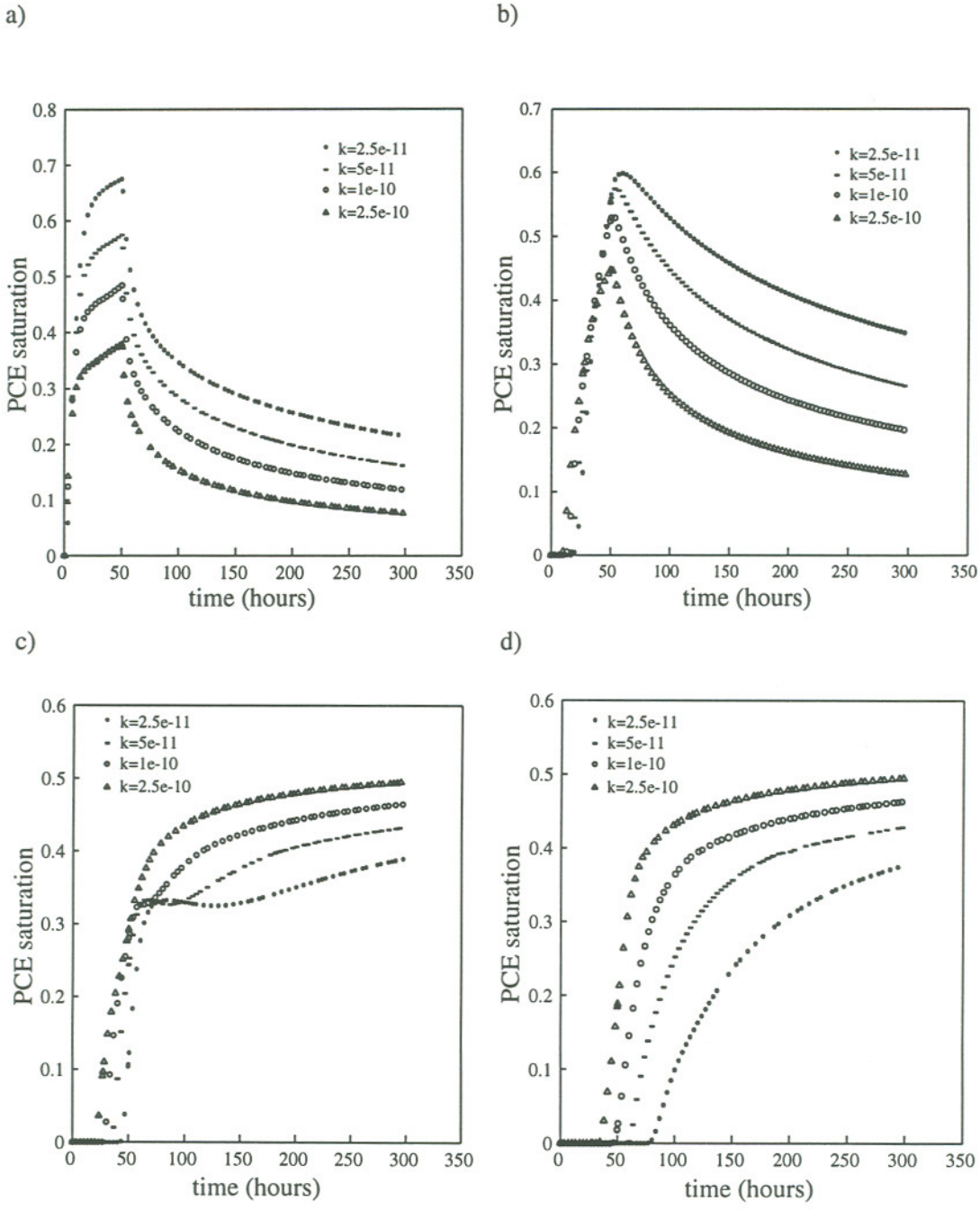

Figure 4.7 PCE saturations at observation point a) "C" and b) "A" above the silica flour, c) "C" and d) "A" above the clay for simulations using a range of sand permeabilities (k).

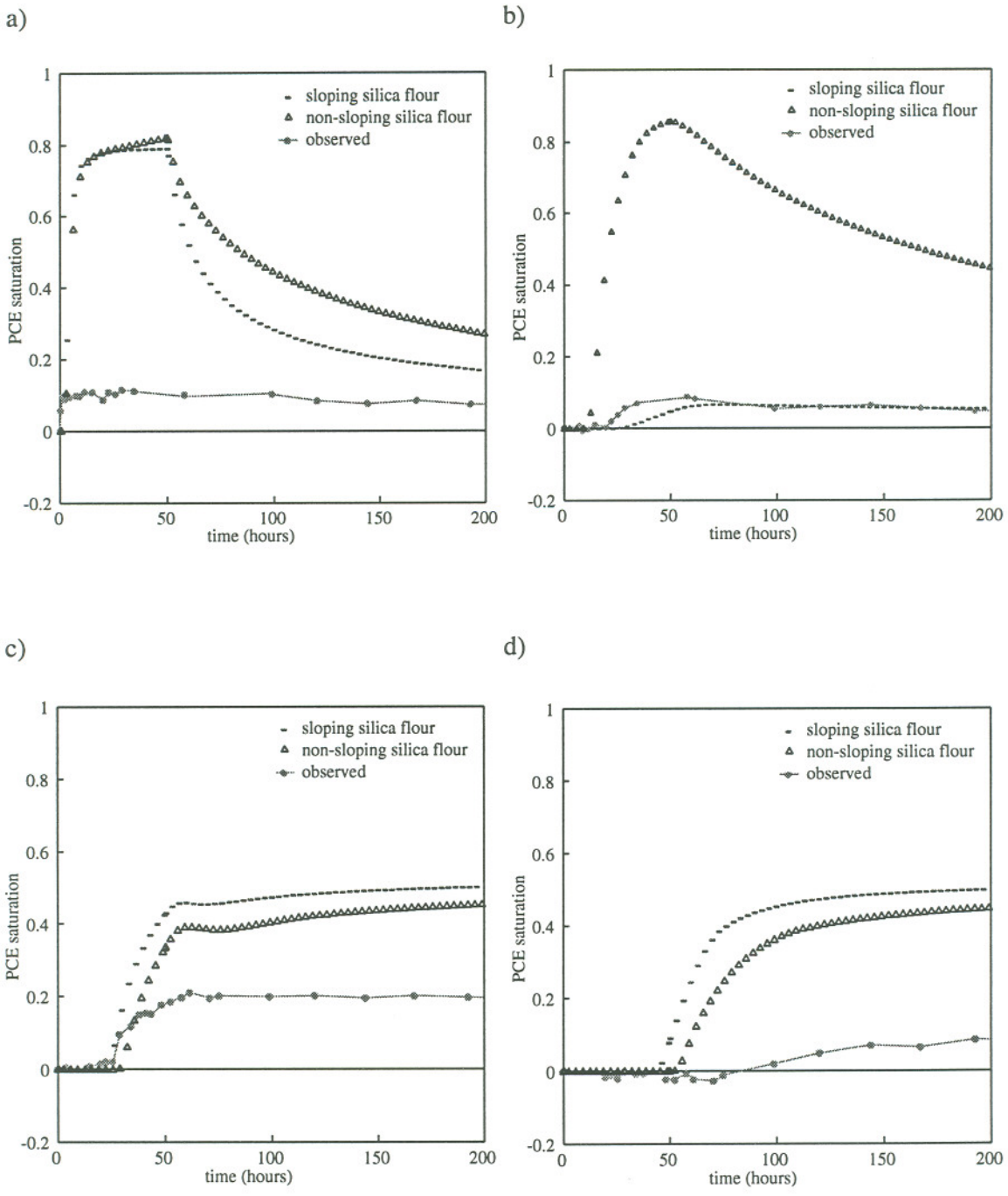

Figure 4.8 PCE saturations at observation points a) "C" and b) "A" above the silica flour, c) "C" and d) "A" above the clay for simulations using sloping and non-sloping silica flour.

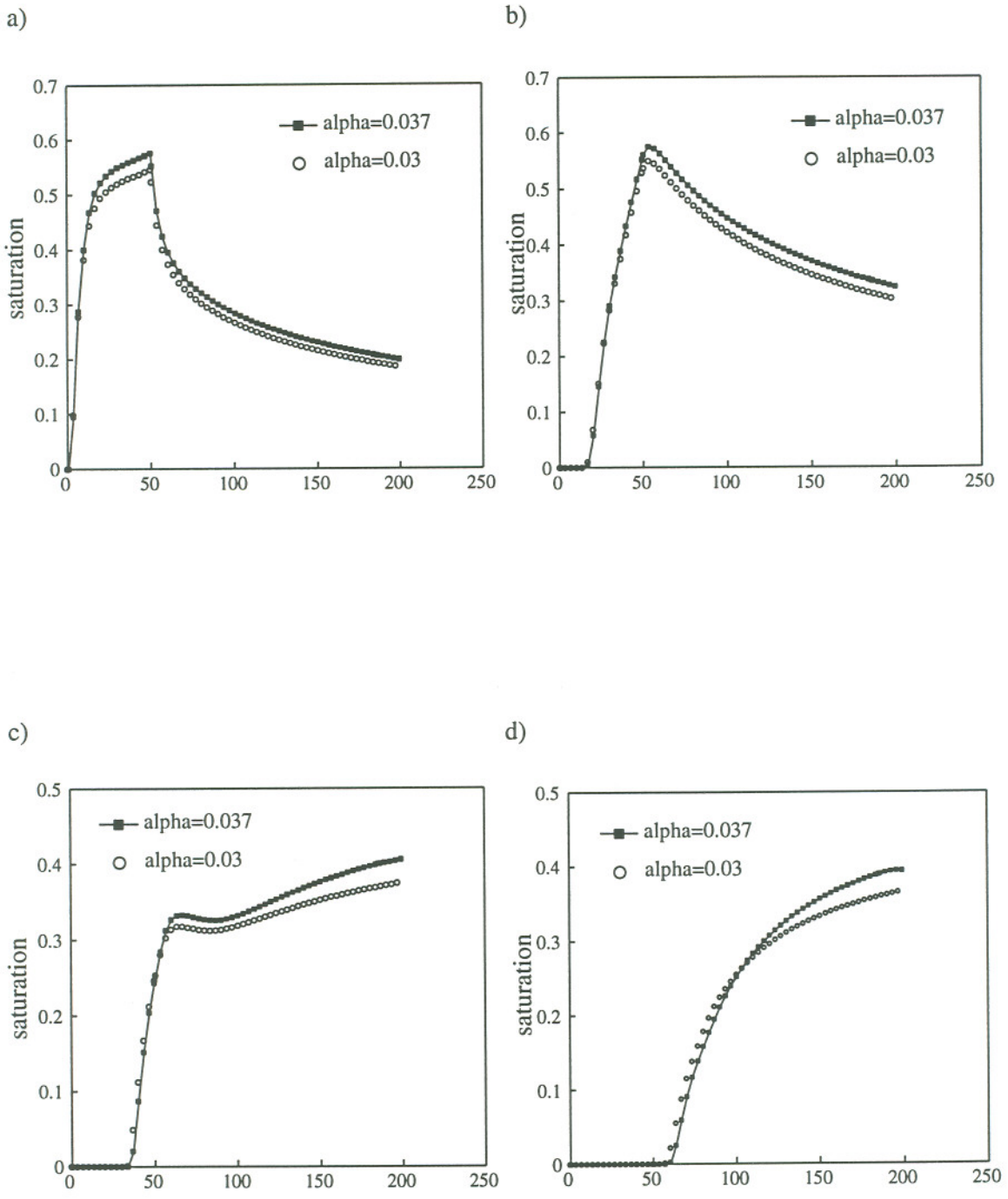

Figure 4.9 PCE saturations at observation points a) "C" and b) "A" above the silica flour, c) "C" and d) "A" above the clay for simulations using alpha = 0.037 and 0.03.

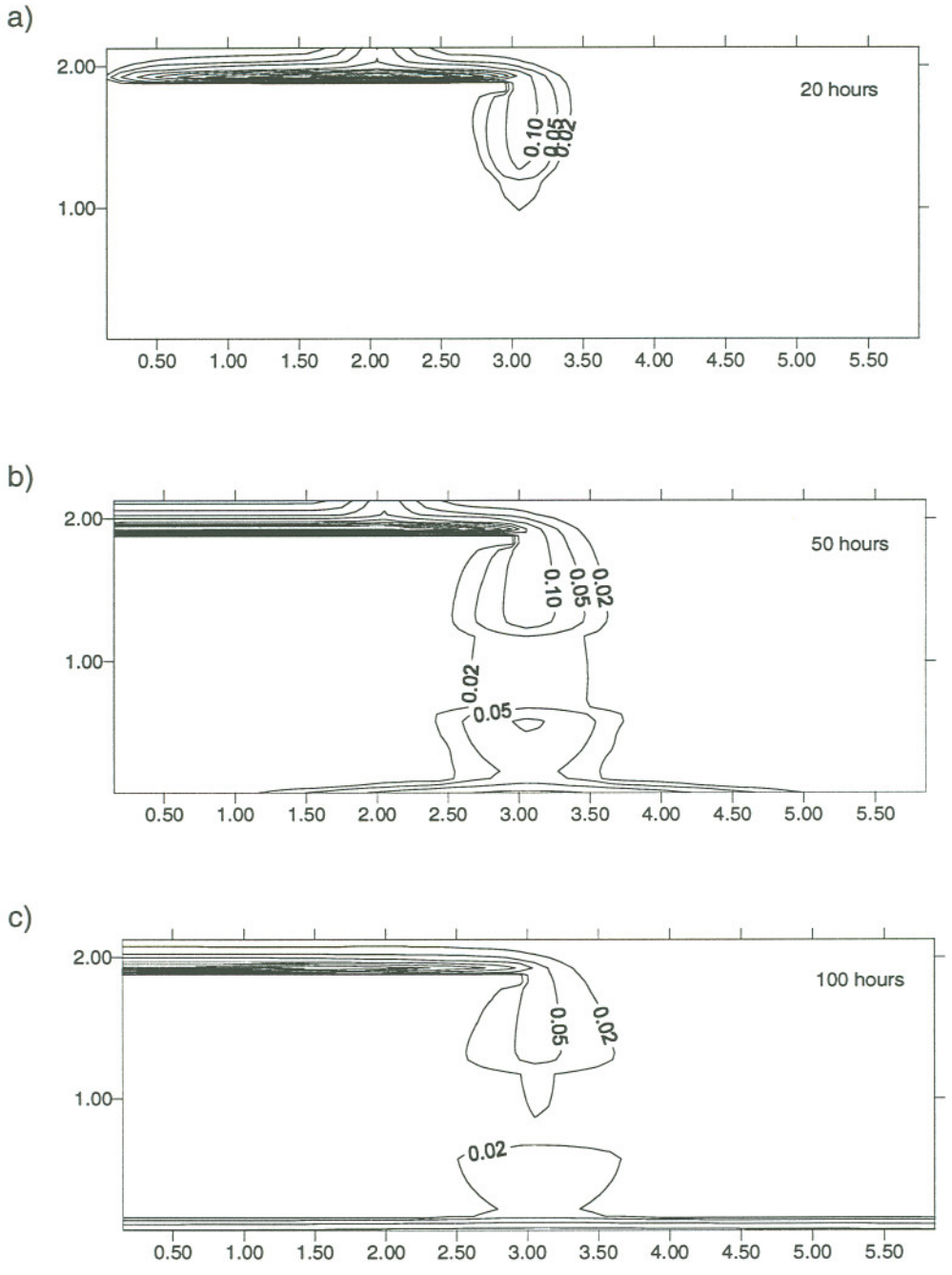

Figure 4.10 PCE saturation contours (0.02, 0.05, 0.1 ... @0.1 intervals) for 2D simulation using a finer grid at a) 20 hours, b) 50 hours, and c) 100 hours.

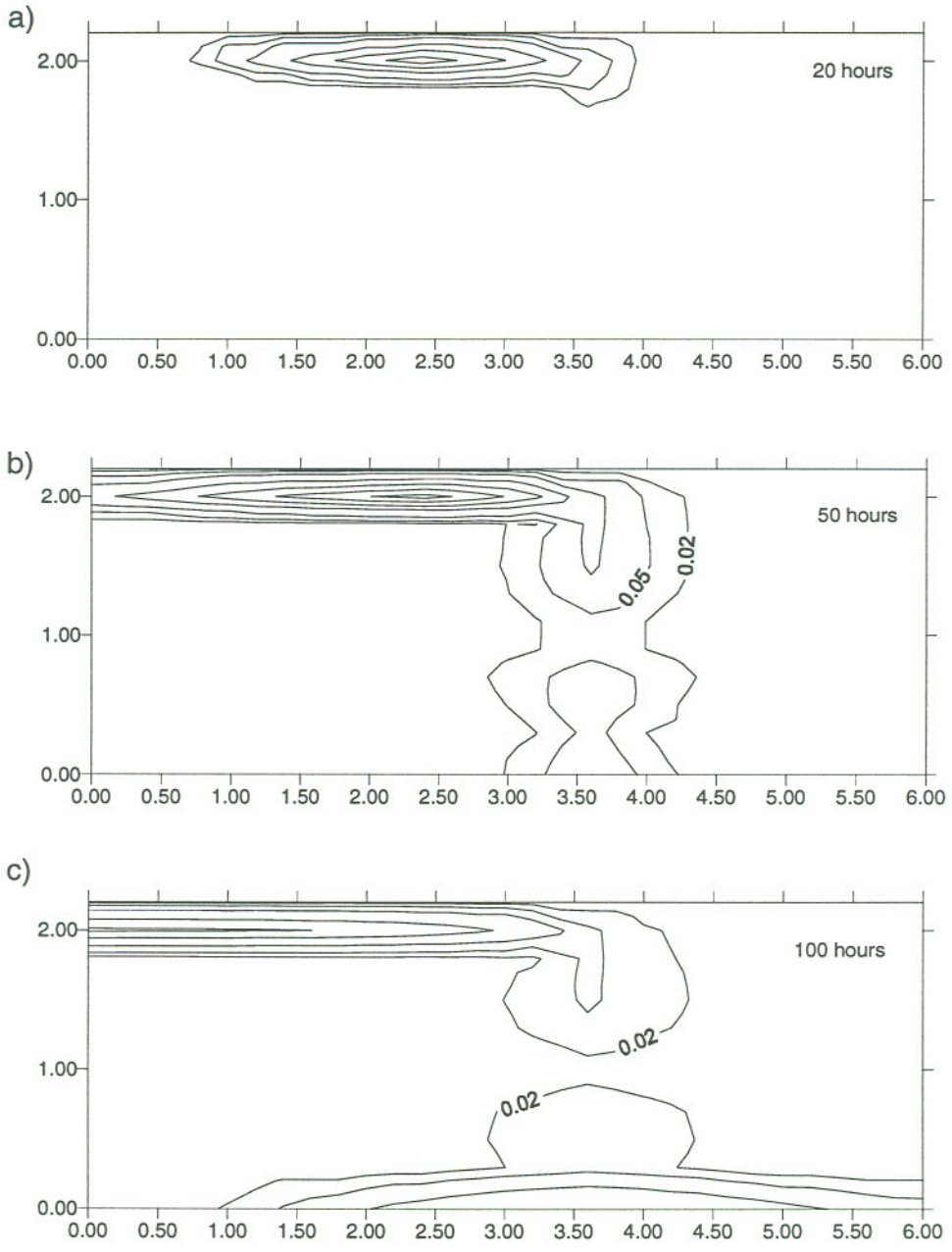

Figure 4.11 PCE saturation contours (0.02, 0.05, 0.1 ... @0.1 intervals) for 2D simulation using a coarser grid at a) 20 hours, b) 50 hours, and c) 100 hours.

a)

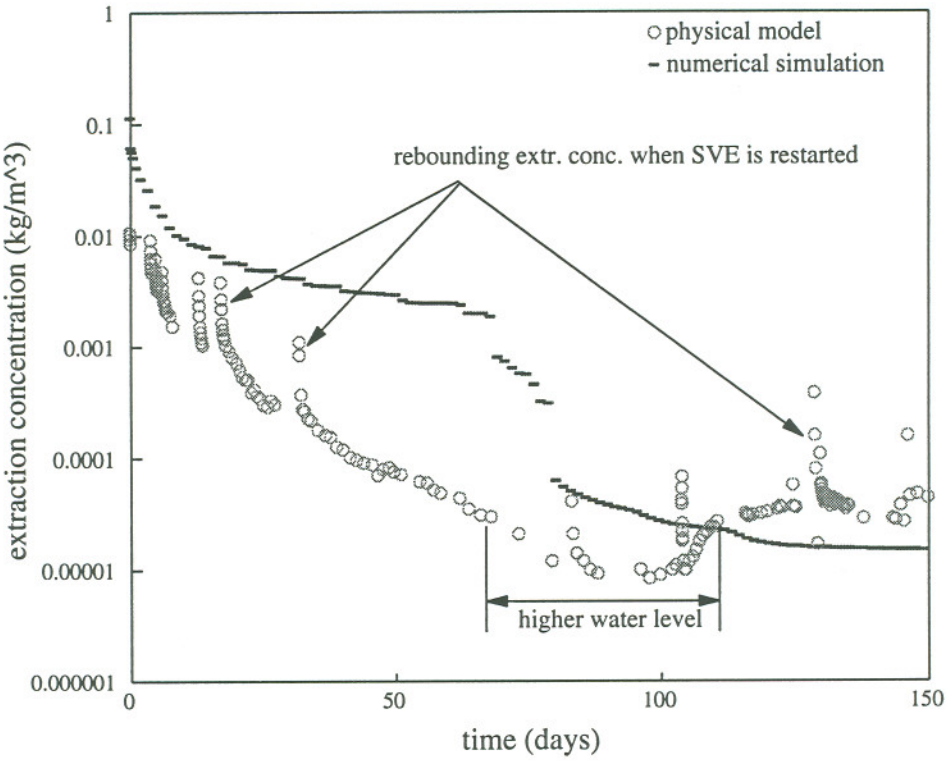

b)

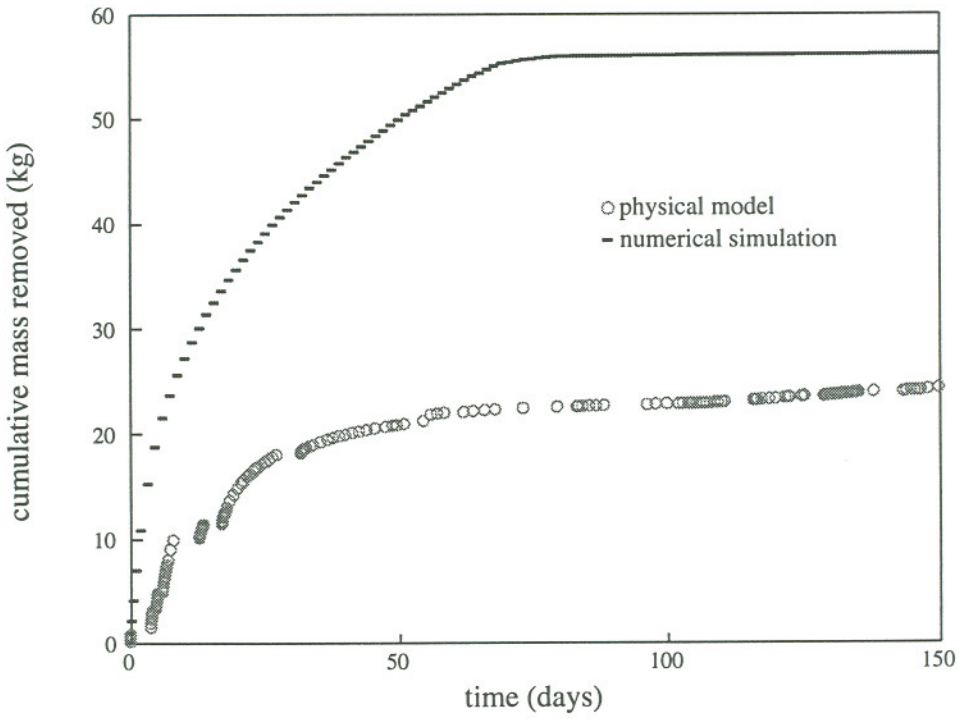

Figure 4.12 Physical model and SVE simulation a) extraction concentrations and b) cumulative mass removed.

a)

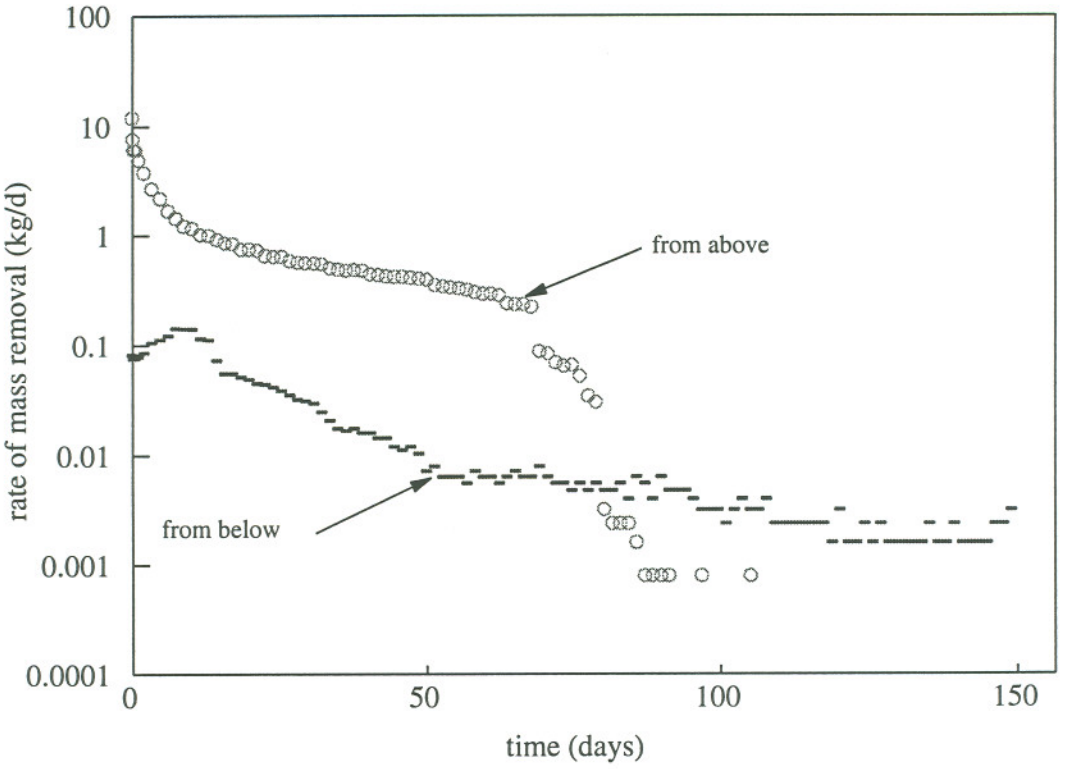

b)

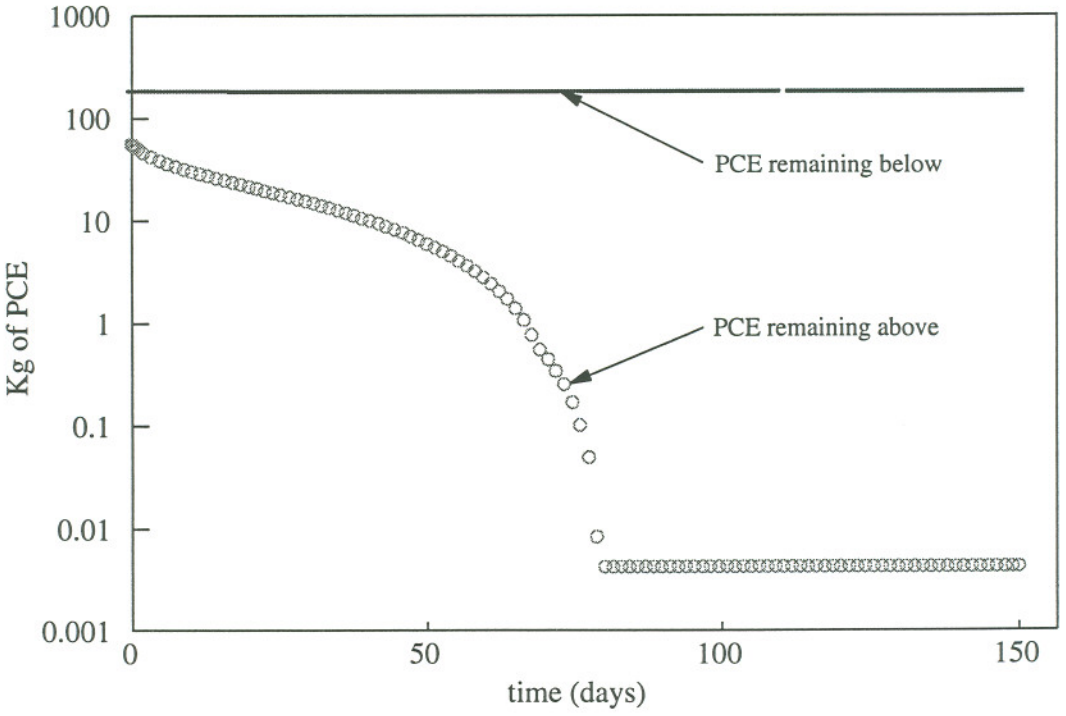

Figure 4.13 Simulated a) mass removal rates and b) mass of remaining PCE for the zones above and below the sand/gravel interface.

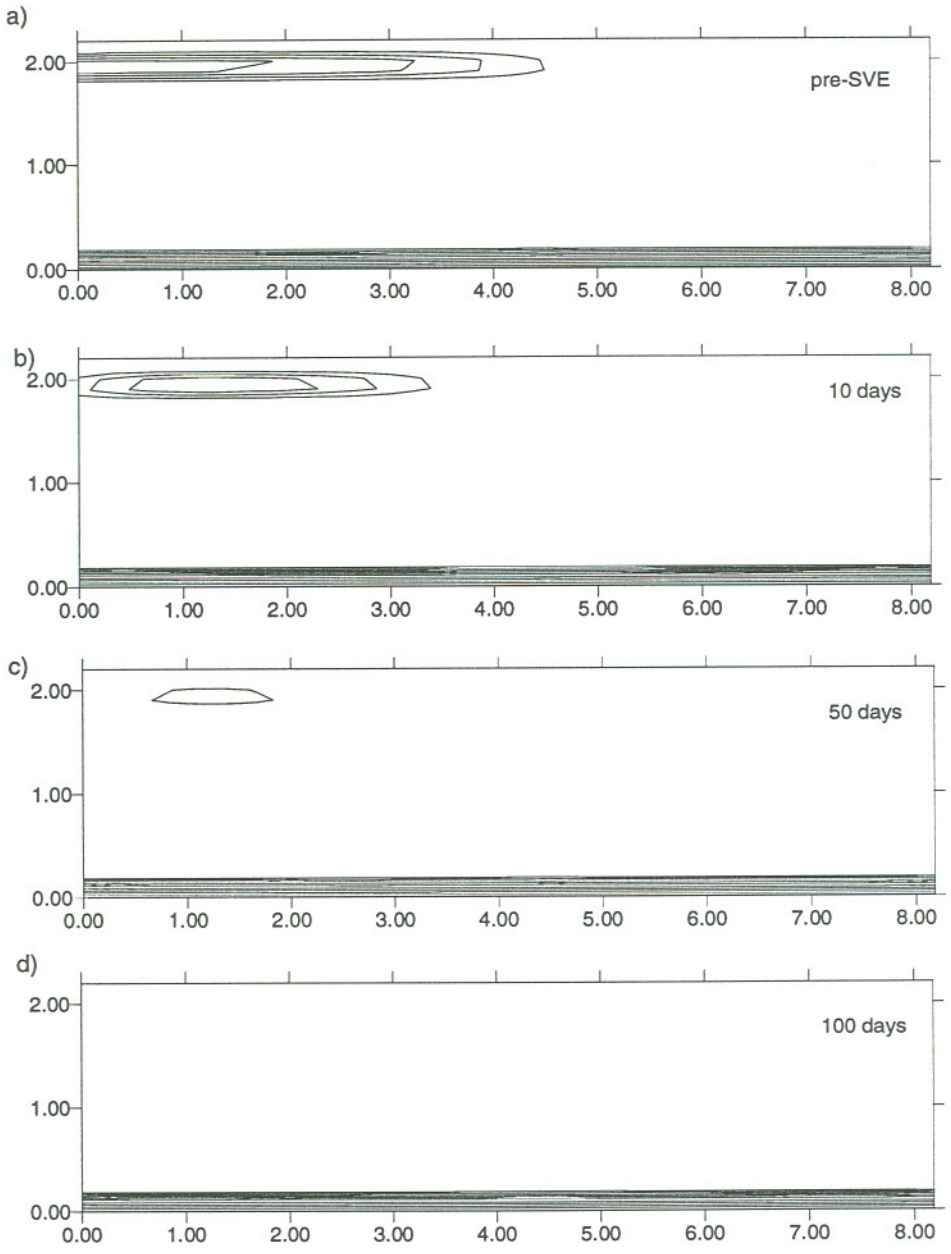

Figure 4.14 PCE saturation contours (0.02, 0.04, 0.06, 0.08, 0.1 ... @0.05 intervals) for SVE simulations a) pre-SVE, b) 10 days, c) 50 days, d) and 100 days.

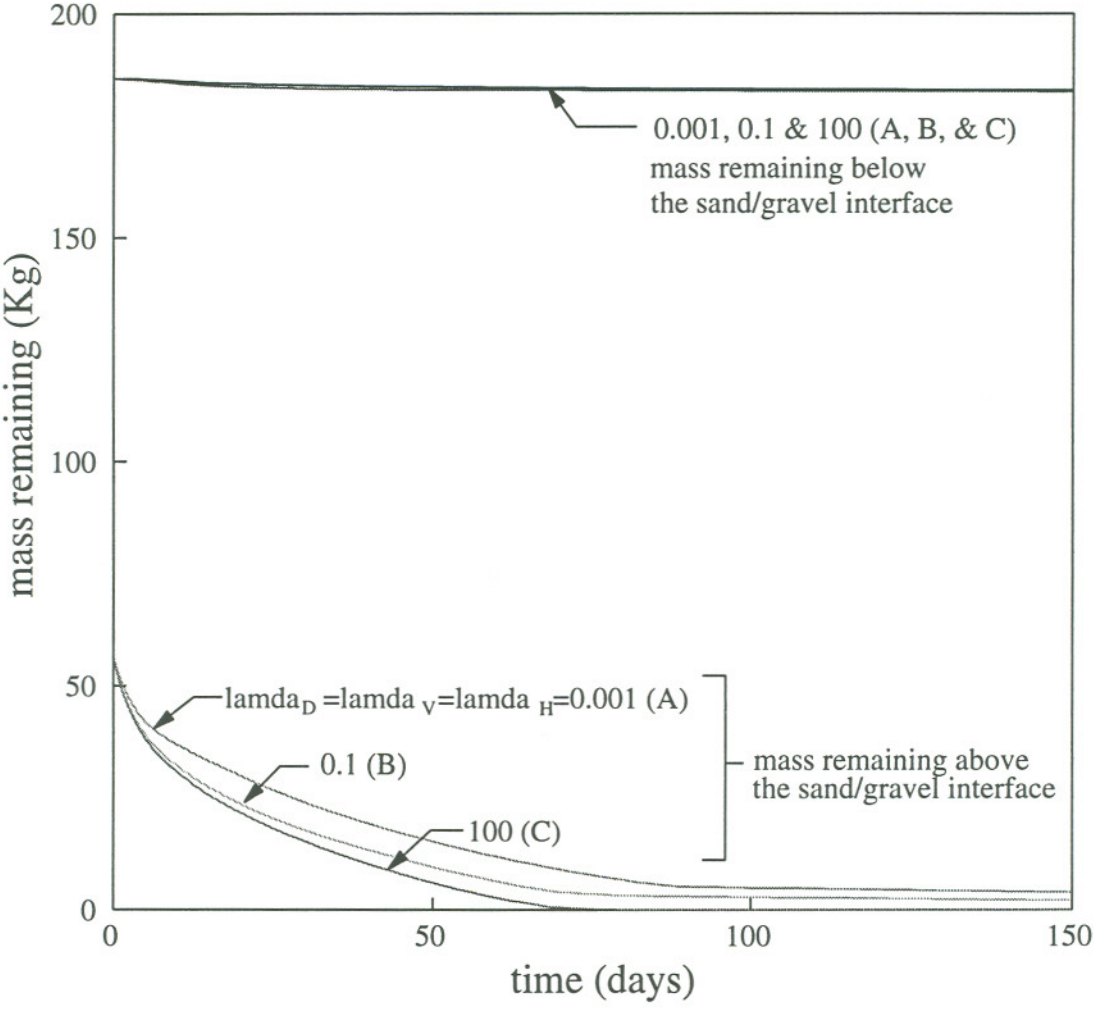

Figure 4.15 Simualted mass of PCE remaining above and below the sand/gravel interface using a range of mass transfer coefficients.

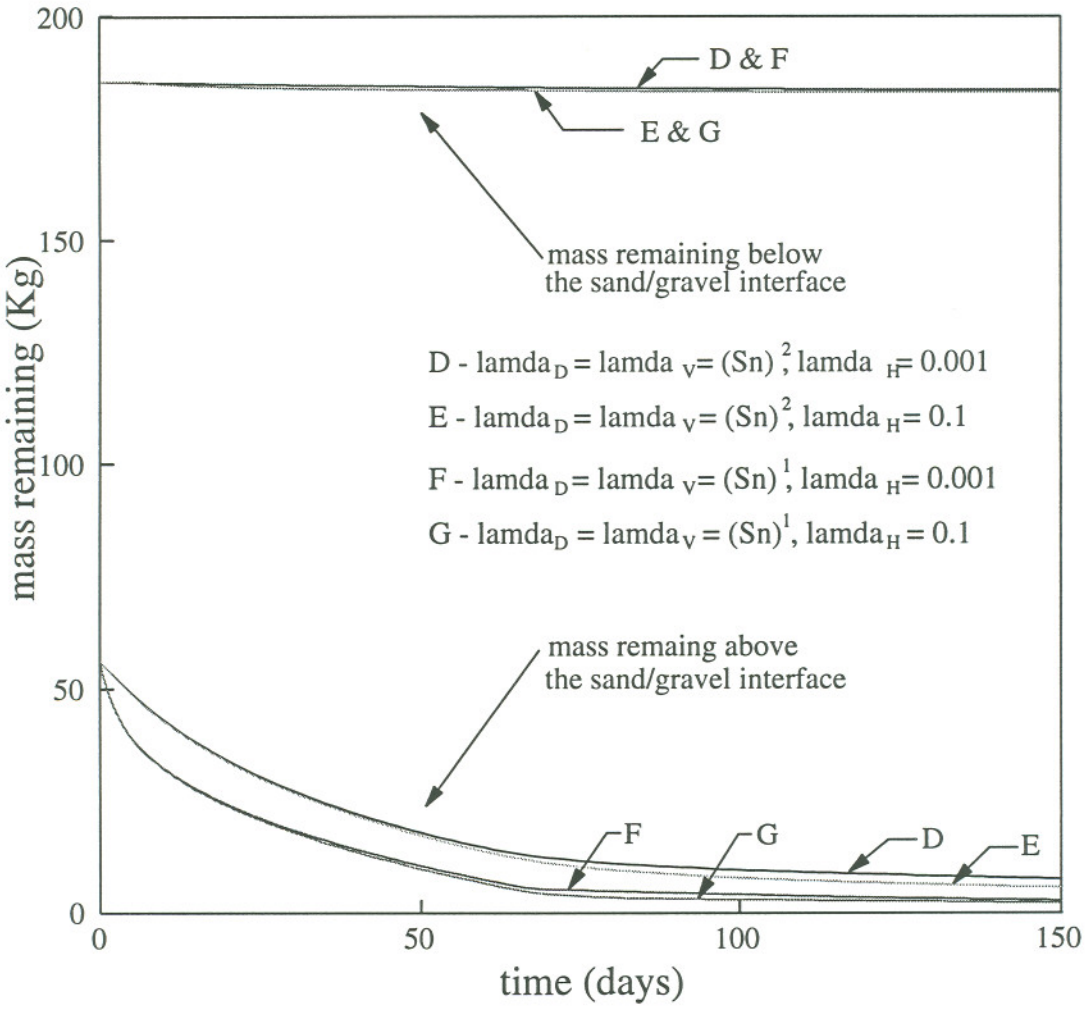

Figure 4.16 Simulated mass of PCE remaining above and below the sand/gravel interface using a range of mass transfer coefficients defined as a function of PCE saturation.

TABLE 4.1 - Porous media, fluid and grid size properties for spill simulations

permeabilities (m^2) :		
	sand	5.00e-11
	gravel	2.00e-09
	silica flour	1.00e-15
fluid densities (kg/m^3) :		
	water	1000
	PCE	1600
	air	1.2
viscosities (Pa-s) :		
	water	0.001
	PCE	0.0009
	air	0.00001
capillary pressure for air/water in sand		
	alpha (m^{-1})	0.00037
	m	0.79
	S_{min}	0.12
capillary pressure for air/water in silica flour		
	alpha (m^{-1})	0.000008
	m	0.5
	S_{min}	0.19
Scaling factors for PCE		
	beta (PCE/water)	2.1
	beta (PCE/air)	1.6
3-dimensional grid		
	dy (m)	0.4 to 0.5
	dx (m)	0.4 to 0.5
	dz (m)	0.2
2-dimensional grid		
	dy (m)	1
	dx (m)	0.2 to 0.25
	dz (m)	0.1
Release rate (m^3/s)		
	3-D	0.000018
	2-D	0.000014

TABLE 4.2 - Parameters used for sensitivity analysis of spill simulations

sand permability (m^2) :			
base	5.00e-11		
	2.50e-11		
	1.00e-10		
	2.00e-10		
beta scaling factors :			
	beta(nw)	beta(ng)	
	1.6	2.1	
	1.86	2.16	
discretization:			
	dx (m)	dz (m)	dy (m)
	0.2-0.25	0.1	1
	0.4-0.5	0.1-0.3	1
	0.1	0.05	1
van Genuchten alpha:			
	alpha (m^{-1})		
	0.00037		
	0.0003		

TABLE 4.3 - Transport parameters for SVE simulations

PCE chemical properties		
	Henry's Constant	0.54
	solubility (kg/m^3)	222
	vapour pressure (kg/m^3)	0.12
	aq. diff. coeff. (m^2/s)	5.60e-10
	gas. diff. coeff. (m^2/s)	0.000007
porous media transport parameters		
	trans dispersivity (m^{-1})	0.2
	long. dispersivity (m^{-1})	0.01
mass transfer coefficients		
	dissolution (s^{-1})	100
	evaporation (s^{-1})	100
	volatilization (s^{-1})	100

TABLE 4.4 - Mass transfer coefficient for SVE simulations

	water/air	NAPL/ water	NAPL/air
	(s^{-1})	(s^{-1})	(s^{-1})
A	0.001	0.001	0.001
B	0.1	0.1	0.1
C	100	100	100
D	$(Sn)^2$	$(Sn)^2$	0.001
E	$(Sn)^2$	$(Sn)^2$	0.1
F	$(Sn)^1$	$(Sn)^1$	0.001
G	$(Sn)^1$	$(Sn)^1$	0.1

REFERENCES

Abriola, L.M. and G.F. Pinder, A multiphase approach to the modelling of porous media contamination by organic compounds, 1. Equation development, *Water Resour. Res., 21(1)*, 11-18, 1995.

Armstrong, J.E., E.O. Frind and R.D. McClellan, Nonequilibrium mass transfer between the vapor, aqueous, and solid phases in unsaturated soils during vapor extraction, *Water Resour. Res., 30(2)*, 355-368, 1994.

Benson, D.A., D. Huntley and P.C. Johnson, Modeling of vapor extraction and general transport in the presence of NAPL mixtures and nonideal conditions, *Ground Water 31(3)*, 437-445, 1993.

Crow, W.L., E.P. Anderson, and E.M. Minugh, Subsurface venting of vapors emanating from hydrocarbon product on the groundwater, *Ground Water Monit. Rev., 7(1)*, 51-57, 1987.

Essaid, H.I., W.N. Herkelrath and K.M. Hess, Simulations of fluid distributions observed at a crude oil spill site incorporating hysteresis, oil entrapment, and spatial variability of hydraulic properties, *Water Resour. Res.*, 29(6), 1753-1770, 1993.

Faust, C.R., Transport of immiscible fluids within and below the unsaturated zone: a numerical model, *Water Resour. Res., 21(4)*, 587-596, 1985.

Faust, C.R., Guswa, J.H. and Mercer, J.W., Simulations of three-dimensional immiscible fluids within and below the unsaturated zone, *Water Resour. Res., 25(12)*, 2449-2464, 1989.

Gierke, J.S., N.J. Hutzler and D.B. McKenzie, Vapor transport in unsaturated soil columns: implications for vapor extraction, *Water Resour. Res., 28(2)*, 323-335, 1992.

Illangasekara, T.H., D.N. Yates, E. Armbruster, J.Wald, and D.D. Reible, *Computational Methods in Water Resources IX. Volume 2: Mathematical Modeling in Water Resources*, Boston, MA., Computational Mechanics Publications, 289-296, 1992.

Johnson, P.C., M.W. Kemblowski and J.D. Colthart, Quantitative analysis for the clean-up of hydrocarbon-contaminated soils by in-situ soil venting, *Ground Water, 28(3)*, 413-429, 1990.

Kueper, B.H. and E.O. Frind, Two-phase flow in heterogeneous porous media, 2. Model application, *Water Resour. Res., 27(6)*, 1059-1070, 1991.

Lenhard, R.J., J.H. Dane, and J.C. Parker, Measurement and simulation of one-dimensional transient three-phase flow of monotonic liquid drainage, *Water Resour. Res., 24(6)*, 853-863, 1988.

Mercer, J.W. and R.M. Cohen, A review of immiscible fluids in the subsurface: properties, models characterization and remediation, *J. Contam. Hydrol., 6*, 107-163, 1990.

Osborne, J.M. and J.F. Sykes, Numerical modeling of immiscible organic transport at the Hyde Park Landfill, *Water Resour. Res., 22(1)*, 25-33, 1986.

Parker, J.C., Lenhard, R.J. and Kuppusamy, T., A parametric model for constitutive properties governing multiphase flow in porous media, *Water Resour. Res.,* 23(4), 618-624, 1987.

Rathfelder, K., W.W-G. Yeh and D. Mackay, Mathematical simulation of soil vapor extraction systems: Model development and numerical examples. *J. Contam. Hydrol., 8*, 263-297, 1991.

Sleep, B.E. and J.F. Sykes, Compositional simulation of groundwater contamination by organic compounds, 1. Model applications, *Water Resour. Res., 29(6)*, 1709-1718, 1993.

Thomson, N.R., *Documentation for 3D3PT: a three-dimensional, three-phase, flow and transport model*, Dep. of Civ. Eng., Univ. of Waterloo, 1995.

Van Geel, P.J., and J.F. Sykes, Laboratory and model simulations of a LNAPL spill in a variably-saturated sand, 2. Comparison of laboratory and model results, *J. Contam. Hydrol., 17*, 27-53, 1994.

CHAPTER 5

SUMMARY, CONCLUSIONS AND IMPLICATIONS

SUMMARY OF RESEARCH

The research presented here has three principal components: 1) physical modeling the release of tetrachloroethylene (PCE) into an into an unsaturated, heterogeneous porous medium; 2) soil vapor extraction (SVE) of the resulting PCE-contaminated soil; and 3) numerical modeling of both the PCE release and remediation by (SVE). The PCE release provided an opportunity to examine the movement of a dense, nonaqueous phase liquid (DNAPL) in an unsaturated porous medium and provided a well-defined source for the subsequent remediation experiments. The SVE experiments, because of the well defined nature of the medium and the NAPL distribution, provided a quantitative understanding of the processes controlling SVE in the physical model. The spill and SVE data for the physical model have made it possible to evaluate the performance of the numerical model and will better allow the model to be applied other spill scenerios.

To examine DNAPL migration, PCE was slowly released into a large-scale, structured, physical model from a point source located near the surface. The physical model consisted of a series of layers of medium sand, gravel, silica flour and clay. Migration of the PCE was monitored throughout the spill and redistribution using a neutron moisture probe (NP) and down-hole video camera. PCE was observed to pool then drain from above the silica flour lens and then pool and spread laterally on the clay bottom. The final DNAPL distribution was confirmed by soil cores.

Following the PCE release, an SVE system consisting of air extraction wells along one side of the physical model and air inlet wells along the other was installed in the physical model. The ground surface was covered with a vinyl cap to reduce leakage. Air flow in the porous medium was controlled by the screened intervals of the injection and extraction wells as well as surface leakage. Two different air flow configurations were used to maximize air flow through the most highly contaminated zones. Gas-phase tracer tests and pressure measurements were performed to characterize the air movement under each of the flow conditions. Mass removal was monitored using extraction air samples collected and analyzed for PCE content using gas chromatography. Two methods of enhanced SVE were also tested: 1) high vacuum extraction from a drive point and 2) SVE coupled with air injection at a drive point.

The PCE release was numerically simulated in two- and three-dimensions using a three-phase flow and transport model where all three fluid phases are active (*i.e.*, capillary and gravitaional forces act on all three phases). The model was also used to simulate air flow and mass transport during SVE. A numerical SVE experiment representing a vertical slice from the center of the physical model was simulated using PCE distributions estimated from the spill simulation. Mass transfer from the PCE pool above the clay was also simulated using a one-dimensional diffusion model.

CONCLUSIONS OF RESEARCH

DNAPL Release Experiments

In the physical model experiments PCE reached the bottom of the model ~26 hours after the release was initiated and essentially all of the movement occured within the first 200 hours. As expected there was evidence of accumulation on the discontinuous impermeable silica flour lens near the top of the model. After the release was terminated, PCE above the lens drained to residual saturation. Approximately 80-90% of the PCE reached the bottom of the model. The final DNAPL distribution was highly irregular, with only ~2% of the soil volume contaminated with PCE. The DNAPL pool on the clay was ~0.16 m thick at the center with an average PCE content of 7% by volume (~0.18 saturation). This pool was located in the tension saturated

portion of the capillary fringe. Mass transfer in that region is primarily by aqueous phase diffusion through the high water content porous medium.

SVE Experiments

Gas-phase tracer tests demonstrated that advective air flow was very low in the portion of the lower sand which contained most of the PCE. This was due to both the presence of the high permeability gravel layer above the sand and low air filled porosity in the contaminated sand above the clay. In addition, despite the presence of a good surface cover, a significant portion of the total air flow through the model resulted from surface leakage.

Of the 320 kg of PCE released into the physical model, only 30 kg was recovered by conventional vapor extraction over a period of 270 days. As mentioned above, the primary limitation to recovery was the fact that nearly all the PCE mass was located at the bottom of the model below the high-permeability gravel and was retained within a high-water-content zone. Diffusion from the pool was simulated using a one-dimensional diffusion model. The calculated rate of mass flux by diffusion through the capillary fringe and transition zone agreed well with the experimentally-observed rate of mass removal.

In an effort to improve mass recovery, two drive points were placed in the sand just above the clay layer. Mass removal by high-vacuum extraction from one of the drive points was significantly higher than by conventional SVE. Approximately 65 kg of PCE was removed (as vapor, gas and liquid phase) over a 20 day period. Mass removal by air injection into a second drive point, coupled with conventional SVE, resulted in some increase in mass recovery over SVE alone, however, it appears that the injection process drove PCE and water from the drive point and prevented sustained high mass recovery.

Numerical Modeling

Two- and three-dimensional numerical simulations of a PCE release into the physical model reproduced the general trends in the migration and final distribution of PCE observed in the physical model. Simulated results showed higher PCE saturations, a longer period of

accumulation above the silica flour, and later arrival at the clay bottom. Sensitivity analysis showed that differences between observed and numerical results were reduced when the sloped surface of the silica flour present in the physical model was represented in the numerical grid and/or when a somewhat higher permeability was used for the sand.

SVE simulations under near-equilibrium conditions showed the same trend in the mass removal rates as was observed in the physical model. There was an initial short period of high mass removal which was followed by a long period of slow mass removal. Distribution of PCE remaining in the soil when simulations mass removal rates became very low matched PCE distributions in the physical model described by soil cores.

The ability of the numerical model to reproduce SVE observations in the physical model was limited by the model description of the initial PCE distribution (2-D characterization of PCE distribution with very low initial PCE saturation in the silica flour).

IMPLICATIONS

The research presented here illustrates the critical roles that soil heterogeneities and irregular NAPL distribution can have on SVE performance. Under the conditions tested, less than 10% of the spilled mass was recovered after 270 days, and teh mass removal rate at that time was very low indicating that significant additional mass removal was unlikely. The research also indicates that if soil heterogeneities and irregular NAPL distributions can be charaterized then reasonable predictions of SVE performance can be made.

Several standard and non-standard methods were used to characterize NAPL and water distributions following the spill, and air flow and mass recovery during SVE. These include: 1) soil gas sampling; 2) NAPL content, water content and permeability measurements from soil cores; 3) water and NAPL distribution using a neutron moisture probe; 4) subsurface pressure measurements and 5) vapor-phase tracer tests. Most of these tools can be utilized at contaminated sites and can provide important insights into the effectiveness of remediation by SVE. Soil gas concentration can provide information on the distribution of volatile contaminants both prior to and during SVE. Soil cores can provide information for the characterization of contaminant distributions as well as characterization of porous media properties including

permeability and fluid content. Cores can be particularly useful for identifying zones with low permeability, high water and/or NAPL content from which mass removal is expected to be slow. Another less conventional monitoring tool evaluated in this research is the neutron moisture probe. This geophysical instrument is simple to operate and can again be used to identify zones of high chlorinated solvent and/or water saturations.

Monitoring tools can also be used to evaluate air flow during SVE. The most common procedure for evaluating air flow relies on air pressure data alone. However, the research presented here has shown how tracers tests can be used simply and effectively in conjunction with pressure field data to measure directly air velocities and identify zones from which mass removal will be diffusion limited.

An understanding of the actual air flow and mass transport limitations, as well as NAPL distributions at a given site should result in improved remediation design, more accurate estimates of the time frame of remediation, as well as more accurate predictions of remediation success using SVE.

VITA

The author was born on August 6, 1967, in Ottawa, Canada, where she attended St. Pius X high school. In the fall of 1985 she enrolled in the civil engineering program at the University of Waterloo. The co-op program at Waterloo provided learning experiences in a classroom as well as in a work place setting. Based on these experiences, as well as a comparison of the lifestyles of her graduate student friends to those of her co-op work-term collegues she decided that she should postpone entering the work force as long as possible.

In September 1990, she made the big move west to begin graduate studies in Environmental Science and Engineering at the Oregon Graduate Institute. After many tons of porous media moved, hundreds of neutron logs, two burnt-out SVE blowers, and many numerical simulations she defended her dissertation in June of 1995.

She is now off to begin a postdoc (and German language classes!) at the University of Stuttgart VEGAS facility.